COPPER CHELATING ANTI-INFLAMMATORY AGENTS OF PSEUDO-MIMICS OF HUMAN SERUM ALBUMIN (HSA): COPPER AND RHEUMATOID ARTHRITIS

A thesis submitted to the Department of Chemistry,
Faculty of Science, University of Cape Town,
in fulfilment of the requirements for the degree of
DOCTOR OF PHILOSOPHY

BY

JOHN NGONI ZVIMBA

Department of Chemistry
University of Cape Town
Rondebosch
7701
Cape Town
South Africa

November 2005

“The task is, not so much to see what no one has yet seen; but to think what nobody has yet thought, about that which everybody sees”

Erwin Rudolf Josef Alexander Shrödinger

DECLARATION

I hereby sincerely and solemnly declare that **COPPER CHELATING ANTI-INFLAMMATORY AGENTS OF PSEUDO-MIMICS OF HUMAN SERUM ALBUMIN (HSA): COPPER AND RHEUMATOID ARTHRITIS** is my own, unaided work, and that all sources I have used or quoted have been indicated and acknowledged by means of complete references. The thesis is submitted for the degree DOCTOR OF PHILOSOPHY, to the Department of Chemistry, Faculty of Science, at the University of Cape Town, and has not been submitted before for any degree or examination at any other university.

.

Signed by candidate

J.N. Zvimba

November 2005

ACKNOWLEDGEMENTS

I would like to express my sincere gratitude to the following:

- My supervisor, Professor Graham Ellis Jackson, for his unwavering guidance and support throughout the course of this study.

- My colleagues in the research group for their useful discussions.

- Dr A. Hunter (Radiobiology) for providing laboratory space for animal experiments, J. Boniaszczuk (Nuclear Medicine Department), J. Visser (Animal Unit), colleagues, S. Odisitse and C. Jackson for their technical assistance in the animal experiments.

- Dr J. R. Zeevart of the South African Nuclear Energy Corporation (Ltd.) at Pretoria for preparation and supplying me with $^{64}CuCl_2$.

- The National Research Foundation (NRF), the Council of the University of Cape Town and Beit Trust for financial support.

- My wife, Norma and family for their continued support and encouragement.

CONFERENCE PROCEEDINGS

Parts of this thesis have been presented at the following conferences:

Solution Chemistry of Metal ions of Biological interest with novel human serum albumin mimicking ligands., J.N. Zvimba and G.E. Jackson; The 37th National Convention of the South African Chemical Institute, Pretoria, South Africa, July 2004.

Human Serum Albumin mimicking ligands as anti-inflammatory agents: Copper and Rheumatoid Arthritis., J.N. Zvimba and G.E. Jackson; The South African Chemical Institute Conference on Inorganic Chemistry, Pietermaritzburg, South Africa, April 2005.

Human Serum Albumin mimicking ligands as anti-inflammatory agents: Copper and Rheumatoid Arthritis., J.N. Zvimba and G.E. Jackson; The International Conference on Solution Chemistry, Portoroz, Slovenia, August 2005.

ABSTRACT

The objective of the study was to develop copper based anti-inflammatory agents for alleviation of inflammation associated with RA.

Four copper chelating agents, N^1-(2-aminoethyl)-N^2-(pyridin-2-ylmethyl)ethane-1,2-diamine [555-N], *N*-(2-(2-aminoethylamino)ethyl)picolinamide [H(555)-N], *N,N'*-(2,2'-azanediylbis(ethane-2,1-diyl))dipicolinamide [H_2(5555)-N] and 2-amino-N-(2-oxo-2-(2-(pyridine-2-yl)ethylamino)ethyl) acetamide [H_2(556)-N], were synthesized, and their formation constants with Cu(II), Zn(II), Ca(II) and Ni(II) investigated potentiometrically at 25 °C and 0.15 mol dm^{-3} Na^+Cl^-. The order of stability of the species formed by the copper-ligand system under physiological conditions was found to be [555-N] > [H(555)-N] > [H_2(556)-N] > [H_2(5555)-N].

UV-Visible spectroscopy showed that the MLH_{-1} and MLH_{-2} species of the Cu(II)-[H(555)-N] and [H_2(556)-N] systems respectively had a square planar geometry, an outcome of the expected Jahn-Teller distortion in copper complexes. Molecular mechanics (MM) calculations based on strain energy of the solution structures gave extra experimental evidence in support of the structures postulated from both potentiometric and spectroscopic data.

This study also considered percutaneous skin absorption estimates of the Cu(II) complexes. In this regard, the octanol/water partition coefficients determined indicated an encouraging trans-dermal absorption of the species formed at physiological pH. However, the IC_{50} values recorded for the copper complexes suggest that they are poor mimics of the Cu-Zn-SOD enzyme.

Speciation modelling calculations of Cu(II) using a computer model of blood plasma indicated that [555-N] and [H(555)-N] should be able to mobilize Cu(II) *in vivo* at low ligand concentrations with no interference with the *in vivo* Zn(II) and Ca(II).

The *in vivo* verification of the modelling results was carried out through animal experiments, in which the tissue distribution of radio-active $^{64}Cu(II)$ was determined in female balb/c mice, following intravenous administration of the [^{64}Cu]Cu(II) complexes. These results indicated significant biological half life of the Cu(II) complexes using these chelating agents.

Overall, these *in vitro* and *in vivo* evaluations of the copper chelating agents have demonstrated their potential in achieving both exogenous trans-dermal administration of Cu(II), its subsequent endogenous mobilization and retention for therapeutic effect at the site of inflammation.

STRUCTURAL FORMULAE OF SOME IMPORTANT LIGANDS MENTIONED IN THIS STUDY

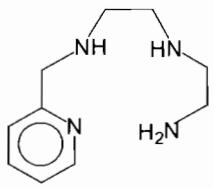

[555-N]

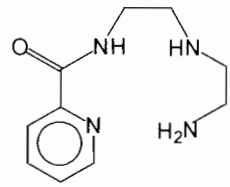

[H(555)-N]

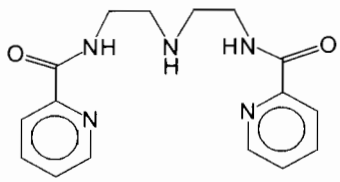

[H_2(5555)-N]

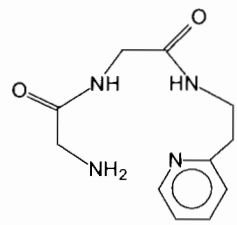

[H_2(556)-N]

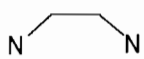

en

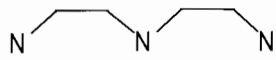

dien

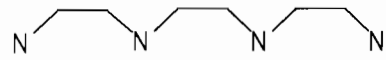

trien

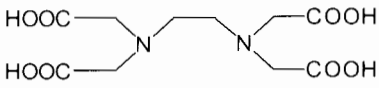

edta

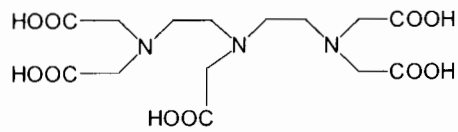

dtpa

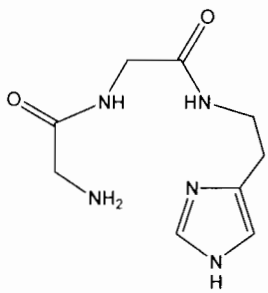

ggha

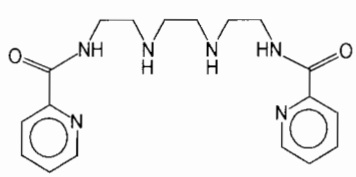

pyctrien

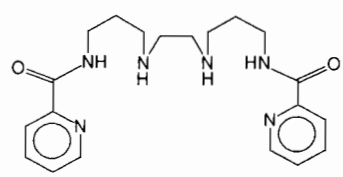

pycdpnen

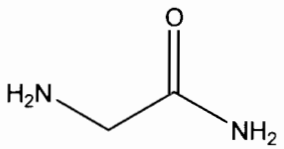

glym

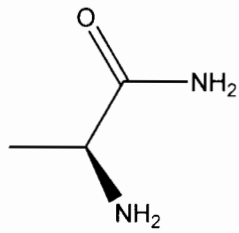

alam

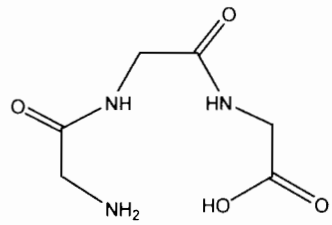

gggc

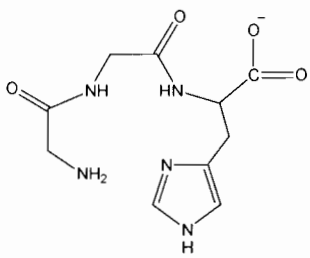

gly-gly-his

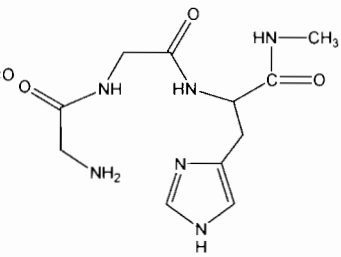

gghma

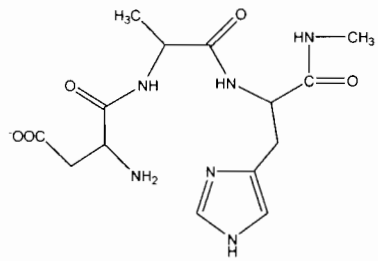

aahm

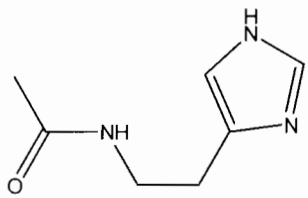

N-aha

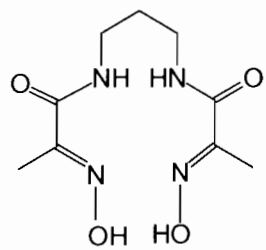

H_2pap

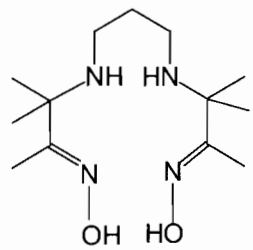

PrAO

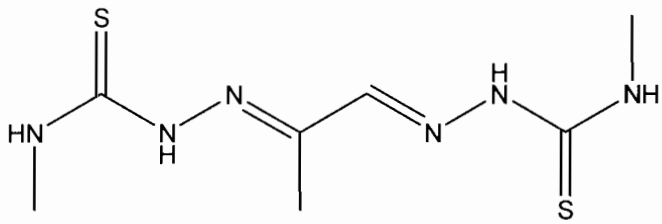

pbmtsc

LIST OF SYMBOLS

δ	-NMR chemical shift (ppm)
J	-NMR coupling constant (Hz)
Hz	-hertz
d	-doublet
t	-triplet
m	-multiplet
Log β_{pqr}	-logarithm of the overall stability constant
σ_{pqr}	-denotes standard deviation in log β_{pqr} for species pqr
T_H	-total proton concentration (mol dm^{-3})
T_H^*	-calculated total proton concentration (mol dm^{-3})
T_L	-total ligand concentration (mol dm^{-3})
T_M	-total metal concentration (mol dm^{-3})
[L]	-free ligand concentration (mol dm^{-3})
pH	-(-Log H^+)- A measure of acidity or alkalinity
K_W	-dissociation constant of water
E_{cell}	-electrode potential (volts)
E^o	-electrode response intercept (volts)
R	-universal gas constant
T	-absolute temperature (Kelvin)
F	-Faraday constant
$[H^+]$	-hydrogen ion activity
s	-electrode response slope
a_i	-activity
f_i	-activity coefficient
c_i	-concentration of i^{th} ionic species
I	-ionic strength (mol dm^{-3})
z_i	-charge of i^{th} ionic species
G	-Gibbs free energy or chemical potential (kJ mol^{-1})
G^o	-Standard Gibbs free energy (kJ mol^{-1})
U_{obj}	-Objective function
N	-total number of experimental titration points
n_p	-number of parameters being optimized

n_e	-total number of electrodes
w_{ni}	-weight of i^{th} residual at n^{th} point
y_{ni}	-electrode emf of i at n^{th} titration point
n_{bar}	-number of protons bound to ligand in the absence of complexation
R_f^H	-Hamiltonian R-factor
R_{lim}^H	-Hamiltonian R limit
Δ or 10Dq	-ligand field splitting
g	-gerade
u	-ungerade
λ_{max}	-wavelength of maximum absorption
h	-Planck's constant
c	-speed of light
I_o	-intensity of incident radiation
I	-intensity of transmitted radiation
$\in$	-molar absorptivity (extinction) coefficient
ν_{max}	-frequency of maximum absorption
V_{total}	-total strain energy
V_b	-bond deformation energy
V_θ	-angle deformation energy
V_φ	-torsion angle deformations energy
V_{nb}	-non-bonded interactions energy
k_b	-force constant
r_o	-ideal bond length
k_θ	-strength of spring holding angles at its ideal value
k_φ	-height of barrier to rotation about torsion angle
φ_{offset}	-offset of minimum energy from a staggered arrangement
IC_{50}	-concentration of drug required to reduce diformazan formation by 50 %
%ID	-percentage injected dose

mCi	-millicurie
MeV	-milli electron volt
kBq	-kilobacquerel

LIGAND ABBREVIATIONS USED

[555-N]	-N^1-(2-aminoethyl)-N^2-(pyridin-2-ylmethyl)ethane-1,2-diamine
[H(555)-N]	-*N*-(2-(2-aminoethylamino)ethyl)picolinamide
[H_2(5555)-N]	-*N,N'*-(2,2'-azanediylbis(ethane-2,1-diyl))dipicolinamide
[H_2(556)-N]	-2-amino-*N*-(2-oxo-2-(2-(pyridin-2-yl)ethylamino)ethyl) acetamide
PHEN	-1,10-phenanthroline
BPY	-2,2'-bipyridyl
en	-ethylenediamine
dien	-diethylenetriamine
trien	-triethylenetetraamine
EDTA	-ethylenediaminetetraacetic acid
DTPA	-diethylenetriaminepentaacetic acid
ggha	-glycylglycylhistamine
ala-gly-ha	alanylglycylhistamine
pyctrien	-1,8-bis(2-pyridylcarbamoyl)-3,6-diazaoctane
pycdpnen	-1,10-(2-bis picolinamide)-4,7-diazadecane
pycdado	-1,8-bis(2-picolinamide)-3,6-dioxaoctane
glym	-glycinamide
alam	-alaninamide
gggc	-glycylglycylglycine
gly-gly-his	-gly-gly-histidine
gghma	-gly-gly-his-*N*-methylamide
aahm	-asp-ala-his-*N*-methylamide
N-aha	-*N*-acetyl histamine
H_2pap	-*N,N'*-bis(2-hydroxyiminopropionyl)propane-1,3-diamine
PrAO	-3,3,9,9-tetramethyl-4,8-diazaundecane-2,10-dione dioxime
Pbmtsc	-pyruvaldehyde bis(N^4-methylthiosemicarbazone)
TTDA	-3,6,9,12-tetraazatetradecanedioate
DTDA	-3,6,9-triazaundecanedioate

OTHER ABBREVIATIONS USED

RA	-rheumatoid arthritis
NSAIDs	-nonsteroidal anti-inflammatory drugs
DMARDs	-disease-modifying anti-rheumatic drugs
GI	-gastrointestinal
CHF	-congestive heart failure
SOD	-superoxide dismutase
CP	-ceruloplasmin
HSA	-human serum albumin
CAT	-catalase
GSSH	-glutathione-peroxidase
HA	-hyaluronic acid
HSAB	-Hard and Soft Acids and Bases
BOP	-benzotriazol-1-yloxytris(dimethylamino) phosphonium hexaflourophosphate
T.M.S	-Tetramethyl silane
UV	-ultraviolet
VIS	-visible
LMCT	-Ligand to metal charge transfer
ESTA	-Equilibrium Simulation for Titration Analysis
OBJE	-task to calculate objective function
ZBAR	-task to calculate the complex formation function
Z-bar	-complex formation function
Q-bar	-deprotonation function
SPEC	-task to calculate the speciation as a function of the pH.
KHP	-potassium hydrogen phthalate
Log $P_{oct/aq}$	-logarithm of partition coefficient in octanol/water mixture
NBT	-nitroblue tetrazolium
ECCLES	-Evaluation of Constituent Concentrations in Large Equilibrium Systems
p.m.i	-plasma mobilising index
l.m.w	-low molecular weight
BFC	-bifunctional chelator

CONTENTS

CHAPTER 3 - POTENTIOMETRY

CHAPTER 4 - ANCILLARY STUDIES

LIST OF FIGURES

LIST OF TABLES

CHAPTER ONE

Introduction

1.1 Rheumatoid Arthritis: Background of the disease

Rheumatoid arthritis (RA) is a chronic, systemic and destructive inflammatory polyarticular joint disease that chiefly affects the synovial membranes of multiple joints in the body [1, 2]. It is characterized by massive synovial proliferation and subintimal infiltration of inflammatory cells, which along with angiogenesis leads to the formation of a very aggressive tissue called pannus [3, 4]. Expansion of the pannus induces bone erosion and cartilage thinning, leading to the loss of joint function with the rheumatoid pannus considered as a local tumor. Progressive degeneration of the joint occurs as a result of unrestrained inflammation, until the joint gets crippled as shown in Figure 1.1.

Figure 1.1: Chronic Rheumatoid Arthritis

The prevalence of the disease is 1 - 2 % of the general population and is found world-wide with 5% of the western world affected [5]. Females with RA outnumber males by a 3:1 margin. In adults the disease is prevalent in the age range 40 - 60 years although it can occur at any age. The cure for RA has

not yet been found, and treatment of chronic RA remains largely symptomatic [6, 7].

In most cases of RA, patients have remissions and exacerbations of the symptoms. Very few patients have complete remission of RA, so it is important that patients continue with their treatment programs prescribed by health care practitioners. The disease rarely goes away, although at times symptoms might temporarily remit.

The etiology of RA and inflammation remains unknown [8] and has been a subject of much research and debate over the years [9, 10, 11]. Metabolic and nutritional factors, the endocrine system, geographic, psychologic, and occupational data have been extensively studied with no conclusive findings [1]. While inflammation may be a normal response, chronic inflammation results in destruction of normal connective tissue due to the activities of catalytic enzymes and cytokines [10, 11, 12]. The destruction is due to the activation of the immune response, the release of hydrolytic enzymes, for instance collagenases, proteases, gelatinases, matrilysin, and subsequent degradation of collagen and other extra-cellular components found in body joints and connective tissues [13]. It now appears that an unknown antigen initiates the auto immune response resulting in RA [14]. There has been continuous suspicion of an infectious origin of the disease process, which has included various bacteria and viruses, but without evidence of precipitating events [1].

RA can affect many joints in the body. These include knee, ankle, elbow and wrist. Joints actively involved with the disease are usually tender, swollen and are likely to demonstrate reduced motion.

1.1.1 Brief Anatomy of a joint

A synovial joint consist of six basic components [15], and these are; joint capsule, joint cavity, synovial membrane (synovium), synovial fluid, bones coming together to form joints and hyaline (articular) cartilage as shown in Figure 1.2.

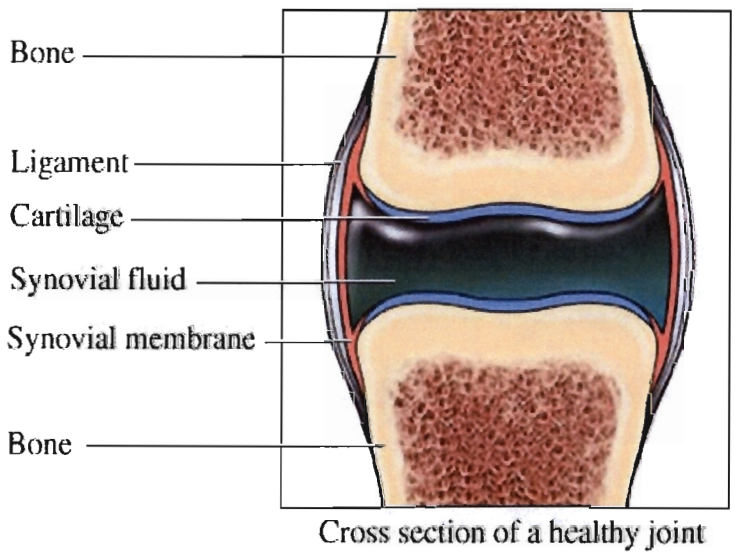

Figure 1.2: Synovial joint

A synovial capsule is composed of two layers, an outer fibrous layer and an inner synovium. The outer layer consists of many joint receptors innervating it, but it is not well vascularized. On the other hand the synovium is well vascularized, but poorly innervated. The articular cartilage has two important functions. These include ability to minimize friction and wear between two opposing joint surfaces during movement as well as to dissipate forces on the joint over a wide area, thus decreasing stresses on the contact joint surfaces. Synovial fluid contains hyaluronate (hyaluronic acid) and a glycoprotein called lubricin. These two substances are responsible for lubrication of the joint, although they have certain specific functions. Hyaluronic acid is important for the lubrication of the joint capsule while lubricin is necessary for cartilage lubrication. Synovial fluid also act as the medium by which nutrients are carried to, and wastes are carried from, the

vascular components of the joint. The ends of the long bones that form the synovial joints are composed of a soft, spongy bone called subchondral bone. Hyaline (articular) cartilage covers this bone and protects it.

Although arthritis and associated mascular skeletal diseases do not dominate the world mortality statistics, they account for substantial socioeconomic costs [16, 17, 18] and are a leading cause of long-term disability [19, 20, 21]. There are no world-wide figures on the costs of inflammation, although the medical and economic costs associated with arthritis in the USA (1992) [19], Canada (1993) [22] and Australia (1997) [16] have been estimated to be $ (US) 64.8 B, $ (CDN) 17.8 B and $ (AUS) 1 - 5 B per annum, respectively. With an ageing population the increasing impact of arthritis on public health in the USA is expected to increase to $ (US) 95 B by 2020 and affect about 22 % of the population [23].

1.2 Therapy for RA: Current status

RA is a complex systemic disease that would require complex treatment involving many aspects of the patient's life. Modern management of such ailments relies principally upon the alleviation of the symptoms with the use of non-steroidal anti-inflammatory drugs (NSAIDs) in conjunction with other non-drug treatment [6, 7]. A review by Sanz and Alboukrek [24] categorises most important agents used by rheumatologists into three categories; namely,

1. Non-steroidal anti-inflammatory drugs (NSAIDs)
2. Glucocorticosteroids
3. Disease-modifying anti-rheumatic drugs (DMARDs).

1.2.1 NSAIDs

NSAIDs are usually the first class of drugs prescribed and most commonly used because they are well tolerated by patients, and they decrease the inflammatory response of the body to disease or injury. They

include salicylates such as aspirin, the first commercially available NSAID introduced into medicine by Frederick Bayer and Company in 1889 [25], and a large number of non-salicylates which are generally weak carboxylic or enolic acid derivatives. NSAIDs have analgesic, antipyretic and anti-inflammatory properties and are thought to function by inhibition of the cyclo-oxygenase pathway of prostaglandins.

However they have little or no effect on the underlying disease and cannot prevent progression of joint destruction or organ damage. NSAIDs remain inadequate and are associated with problematic side effects. Gastropathy and renal toxicity are major side effects of NSAIDs. Specific side effects include renal insufficiency and failure [26, 27, 28], gastrointestinal (GI) ulceration, bleeding or perforation, [29, 30, 31, 32] exacerbation of hypertension and congestive heart failure (CHF) [33].

The damage to the GI mucosa by NSAIDs can occur via a number of mechanisms. These include direct topical irritation to the GI epithelium, impaired barrier properties of the mucosa, reduced gastric mucosal blood flow, interference with the repair of superficial injury and suppression of gastric prostaglandin synthesis [34], particularly inhibition of the COX iso-enzyme system [35].

1.2.2 Glucocorticosteroids

The glucocorticosteroids are potent, fast-acting, anti-inflammatory agents that include compounds such as cortisone, prednisone and dexamethasone to mention a few. They have numerous metabolic and physiological effects, affecting lympocytes, granulocytes, macrophages and cell membranes as well as inhibiting the immune system [36]. Corticosteroids are, however, not considered to have disease-remitting potential, although this has recently been questioned since protection against joint erosion has been reported [24]. Their precise method of action is yet to be determined.

The use of corticosteroids in treatment of RA has many serious side effects, especially their effect on bone and gastrointestinal tract. Other complications include glucose intolerance, increased susceptibility to infections and impaired wound healing. It is also difficult to discontinue their use once patients have developed a steroid-dependence.

1.2.3 DMARDs

DMARDs are thought to have some effect on changing the progression of RA. However DMARDs are slower acting and take long for benefits of the drug to be noted. Classes of DMARDs include anti-malarial drugs, gold compounds, penicillamine and sulfasalazine. DMARDs are however toxic and patients need to be frequently re-evaluated by their physicians. Toxicity varies from 20 % in sulfasalazine up to 60 % in penicillamine. Side effects of DMARDs include retinal toxicity, dermatitis, nausea and anaemia.

1.3 Use of copper in chemotherapy

Copper was believed to be of therapeutic value as long as 1000 years B.C. and the copper bracelet has long been used as a folk remedy for treatment of arthritis [37]. Copper devices such as bracelets, may serve as a source of copper taken into the body with cupriphores from sweat [38]. Pharmacological evidence suggests use of copper complexes to be beneficial in alleviation and treatment of RA and that these compounds have disease remitting qualities [39, 40, 41]. Sorenson, [42] have discussed the physiological basis for pharmacological activities of copper complexes as well as the anti-arthritic, anti-ulcer and analgesic activities of copper complexes.

1.3.1 Biological roles and bio-distribution of copper

Copper occurs as the metal in oxidation states (0), (I), (II) and unstable (III) is also known. In an aqueous solution copper is present mainly as the Cu(II) ion, and this depends on pH, temperature, presence of bicarbonate and sulphide, and the presence of potential complexing agents such as humic,

fulvic, amino acids, certain peptides and detergents [43]. Copper is a very important element in mammalian nutrition as well as in many enzymatic reactions. Thus it is a biologically essential metal ion. It was first shown to be essential in the 1920^{s} when anaemia was discovered to result from copper-deficient diets in animals [44]. Copper serves as a catalytic component in many enzymes. It is an important constituent of some metalloproteins [45] and enzymes such as lysyl and cytochrome oxidase [46]. The enzymes requiring copper include monoamine oxidase, for pigmentation and control of neurotransmitters and neuropeptides; lysyl oxidase, essential for maintenance of connective tissue in lungs and bones; cytochrome c oxidase, involved in oxidative metabolism, brain functioning, haem synthesis, and phospholipid synthesis; and superoxide dismutase (SOD), required for destruction of superoxide radicals [47].

Copper deficiency has been observed in malnourished children and symptoms that included anaemia, neutropenia, and bone formation disturbances, responded to copper supplimentation [48]. The daily intake of copper in humans is about 1.5 - 3.0 mg per day [46]. The body of an average healthy adult male (70 kg) contains approximately 110 mg of copper, much of which is in the skeleton (46 mg), skeletal muscle (26 mg), liver (10 mg), brain (8.8 mg) and blood (6 mg) [49]. Copper is the third most abundant transition metal element in biological systems [50]. The normal human body contains 80 - 120 mg of copper as compared with 4 - 5 g of Fe and 1.4 - 2.3 g of Zn [50].

The distribution of copper in the body is such that the brain and liver have the highest tissue levels, while lesser concentrations are found in the heart, spleen, kidneys and blood. The iris and choroid of the eye have very high copper levels [51]. Metabolic balance studies show that people with daily intakes of 2 - 5 mg of copper per day absorb 0.6 - 1.6 mg (32 %), excrete 0.5 - 1.3 mg in the bile, pass 0.1 - 0.3 mg directly into the bowel, and excrete 0.01 - 0.06 mg in the urine [47]. As these data indicate urinary excretion plays a minor role in copper clearance, and principal route of excretion is in the bile.

Table 1.1 shows normal human copper concentrations in various biological media and daily excretion levels [52].

Table 1.1: Copper concentrations in various biological fluids and daily excretion in humans.

Tissue	Humans	Daily excretion (µg)
Whole body	800 - 1300 µg L^{-1}	
Serum / plasma	800 - 1750 µg L^{-1}	
Urine	12 - 80 µg L^{-1}	30 - 70
Gastric juice	0.39 µg L^{-1}	1000
Bile	4.0 µg L^{-1}	2500
Pancreatic fluid	0.13 - 0.90 µg L^{-1}	400 - 1300
Duodenal fluid	0.17 µg L^{-1}	400 - 2200
Synovial fluid	0.2 - 0.5 µg L^{-1}	

In humans, copper absorption varies inversely with dietary copper intake [53]. Most copper absorption takes place from the stomach through to the small intestine [54], predominantly in the stomach and duodenum (acidic pH) of the GI tract. Maximum blood copper levels have been observed within 1 to 3 hours following oral administration, with about 50 % of ingested copper being absorbed [51]. The presence of zinc, iron, and molybdenum, decreases copper absorption, while high protein diets increase copper absorption [54, 55]. The low pH value of gastric juices also contribute to the freeing of copper bound to foodstuffs prior to GI absorption [54]. This is important when investigating the fate of copper complexes as anti-inflammatory agents and the development of their pharmaceutical formulations.

Copper absorbed from the GI tract is transported rapidly to blood serum and deposited in the liver bound metallothionen, where it gets released

and incorporated into ceruloplasmin (CP), a specific copper transporting protein. Thus in blood plasma, about 90 % of the copper is irreversibly bound to ceruloplasmin in a non-exchangeable form, while about 10 % is reversibly bound to serum albumin. A small amount of copper, (less than 1 %) is distributed amongst low molecular weight (l.m.w) complexes, predominantly [Cu(histidinate)(cystinate)] [56] as the exchangeable copper fraction in blood [49].

Serum albumin (SA) has been considered to facilitate the transport of trace metals between tissues and blood [57]. Albumin and CP appear to be the primary copper carrier proteins in the body. These proteins transfer a large amount of exchangeable copper in the circulatory system and release it for specific cell uptake [58]. Albumin is the major metal binding protein in the body, with about 40 µg of copper able to bind to the albumin contained in 1 ml of human plasma [58].

The Cu(II) transport site of serum albumin is one of the most extensively studied binding sites of any protein [56]. The proposed structure of the major Cu(II) binding site in HSA involves the α-NH_2 nitrogen, two peptides nitrogens, and the imidazole nitrogen of the N-terminal Asp-Ala-His residue [60, 61, 62]. Figure 1.3 shows the proposed copper binding site of Cu(II) in human serum albumin (HSA).

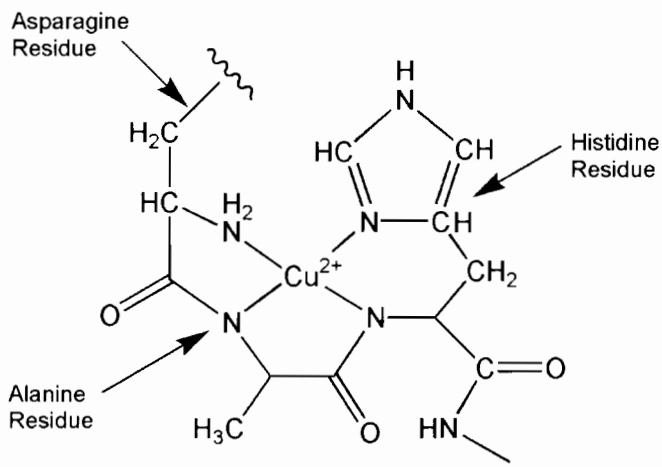

Figure 1.3: Copper binding site in HSA [52].

1.3.2 The anti-inflammatory role of copper

A potential scientific basis for the anti-inflammatory copper bracelet remedy emerged when it was shown that metallic copper can be dissolved and be absorbed through the skin [37]. Copper is believed to possess anti-inflammatory activity [41, 63]. Generally patients with RA exhibit changes in the copper distribution in the blood [36, 64]. There is an observed increase in total serum copper in arthritis sufferers compared with controls. This is observed as an increase in CP-bound copper and a decrease in albumin-bound and l.m.w copper resulting in lower levels of bio-available copper, in the blood [36, 64]. Altered copper concentrations have also been observed in the synovial fluid of RA patients [63]. The reasons for these observations are still debatable. Some researchers suggest that alterations in copper are a cause of the disease while others do believe that it is a physiological response to the disease and that copper plays an essential role in its control and treatment [36].

Whilst the roles of copper in inflammation are not yet clear, a change in its metabolism is observed in acute and chronic inflammatory conditions. In acute inflammation, there are significant increases in both total Cu(II) and CP concentrations in serum, without notable changes in the copper concentrations in the liver. Likewise, in chronic inflammation, copper serum concentrations are increased during the acute phase, with appreciably higher than normal CP levels found in the synovial fluid of patients with RA and a net accumulation of copper in inflamed areas [65]. It is proposed that there is increased demand for copper during inflammatory conditions, which is compensated for by enhanced intestinal absorption and decreased intestinal excretion of copper [65].

It has been suggested that the mode of action of anti-inflammatory drugs may involve chelation of bioactive metal ions such as Cu(II), facilitating the transfer of the metal to and from a site of inflammation or pain [39]. The beneficial role of copper in minimizing inflammation has been attributed to its redox activity, particularly the ability of copper in such enzymes as SOD to

remove the highly pro-inflammatory superoxide radical anion $O_2^{\cdot-}$ [66]. SOD has been used clinically in treatment of inflammation in animals. The dismutation [66] of $O_2^{\cdot-}$ by copper in SOD is summarized as follows;

$$Cu(II) + O_2^{\cdot-} \rightarrow Cu(I) + O_2 \quad (1.1)$$

$$Cu(I) + O_2^{\cdot-} + 2H^+ \rightarrow Cu(II) + H_2O_2 \quad (1.2)$$

$$\text{Net: } 2O_2^{\cdot-} + 2H^+ \rightarrow H_2O_2 + O_2 \quad (1.3)$$

Superoxide, generated in biological systems by the one-electron reduction of O_2 is capable of tissue damage by virtue of its ability to act as a weak base, undergoing protonation ($pK_a = 4.80$) to $HO_2^{\cdot}$ and as a one-electron reductant of oxidized metal enzymes, eg ferricytochrome c. Along with hydrogen peroxide (H_2O_2) and the hydroxyl radical ($^{\cdot}OH$), superoxide has been implicated in oxidative damage phenomena related to aging, inflammation and post-ischemic injury via reperfusion. The damaging effects of H_2O_2 in cells are minimized by its conversion to water by the enzymes catalase (CAT) and glutathione-peroxidase (GSSH) [67]. The superoxide radical, $O_2^{\cdot-}$ has also been implicated in the promotion of arthritis due to its ability to degrade hyaluronic acid (HA) [68]. HA is an important component of the synovial fluid maintaining internal joint homeostasis by acting as a lubricant. It assists with the nutrition of articular cartilage and provides direct anti-inflammatory action [69]. When $O_2^{\cdot-}$ is added to the synovial fluid, the viscosity decreases, indicating de-polymerization of HA [68]. Introduction of SOD provides complete protection against this degradation [68] by removal of potentially damaging $O_2^{\cdot-}$ from cells (Equations 1.1 - 1.3) [70].

Copper-chelating agents have been observed to exhibit significant anti-inflammatory effect [2] against inflammation associated with RA as well as SOD-mimetic activity [41]. Thus the use of SOD as a pharmaceutical has been proposed for treatment of a number of diseases. These include hyperoxia, reperfusion injury, auto-immune deficiency diseases (AIDS), ulcerative colitis, bronchopulmonary dysplasia in premature neonates, as well as inflammation and inflammation-associated diseases, such as RA [71].

However, the mechanism by which copper exhibits anti-inflammatory activity is not completely understood. There are several possible mechanisms that have been proposed for the anti-inflammatory activity of copper-chelating agents. The copper may induce lysyl oxidase activity [72], modulate prostaglandin synthesis [73, 74], induce or mimic superoxide dismutase activity [68, 75], decrease the permeability of human synovial lysosomes [76] and modulate the physiological effects of histamine [77].

Whatever the mechanism of anti-inflammatory action of copper *in vivo*, its therapeutic beneficial function has long been recognized and clinical effect investigated for a long period of time [78]. It is therefore essential to investigate the effect of copper chelating agents in improving the bioavailability of copper, and explore their possible use in copper chemotherapy as anti-arthritic agents. However the initial task in such a study would be the design and synthesis of appropriate copper-chelating agents, preferably peptide molecules [79, 80, 81, 82], in this case pseudo-mimics of the specific Cu(II)-transport site of human serum albumin [60, 83, 84, 85, 86], that would provide an ideal opportunity to study in detail the nature of coordination equilibria existing under approximated physiological conditions, and then assess their possible use as therapeutic agents in copper chemotherapy.

1.4 Aims and Objectives of the Research

The objective in designing Cu(II)-based anti-inflammatory drugs is to increase the concentration of the low molecular weight (l.m.w), membrane-penetrable, plasma fraction of Cu(II) *in vivo*. To achieve this, the ligands designed were pseudo-mimics of HSA (Figure 2.1) that could possibly compete for and mobilize endogenous reversibly bound serum albumin Cu(II). The same ligands could be used for exogenous administration of Cu(II) orally or topically as membrane-penetrable, low molecular weight complexes.

Equilibrium and solution structures of these complexes were the subject of this study on the basis of potentiometric and UV-Visible spectroscopic measurements.

The broad objectives of this study were therefore, to investigate the potential use of copper chelating pseudo-mimics of HSA as anti-inflammatory agents against inflammation associated with RA, using the following methodology;

- Design, synthesis and characterization of ligands, [555-N], [H(555)-N], [H_2(5555)-N], and [H_2(556)-N].
- Measure the formation constants of these ligands with Cu(II), Ni(II) and the most common blood plasma metal ions, Zn(II) and Ca(II) using glass electrode potentiometry. Formation constants of Zn(II) and Ca(II) will give some insight on the potency of Zn(II) and Ca(II) as abundant *in vivo* competitors. The Ni(II) solution equilibria are investigated for comparison since this metal normally forms stable complexes with ligands which coordinate strongly to Cu(II).
- Study specific structures formed between Cu(II) and these ligands in solution using UV-Visible spectroscopy.
- Use a computer model of blood plasma, together with measured formation constants, to evaluate the plasma mobilizing ability of these ligands.
- Measure partition coefficients between aqueous and organic solvents using octanol/water system, as an estimation of the dermal absorption for Cu(II) complexes of these ligands.
- Measure the S.O.D activity of Cu(II) complexes with selected ligands using a simple *in vitro* assay.
- Verify the postulated solution structures for Cu(II) complexes using molecular mechanics calculations.
- Perform animal experiments so as to determine the tissue distribution and *in vivo* stability of the most promising complexes.

References

1. Schumacher H.R. Jr, (1993), Primer on the Rheumatic Diseases, 10th ed. Arthritis Foundation, Atlanta, Georgia.
2. Omoto A., Kawahito Y., Prudovsky I., Tobouchi Y., Kimura M., Ishino H., Wada M., Yoshida M., Kohno M., Yoshimura R., Yoshikawa T., Sano H., (2005), *Arthritis Res. & Therapy*, **7**, R1174.
3. Feldmann M., Brennan F.M., Maini R.N., (1996), *Cell*, **85**, 307.
4. Koch A.E., (1998), *Arthritis Rheum.* **41**, 951.
5. McCarty D.J., (ed.), (1989), Arthritis and Allied Conditions. 11th ed., Lea and Febiger, Philadelphia London.
6. Felson D.T, Lawrence R.C., Hochberg M.C, McAlindon T., Dieppe P.A., Minor M.A., Blair S.N., Berman B.M., Fries J.F., Weinberger M., Lorig K.R., Jacobs J.J, Goldberg V., (2000), *Ann. Int. Med.*, **133**, 726.
7. Blackburn W.D., (1996), *Am. J. Med.*, **100**, 24.
8. Rafter G.W., (1982), *Medical Hypothesis*, **9**, 437.
9. Arrigoni-Martelli E., (1985), *Int. J. Tissue React.*, **7**, 513.
10. Bonta T.L., Thompson J., Brune K., (1977) (eds.) Inflammation: Mechanisms and their Impact on Therapy, Birkhauser Verlag, Basel.
11. Vane J.R., Ferreira S.H., (1978) (Eds.), Inflammation, vol. 1 & 2, Springer-Verlag, Berlin.
12. Maiotti M., Monteleone G., Tarantino U., Fasciglione G.F., Marini S., Coletta M., (2000), *Arthroscopy,* **16**, 522.
13. Song X.Y., Zeng L., Jin W.W., Thompson J., Mizel D.E., Lei K.J., Billinghurst R.C., Poole A.R., Wahl S.M., (1999), *J. Exp. Med.,* **190**, 535.
14. Reynolds P.G.M., (1976) Rheumatoid Arthritis, Medical News, Postgraduate Series on Rheumatism, Nov; 10.
15. http://www.duq.edu/PT/RA/BackgroundOfTheDisease.html /EffectsOnJoints.html
16. Muirden K.D., (1997), *Med. J. Aust.,* **166**, 344.

17. Yelin E., Callahan L.F., Arnett F., Dennis D., Deyo R., Felson D., Felts W., Giannini E., Helmick C., Heyse S., Hirsch R., Hochberg M., Hunder G., Lawrence R., Liang M., Pillemer S., Shulman L., Steen V., Wolfe F., (1995), *Arthritis Rheum.,* **38**, 1351.
18. de Pouvourville G., (1995), *Br. J. Rheum.,* **34**, 19.
19. Lappin D.R., (1997), Arthritis: What We know Today; National Institute of Arthritis and Mascularskeletal and skin Diseases. http://www.elitehealthshop.com/Articles/ArthritisFacts-Mythis.htm.
20. Gordon E., (1999), In: House of Commons Hansard (UK), http://www.parliament.the-stationery-office.co.uk/cgi-bin/empower.
21. Ryall C., (1998), In: Facts, Figures and Estimated Costs of Arthritis; British Society for Rheumatology. http://www.rheumatology.org.uk/noframes/general/facts.htm.
22. Canadian Arthritis Network, (1999), http://can.klickit.com/content.cfm?page=/info_exchange_disease_arthritis
23. Elders M.J., (2000), *J. Rheumatol.,* **27**, 6.
24. Sanz I., Alboukrek D., (1991) In: Rheumatoid Arthritis. M. Fischbach (ed.), Churchill Livingstone, New York Edinburgh.
25. Goodman L.S, Gilman A., (1975), (Eds), The Pharmacological Basis of Therapeutics, 5th ed., Mcmillan, New York, pg. 1704.
26. Alexopoulos E., (1998), *Renal Failure,* **20**, 809.
27. Rodriquez F., Llinas M.T., Gonzalez J.D., Rivera J., Salazar J., (2000), *Hypertension,* **36**, 276.
28. Komhoff M., Wang J.L., Cheng H.F., Langenbach R., Mckanna J.A., Harris R.C., Breyer M.D., (2000), *Kidney Int.,* **57**, 414.
29. Ares J.J., Outt P.E., (1998), *Curr. Pharm. Des.,* **4**, 17.
30. Hernandez-Diaz S., Rodriquez L.A.G., (2000), *Arch. Int. Med.*, **160**, 2093.
31. Schoenfeld P., Kimmey M.B., Scheiman J., Bjorkman D., Laine L., (1999), *Aliment. Pharmacol. Ther.,* **13**, 1273.
32. Holvoet J., Terriere L., Van Hee W., Verbist L., Fierens E., Hautekeete M.L., (1991), *Gut,* **32**, 730.
33. Page J., Henry D., (2000), *Arch. Int. Med.*, **160**, 777.

34. Kuwano S., Tsuji S., (2000), *J. Gastroenterol. Hepatol.*, **15**, D1.
35. Frölich J.C., (1997), *Trends Pharmacol. Sci.*, **18**, 30.
36. Bonta I.L., Parnham M.J., Vincent J.E., Bragt P.C., (1980), In: G.P. Ellis, G.P. West (Eds.) Progress in Medicinal Chemistry, North Holland Biomedical Press, North Holland, pg. 185.
37. Walker W.R., Keats D.M., (1976), *Agents Action,* **6/4**, 454.
38. Fernandez-Madrid, (1989), In: R. Milanino, K.D. Rainsford, G.P. Velo (Eds.) Copper and Zinc in Inflammation, Kluwer Academic Publishers, Dordrecht, pg. 49.
39. Sorenson J.R.J., (1976), *J. Med.Chem.*, **19**, 135.
40. Sorenson J.RJ. (1982), In: Metal Ions in Biological Systems, 14 H. Sigel (ed) Marcel Decker, New York.
41. Sorenson J.R.J., (1984), *Chem. in Britain*, **19**, 1110.
42. Sorenson J.R.J. (1987), In: J.R.J. Sorenson (Ed.) Biology of Copper Complexes, Humana Press, Clifton, New Jersey, pg. 3.
43. Stiff M.J., (1971), *Water Res.*, **5**, 585.
44. Hart E.B., Steenbock H., Waddell J., Elvehjem C.A., (1928), *J. Biol. Chem.*, **77**, 777.
45. Sun W.H., Tsuji M., Gunawan E.S, Sawaoka H., Kawai N., Lijima H., Kimura A., Kakiuchi Y., Yasumaru M., Sasaki Y., Kawano S., Hori H., (2000), *J. Gastroenterol. Hepatol.*, **15**, 752.
46. Cox D.W., (1999), *Br. Med. Bull.*, **55**, 544.
47. Davies G.K., Mertz W., (1987) In: Trace elements in human and animal nutrition. Vol. 1. 5th ed. W. Mertz (ed.) Academic Press, New York, NY.
48. Hambidge K.M., Nicholas B.F., Jr (ed.), (1978) Zinc and Copper in clinical medicine. Spectrum Press, New York, NY.
49. Linder M.C., Hazegh-Azam M., (1996), *Am. J. Clin. Nutr.*, **63**, S 797.
50. Hathaway B.J., (1987), Comprehensive Coordination Chemistry. The Synthesis, Reactivity, Properties & Application of coordination compounds. Vol 5, Pergamon Press, Oxford pg. 634.
51. U.S Environmental Protection Agency, (1980), Ambient Water Quality for copper. Public. No. PB81-117475. Office of Water Regulations and Standards, Criteria and Standards Deviation Washington, DC.

52. Weder J.E., Dillon C.T., Hambley T.W., Kennedy B.J., Lay P.A., Biffin J.R., Regtop H.L., Davies N.M., (2002), *Coord. Chem. Reviews*, **232**, 105.
53. Turnlund J.R., Keyes W.R., Peiffer G.L., Scott K.C., (1998), *Am. J. Clin. Nutr.*, **67**, 1219.
54. Wapnir R.A., (1998), *Am. J. Clin. Nutr.*, **67**, S 1054.
55. Lonnerdal B., (1996), *Am. J. Clin. Nutr.*, **63**, 821.
56. May P.M., Linder P.W., Williams D.R., (1977), *J. Chem. Soc. Dalton Trans.*, 588.
57. Bearn A.G., Kunkel H.G., (1954), *Proc. Soc. Exp. Biol.*, **85**, 44.
58. Linder M.C., Wooten L., Cerveza P., Cotton S., Shulze R., Lomeli N. (1998), *Am. J. Clin. Nutr.*, **67**, 965.
59. Laussac J., Sarkar B., (1971), *J. Biol. Chem.*, **246**, 5040.
60. Peters T., Jr. Blumenstock F.A., (1967), *J. Biol. Chem.*, **242**, 1574.
61. Neumann P.Z., Sass-Kortsak A.J., (1967), *J. Clin. Invest.*, **46**, 646.
62. Sarkar B., Wigfield Y., (1968), *Can. J. Biochem.*, **46**, 601.
63. Sorenson J.R.J., (1989), *Prog. Med. Chem.*, **26**, 437.
64. Freeman P.C., O'Callaghan P.O., (1987), *Br. J. Pharmacol.*, **90**, 49 P.
65. Milanini R., Mauro U., Marrella M., Pasqualiccio M., Gasperini R., Velo G., (1995), In: G. Berthon (Ed.), Handbook of Metal-Ligand Interactions in Biological Fluids, Marcel Derker, New York, pg. 886.
66. Grisham M.B., Jourd'Heuil D., Wink D.A., (1999), *Am. J. Physiol.*, **276**, G 315.
67. Aruoma O.I., (1998), *J. Am. Oil Chem. Soc.*, **75**, 199.
68. McCord J.M., (1974), *Science* (Washington D.C), **185**, 529.
69. Netter P., Bannwarth B., Royer-Morrot M.J., (1989), *Clin. Pharmacokinet.* **17**, 145.
70. Auer D.E., Ng J.C., Seawright A.A., (1990), *J. Vet. Pharmacol. Ther.*, **13**, 59.
71. Henke S.L., (1999), *Expert Opin. Ther. Pat.* **9**, 169.
72. Harris E.D., (1976), *Proc. Natl. Acad. Sci.*, USA, **73,** 371.
73. Boyle E., Freeman P.C., Goudie A.C., Megan F.R., Thomson M. J., (1976) *Pharm. Pharmacol.*, **28**, 865.

74. Vargaftig B.B, Trainer Y., Chignard M., (1975), *Euro. J. Pharmacol.*, **33**, 19.

75. Huber W., Menander-Huber K.B., In: Huskisson E. (Ed.) (1980), Clinics in Rheumatic Diseases: Anti-Rheumatic Drugs, vol. 2 Saunders, London, pp. 465 ff.

76. Chayen J., Bitensky L., Butcher R.G., Poulter L.W., (1969), *Nature*, **222**, 281.

77. Sorenson J.R., (1978), In: Ellis G.P., West G.P., (Eds.) Progress in Medicinal Chemistry, vol. 15 Elsevier, Amsterdam, pp. 211.

78. Sorenson J.R.J., (1995), Handbook of Metal-Ligand Interactions in Biological Fluids, vol 2, 1st ed., Marcel Decker, New York, pg. 1318.

79. Sarkar B., (1972), *Proc. Can. Fed. Biol. Soc.*, **15**, 659.

80. Sarkar B., (1973), *Proc. Int. Congr. Biochem.*, **9**, 122.

81. Sarkar B., Kruck T.P.A., Lau S., (1973), *Proc. Int. Conf. Coord. Chem.*, **15**, 472.

82. Lau S., Kruck T.P.A., Sarkar B., (1974), *J. Biol. Chem.*, **249**, 5878.

83. Bradshaw R.A., Peters T. Jr., (1969), *J. Biol. Chem.*, **244**, 5582.

84. Shearer W.T., Bradshaw R.A., Gurd F.R.N., Peters T. Jr., (1967), *Biol. Chem.*, **242**, 5451.

85. Breslow E., (1964), *J. Biol. Chem.*, **239**, 2352.

86. Bradshaw R.A., Shearer W.T., Gurd F.R.N., (1968), *J. Biol. Chem.*, **243**, 3817.

CHAPTER TWO

Ligand design and synthesis

2.1 Ligand design

2.1.1 Introduction

The design of the copper-chelating agents (ligands) for the alleviation of inflammation associated with RA was based upon two important assumptions [1]. The therapeutic activity depends upon increasing the total labile Cu(II) concentration in some body compartments other than plasma and only neutral complexes will pass through a membrane separating these compartments whereas charged complexes generally do not, in the absence of a specific uptake pathway.

The two ways by which Cu(II) concentration can be increased at the site of inflammation are summarized in the scheme below;

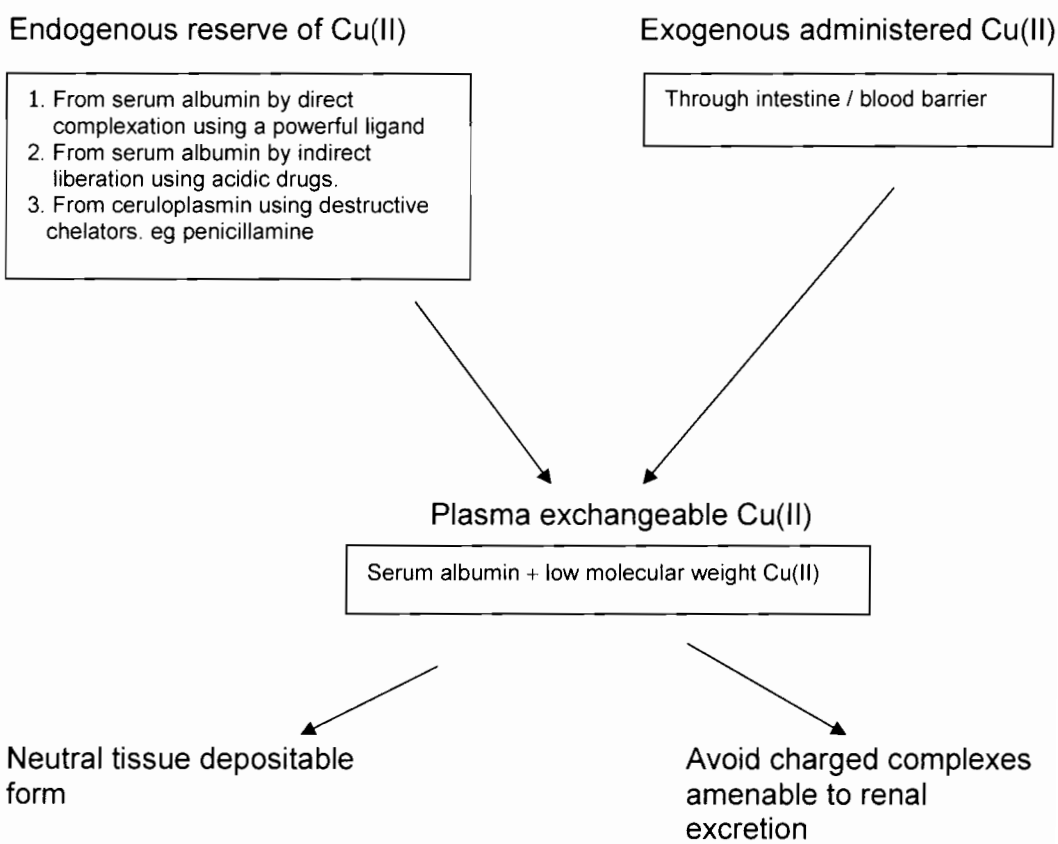

Scheme 2.1

2.1.2 Design strategy

Clearly the strength of the complex formation will be the predominant factor in the designing strategy. Very strong or kinetically inert complexes which persist from the intestine through plasma to the tissue have been proposed. However, this idea is not attractive since such complexes would be unlikely to yield Cu(II) ions to the biological mechanism that requires Cu(II). Alternatively, weakly bonded complexes which would release the metal ion to proteins and amino acids in plasma can be chosen. The design of the ligands in this instance should be focused upon its role in enhancing Cu(II) absorption from the intestine. The concentration of all labile Cu(II) complexes in plasma will thus be elevated although the percentage distribution of endogenous and added Cu(II) amongst the l.m.w will remain essentially constant. As a result, the overall concentration of the neutral Cu(II) complexes normally present will be increased.

A third alternative is to design a ligand which will not only increase absorption of exogenous copper but will also take advantage of the large pool of endogenous copper bonded to serum albumin. Ligands in this category would have to be powerful enough to compete with serum albumin but not so powerful that they promote copper excretion.

There are desirable features required for a ligand for RA therapy which exploits Cu(II) bound to serum albumin. Powerful Cu(II) complexing properties are reflected in a high plasma mobilizing index (p.m.i), defined as the ability to move metal from a protein bound form to a low-molecular weight form. This can be best achieved by designing a multidentate ligand with the structural characteristics that makes it effective to mobilize Cu(II) *in vivo*. More details about p.m.i will be discussed in chapter 5. In general the ability of organic chelates to mobilize Cu(II) has been shown [2] to be affected by size of the chelate rings formed upon co-ordination, donor atoms, number of donor atoms and anionic groups.

Multidentate ligands generally lead to complexation in which chelate rings are formed. Chelate rings are associated with enhanced stability compared to that of similar complexes involving monodentate binding. This is known as the chelate effect, first defined by Schwarzenbach [3] and is one of the oldest known phenomena in chemistry. This phenomenon defines that ligands containing two or more donor groups in such an arrangement that they are able to form five or six-membered rings on coordinating to the metal ion yield complexes with substantially larger formation constants than those of the analogous complexes of corresponding monodentate ligands. The chelate effect is observed in Cu(II) complexes of ethylenediamine, $[Cu(en)_2]^{2+}$ which is about 10^7 times more stable than $[Cu(NH_3)_4]$ [4]. The increase in the number of chelate rings enhances stability. The simplest explanation for the increased stability of chelate complexes is the entropy increase associated with their formation [5, 6].

It is a well-known fact of coordination chemistry that an increase in the size of the chelate ring above 5 usually leads to a drop in complex stability. This observation was originally modelled [3] in terms of entropy effects associated with the longer connecting link between the donor atoms of ligands that form six-membered as opposed to five-membered chelate rings. However, the available evidence [7] show that such a drop in complex stability, associated with increases in the size of the chelate ring, are almost entirely due to favourable enthalpy contributions as seen in the thermodynamics of complex formation of ethylenediamine and propylenediamine complexes or of trimethylenediaminetetraacetic acid and ethylenediaminetetraacetic acid. Cu(II) complexes of ligands which give rise to a 5,6,5 membered chelate system are generally more stable than their 5,5,5 chelate analogues. This is due to steric constraints of the three contiguous, small rings in the latter. However, systems in which the 5,5,5 chelate complex is more stable than the 5,6,5 complex have been reported in literature [8].

Ligands that have predominantly nitrogenous donor groups confer a high degree of selectivity towards Cu(II) upon such chelating agents. Other

cations, in particular Ca(II) and Zn(II), can drastically interfere with a ligand designed to bind Cu(II) *in vivo*, particularly if predominantly oxygen donor groups are present. According to HSAB principles, the "soft" nitrogen and sulphur donor atoms are selective for a number of the "borderline" +2 metal ions, Fe(II), Ni(II), Cu(II) and Zn(II). However Cu(II) shows remarkable ability to form bonds at pH ≈ 7.00 to peptide and amide nitrogen atoms in their ionized state, giving it a selectivity factor of Cu(II)/Zn(II) of about 10 000 [9]. Sulphur could be considered an alternative donor atom in the ligand system but it is preferred by the softer Cu(I) ion. Moreover, thiol groups bring about reductive chelation of Cu(II) and are known to be toxic. Since we wish to form a neutral Cu(II) complex, the ligand has to contain two anionic groups or dissociable protons. Ligands containing amide groups where amide hydrogen atoms dissociate on complexation have been preferred in this study because they are reasonable models of peptide bonds of proteins. More over, upon loss of amide protons, such ligands can coordinate to a metal ion via four nitrogen atoms, giving rise to three chelate rings.

Although the imine nitrogen of the imidazole ring is possibly the most basic heterocyclic nitrogen atom known, having a pk_a of 6.95 [10], Jackson and Kelly [2] have reported that ligands containing an imidazole residue are not particularly good at mobilizing Cu(II) *in vivo*. This is rather surprising in view of the wide biological involvement of histidine as a chelating agent. Thus, best mobilization of Cu(II) has been reported [2] when ligands form a 5,6,5 and 5,5,5 membered ring systems and comparison of donor atom basicity on Cu(II) mobilization has been observed to follow the order amino > py > 4-Im > 2-Im > An.

Although the unsaturated nitrogen donor pyridine is a stronger base than any of the saturated nitrogen donors in the gaseous phase, it is a weaker base than the saturated nitrogen donors in aqueous solution [11]. Thus, the order of basicity of nitrogen donors in an aqueous solution can be stated as follows; amino > imidazole > pyridine. However the unsaturated nitrogen donor is sp^2 hybridized, which leads to greater character in the orbitals used

for bonding to the metal ion and hence more covalent bonding. Thus ligands where such hetero-atomic donors are present can exert very high ligand field strengths, even though their proton basicity may be significantly less than that of the sp^3-hybridised saturated nitrogen donors. The low proton basicity of the unsaturated nitrogen donors can be of considerable use in designing ligands, since what ultimately counts in many situations is not the formation constant of the metal ion with the ligand alone but also the relative difficulty of removing protons from the donor groups of the ligand so as to permit complex formation.

Unsaturated donors such as the pyridyl or imidazole group also have the ability to impart rigidity to the ligand system, due to the rigidity of aromatic ring systems. For instance, the ligand 1,10-phenanthroline (PHEN) forms a complex that is 1.1 log units more stable than that formed by BIPY (2,2'-bipyridyl) with Cu(II). This effect is due to the fact that the PHEN is more effectively pre-organized for coordination relative to BPY. The BPY is highly strained while this problem is overcome by fusion of two rings in PHEN. Thus, this idea of pre-organization [12] is of considerable importance in ligand design.

Part of the effort to design ligands that will complex metal ions more strongly is the design of more sterically efficient chelating agents, and the idea is to increase selectivity of the ligand for one metal ion over others by making them sterically efficient with that metal ion only. The choice of the ligands structures in this study has been driven by the desire to design Cu(II) chelating agents that are pseudo-mimics of the Cu(II) binding site *in vivo*, particularly those of human serum albumin (HSA). The target ligands have also been designed to facilitate trans-dermal transport of exogenous Cu(II) and subsequent mobilization of endogenous Cu(II). The interest in HSA pseudo-mimics is due to their biological significance as models of the peptide bonds of proteins [13] in peptide-metal binding.

It was therefore decided to investigate a series of tetradentate copper-chelating agents, incorporating ionizable amide nitrogen donor atom in order

to achieve the desired Cu(II) ion selectivity. The dissociation of the amide protons would enable formation of the required electrically neutral species with some of the chelating agents while incorporation of the hydrophobic pyridyl groups would hopefully result in the formation of less hydrophilic complexes particularly for charged copper complexes. Previously, other workers have reported [14] neutral but hydrophilic Cu(II) complexes to suffer undesirable renal filtration in the urine of laboratory animals. In light of the structural factors considered, the bulky (three) of the ligands of choice have been unsymmetrical tetra-dentate compounds which are only investigated rarely [15, 16], and these are given in Figure 2.1 below. This series of ligands varies generally in the number of ionizable amide nitrogen atoms present, and this has the effect of changing the overall charge of the complex formed. The effect of the number of ionizable amide nitrogen atoms to complex formation can therefore also be established.

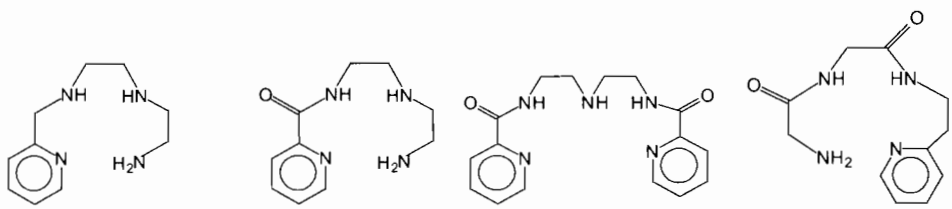

[555-N] [H(555)-N] [H_2(5555)-N] [H_2(556)-N]

Figure 2.1: Ligands studied

2.1.3 Ligand requirements

The above ligands have been carefully designed to achieve successful metal ion administration and subsequent mobilization in the body fluids. Thus their choice has been carried out so as to fulfil the following general requirements;

- strong chelation with formation of thermodynamically stable complexes with Cu(II) under physiological conditions of temperature and pH, minimizing loss to competing serum proteins.

- formation of kinetically labile complexes so as to give up the metal ion at the biologically active site.
- selectivity for metal ion of interest so that other *in vivo* metal ions essential for correct body function are not disturbed.
- formation of uncharged lipophilic complexes to enable transport across cell membranes and prevent loss via urinary excretion. Thus the chelating agents [H_2(5555)-N] and [H_2(556)-N] have been designed to form neutral complexes while [H(555)-N] is capable of forming a single charged species. More Hydrophobic complexes are essential since hydrophilic complexes have been reported [14] to be rapidly excreted in the urine of laboratory animals despite their electrical neutrality. The inclusion of hydrophobic pyridyl rings in these ligands would hopefully result in formation of less hydrophilic complexes capable of significant skin permeation without much renal excretion.

2.2 Synthesis

2.2.1 Introduction

The use of the di-tert-butyl dicarbonate (N-tert-butoxycarbonyl) as a protecting group in organic synthesis is well known [17] and this method has been widely used [18, 19, 20, 21] in literature for protecting amines. From a practical point of view, selective protection of one end of an amine, for instance, ethylenediamine, is difficult and this would involve use of excess amine so as to increase the yield of the mono-protected amine. However the separation of the mono and di-protected amines is a relatively easy task achieved by either extraction or chromatography.

This approach of amine protection was unsuccessful and so manipulation of starting material ratios approach was adopted. Such an approach has been used successfully by other workers [22] for related compounds. The synthesis of each ligand was followed by a complete characterization procedure using standard physical techniques, including

nuclear magnetic resonance (n.m.r), microanalysis, acid-base titration and melting points determination.

2.2.1.1 Preparation of N^1-(2-aminoethyl)-N^2-(pyridin-2-ylmethyl) ethane-1,2-diamine, [555-N]

N^1-(2-aminoethyl)-N^2-(pyridin-2-ylmethyl)ethane-1,2-diamine, was synthesised by reacting a mixture of diethylenetriamine (25 ml; 229.1 mmol) and sodium carbonate (2.218 g; 20.9 mmol) dissolved in ethanol, with 2-(chloromethyl) pyridine hydrochloride (3.500 g; 20.9 mmol). The 2-(chloromethyl) pyridine hydrochloride was dissolved in ethanol and added dropwise over 2 hours at reflux temperature of 90 - 100 °C. The resulting mixture was then refluxed for at least 21 hours under nitrogen. After reflux, excess solvent was removed under reduced pressure and the resulting solution suspended in sodium hydroxide solution (2 M). Extraction by dichloromethane (4 x 50 ml) then followed and the combined extract dried over anhydrous potassium carbonate. The resultant sample was then purified by column chromatography using silica as a stationary phase and a methanol-dichloromethane (1:4) mobile phase system. The purified sample was regenerated as a hydrochloride by bubbling dry HCl gas into the sample dissolved in ethanol. The resultant salt was filtered and dried under vacuo. The structure of the compound was confirmed by n.m.r spectroscopy and the purity checked by elemental microanalysis (C, H, N), acid-base titration and melting point determination.

(Yield ca. 21 %, m.p 195 - 200 °C, Purity 97.2, Found: C, 35.31; H, 6.52; N, 16.64. $C_{10}H_{18}N_4 \bullet 4HCl$ requires C, 35.31; H, 6.53; N, 16.47 %); (δ_H : δ_C 400 MHz, solvent D_2O), 7.85(d, 1H, *J* 8.0 Hz : 126.46); 7.79(t, 1H, *J* 6.8; 6.8 Hz : 144.08); 8.29(t, 1H, *J* 6.8; 8.0 Hz : 126.66); 8.70(d, 1H, *J* 4.0 Hz : 145.95); 4.55(s, 2H : 49.77); 3.54(m, 2H : 44.87); 3.54(m, 2H : 44.27); 3.47(t, 2H, *J* 3.6; 3.2 Hz : 43.58); 3.39(t, 2H, *J* 5.2; 2.0 Hz : 35.60).

2.2.1.2 Preparation of *N*-(2-(2-aminoethylamino)ethyl)picolinamide, [H(555)-N] and *N,N'*-(2,2'-azanediylbis(ethane-2,1-diyl)) dipicolinamide, [H_2(5555)-N].

As the preparation of [H(555)-N] and [H_2(5555)-N] is similar and both are formed from the same reaction mixture, the details of one method will be given. *N*-(2-(2-aminoethylamino)ethyl)picolinamide, and *N,N'*-(2,2'-azanediylbis(ethane-2,1-diyl))dipicolinamide were synthesized by reacting diethylenetriamine (50 ml; 458.2 mmol) with picolinic acid (5.368 g; 43.2 mmol). The picolinic acid was dissolved in pyridine (50 ml) and added drop-wise over 2 hours with stirring at reflux temperature (120 °C). The mixture was then refluxed under nitrogen for at least 36 hours at 120 °C. After reflux excess solvent was removed under diminished pressure resulting in brownish-yellow oil. The oil was then distilled under reduced pressure to remove the excess diethylenetriamine and this generated blood-red oil. The resulting oil sample was purified by column chromatography using silica as stationary phase and a methanol-dichloromethane (1:4) mobile phase system. [H_2(5555)-N] eluted first and [H(555)-N] second during the chromatographic process. After removal of the eluting mobile phase under reduced pressure each oil sample was taken up in ethanol and dry HCl gas bubbled into each sample generating a hydrochloride of each compound. The solid hydrochloride was filtered under suction, washed with methanol three times and then dried under vacuo. The structure of the compound was confirmed by n.m.r spectroscopy and the purity checked by elemental microanalysis (C, H, N), acid-base titration and melting point determination.

[H(555)-N], (Yield ca. 37 %, m.p 181 - 185 °C, Purity 98.0, Found: C, 34.82; H, 6.20; N, 15.79. $C_{10}H_{16}N_4O \bullet 3HCl \bullet 1.5H_2O$ requires C, 34.85; H, 5.99; N, 15.82 %); (δ_H : δ_C 400 MHz, solvent D_2O), 8.41(d, 1 H, *J* 8.0 Hz : 129.95); 8.13(t, 1H, *J* 6.4; 6.8 Hz : 125.16); 8.62(t, 1H, *J* 8.0; 7.8 Hz : 144.04); 8.84(d, 1H, *J* 5.6 Hz : 146.98); 3.82(t, 2H, *J* 5.6; 6.9 Hz : 47.83); 3.42(m, 6H : 44.79, 36.94, 35.77).

Since [H_2(5555)-N] was obtained in lower yield during this procedure it was synthesized again using a procedure that has been used by other workers [23, 24, 25, 26] for similar bis(amides) of pyridine-2-carboxylic acid. The structure of the compound in this case was also confirmed by the same physical techniques as mentioned above.

[H_2(5555)-N], (Yield ca. 49.0 %, m.p 170 - 173 °C, Purity 98.4, Found: C, 41.93; H, 5.10; N, 15.15. $C_{16}H_{19}N_5O_2$•3HCl•2H_2O requires C, 41.89; H, 5.71; N, 15.26 %); (δ_H : δ_C 400 MHz, solvent D_2O), (- : 143.24); 8.31(d, 2 H, *J* 8.0 Hz : 129.81); 8.06(t, 2 H, *J* 6.8; 5.6 Hz : 125.02), 8.52(t, 2 H, *J* 6.8; 9.2 Hz : 144.23), 8.78(d, 2 H, *J* 5.6 Hz : 146.58), (- : 162.58), 3.81(t, 4 H, *J* 5.2; 6.4 Hz : 47.41), 3.40(t, 4 H, *J* 5.6; 3.6 Hz : 36.89).

2.2.1.3 Preparation of 2-amino-*N*-(2-oxo-2-(2-(pyridin-2-yl)ethyl amino)ethyl)acetamide, [H_2(556)-N]

2-amino-*N*-(2-oxo-2-(2-(pyridin-2-yl)ethylamino)ethyl)acetamide, [H_2(556)N] was prepared from BOC-glycylglycine and 2-(2-aminoethyl) pyridine according to a procedure used for synthesis of glycylglycylhistamine [27].

BOC-glycylglycine (1.8440 g; 7.94 mmol) and 2-(2-aminoethyl) pyridine (1.00 ml; 7.94 mmol) were dissolved in a mixture of chloroform (30 ml) and N-ethyl-diisopropylamine (6.5 ml, 27.8 mmol) with stirring. BOP (benzotriazol-1-yloxytris(dimethylamino) phosphonium hexafluorophosphate) (3.5830 g; 7.94 mmol), a coupling agent was added to the resulting solution. The mixture was then refluxed for about 12 hours continuously under nitrogen at 60 °C. Excess solvent was removed under diminished pressure resulting in a blood-red sample. This sample was then cleaned by column chromatography using a silica stationary phase and a methanol-ethyl acetate (1:4) mobile phase. The sample was taken up into ether and dry hydrochloric acid gas bubbled through for at least three hours with stirring until pH 1.00 - 2.00 which was measured by use of universal pH paper indicators. The solution mixture was

stirred again for another two hours to ensure removal of the protecting group. The de-protecting procedure generated the final product as a solid hydrochloride which was filtered and re-crystallised from a methanol-diethyl ether mixture. The structure of the compound was confirmed by n.m.r spectroscopy and the purity checked by elemental microanalysis (C, H, N) and acid-base titration. Melting point was difficult to determine because the compound was very hygroscopic.

(Yield ca. 68.0 %, m.p very hygroscopic, Purity 95.3 %, Found: C, 34.73; H, 6.73; N, 14.98. $C_{11}H_{16}N_4O_2 \bullet 2HCl \bullet 4H_2O$ requires C, 34.65; H, 6.87; N, 14.69 %); (δ_H : δ_C 400 MHz, solvent D_2O), (- : 153.85); 7.72(m, 1 H : 125.26); 8.31(t, 1 H, *J* 8.2; 7.8 Hz : 140.86); 7.72(m, 1 H : 127.90); 8.45(d, 1 H, *J* 6.0 Hz : 146.92); 3.06(t, 2 H, *J* 6.6; 6.0 Hz : 33.16); 3.46(t, 2 H, *J* 6.3; 6.6 Hz : 38.15); (- : 167.68); 3.67(s, 2H : 40.43); (- : 171.20); 3.67(s, 2H : 42.25).

2.3 Experimental

The various chemicals used in the synthesis of the ligands are listed in Table 2.1 below;

Table 2.1: Starting materials for the synthesis of the ligands

Chemical	Source	Purity	Comments
Diethylenetriamine	Aldrich	99 %	Starting materials with purity 98 % and better were used without any further purification.
2-(chloromethyl) pyridine hydrochloride	Aldrich	98 %	
Picolinic acid	Aldrich	99 %	
BOC-glycylglycine	Bachem	99 %	
2(2-aminoethyl) pyridine	Aldrich	95 %	2(2-aminoethyl) pyridine was purified by distillation under vacuum.
BOP	Fluka	98 %	
N-ethyl-diisopropyl-amine	Aldrich	99 %	

All solvents used for synthesis were analytical grade. The solvents were purified according to procedures in Vogel [28] and stored in bottles containing molecular beads before use.

^{1}H and ^{13}C n.m.r spectra were recorded on a Varian Unity Plus 400 MHz instrument. Chemical shifts were recorded in ppm with tetramethyl silane (T.M.S) (δ scale) as internal reference.

Microanalysis was carried out on a Fisons elemental analyser CHNOS, while melting points were determined on a Reichert Thermovar melting point apparatus.

References

1. Jackson G.E., May P.M., and Williams D.R., (1977), *J. Inorg. Nucl. Chem.*, **40**, 1227.
2. Jackson G.E., Kelly M.J., (1988), *Inorg. Chim. Acta*, **152**, 215.
3. Schwarzenbach G., (1952), *Helv. Chim. Acta.*, **35**, 2344.
4. Burgess J. (1988), Ions in Solution. Ellis Horwood, Chichester.
5. Spike C.G., Parry R.W., (1953), *J. Am. Chem. Soc.*, **75**, 2726.
6. Cotton A., Harris F.E., (1955), *J. Phys. Chem.*, **59**, 1203.
7. Martell A.E., Smith R.M., Critical Stabilty Constants; Plenum Press: New York; Vols. 1-6, (1974, 1975, 1976, 1977, 1982, 1989).
8. Jackson G.E., Linder P.W., Voye A., (1991), *Communication*, **10**, 8, 883.
9. Frausto da Silva J.J.R., Williams R.J.P., (1991), The Biological Chemistry of the Elements. Clarendon Press, Oxford.
10. Neckers D.C. and Doyle M.P., (1977), Organic Chemistry, John Willey & Sons, New York London Sydney Toronto.
11. Hancook R.D., Martell A.E., (1989), *Chem. Rev.* **89**, 1875.
12. Cram Donald. J., Kaneda Takahiro., Helgeson Roger. C., Brown S. Bruce., Knobler Carolyn .B., Maverick Emily., Trueblood Kenneth. N., (1985), *J. Am. Chem. Soc.*, **107**, (12), 3645.
13. Bai S.K., Martell A.E., (1969), *J. Am. Chem. Soc.*, **91**, 16, 4412.
14. Jackson G.E., and Kelly M., (1989), *J. Chem. Soc. Dalton Trans.* 2429.
15. Wallis W.N., Cummings S.C., (1974), *Inorg. Chem.*, **13**, 991.
16. Prince R.H., Slotter D.A., (1974), *Inorg. Chim. Acta*, **10**, 89.
17. Solomons T.W., (1993), Organic Chemistry, 3rd edition, John Willey & Sons, University of South Florida. pg 1042.
18. Kofoed T., Hansen H.F., Ørum H., Koch T., (2001), *J. Pept. Scie.*, **7**, 402.
19. Ragnarsson U., Grehn L., Maia H.L.S., Monteiro L. S., (2002), *J. Chem. Soc. Perkin Trans 1*, **1**, 97.
20. Thompson L.A., Ellman J.A., (1996), *Chem. Rev.*, **96**, 555.
21. Jarowicki K., Kocien'ski P., (1999), *J. Chem. Soc. Perkin Trans 1*, 1589.

22. Nonoyama K.T., (1975), *Inorg. nucl. Chem.*, **37**, 2449.

23. Barnes D.J., Chapman R.L., Vagg R.S., Watton E.C., (1978), *J. Chem. Engineer. Data*, **23**, 349.

24. Mutin Yu V., Glunskaya O.V., (1969), *Tetrahedron Lett.*, 5267.

25. Yamazaki N., Higashi F., (1972), *Tetrahedron Lett.*, 5047.

26. Yamazaki N., Higashi F., (1974), *Tetrahedron Lett.*, **30**, 1323.

27. Henry B., Gajda T., Selve C., Delpuech J.J., Arnould J.M., (1993), *Amino Acids*, **5**, 113.

28. Furniss B.S., Hannaford A.J., Smith P.W.G., Tatchell A.R., (1989), Vogel's Practical Organic Chemistry, 5th edn., Longman Scientific & Technical, pg 395.

CHAPTER THREE

Potentiometry

3. Potentiometry

3.1 Introduction

Although a large number of stability constants, also known as formation constants, have been determined in literature [1], a considerable proportion of these are of doubtful accuracy [2]. It is therefore essential that before measuring any formation constants great caution is taken to ensure that the experimental method to be used gives a reliable result. There are two major problems involved in solving complex formation equilibria [3]. These include the selection of species as well as the calculation of stability constants. The reliability of the formation constant is determined by the adequacy of the experimental method, exactness of the experimental work, consideration of all relevant equilibria, calculation method and reliability of the auxiliary data used. However the source of the greatest error is evidently the inadequacy of the experimental method applied.

Any method which can determine the concentration of at least one of the species in the equilibrium with reasonable accuracy can be used to determine the formation constant [4]. Any complexation method is only sensitive when there is a change in pH. Hence any equilibrium which does not involve a change pH cannot be measured using such a technique. In general, the applicability of any method is limited to the region where there is a change in complexation; thus if complex is fully formed or amount is negligible the equilibrium cannot be measured under those conditions.

Several analytical techniques can be used to determine formation constants [5], and these include spectroscopic, distribution, electrochemical and calorimetric methods. Potentiometry is one of the oldest analytical methods still in wide use because of its convenience and success for metal complex equilibrium measurements. It has thus been described [6] as by far the most accurate, reproducible, non-invasive and widely applicable technique currently available for the study of ionic equilibria. The applicability of potentiometry in the determination of stability constants is however possible

only when the proton displacement reaction can be monitored. The monitoring of this reaction is also possible only when the interacting ligand is a weak Bronsted-Lowry acid or base and the displacement reaction is in equilibrium.

This chapter focuses on the general theory of potentiometry as a measurement method applied to complex equilibria, presentation and discussion of experimental results.

3.1.1 Theory

Theory on formation constants and the various techniques used to determine these constants has been extensively covered in literature [2, 4, 6, 7]. In potentiometry, an electrode responding to one of the species is used to measure the species' activity or concentration, depending on the experimental conditions. When a glass electrode is used the electrode responds to hydrogen ion activity.

Considering a general metal-ligand formation equilibria involving **M**, as a metal and **L** as a ligand, the stepwise formation of parent complexes can be described by the following set of formation constants,

$$\mathbf{M} + \mathbf{L} \rightleftharpoons \mathbf{ML} \qquad \mathbf{K}_1 = \frac{[\mathbf{ML}]}{[\mathbf{M}][\mathbf{L}]} \tag{3.1}$$

$$\mathbf{ML} + \mathbf{L} \rightleftharpoons \mathbf{ML}_2 \qquad \mathbf{K}_2 = \frac{[\mathbf{ML}_2]}{[\mathbf{ML}][\mathbf{L}]} \tag{3.2}$$

$$\mathbf{ML}_{n-1} + \mathbf{HL} \rightleftharpoons \mathbf{ML}_n + \mathbf{H} \qquad \mathbf{K}_n = \frac{[\mathbf{ML}_n][\mathbf{H}]}{[\mathbf{ML}_{n-1}][\mathbf{HL}]} \tag{3.3}$$

The product of individual formation constants also give characteristic constants, called overall formation constants denoted by the symbol **β**, as given below. The charges of the species have been omitted for clarity.

$$\mathbf{M} + \mathbf{L} \rightleftharpoons \mathbf{ML} \qquad \beta_1 = \mathbf{K}_1 = \frac{[\mathbf{ML}]}{[\mathbf{M}][\mathbf{L}]} \tag{3.4}$$

$$M + 2L \rightleftharpoons ML_2 \qquad \beta_2 = K_1K_2 = \frac{[ML_2]}{[M][L]^2} \tag{3.5}$$

Therefore, $$\beta_n = K_1 \cdot K_2 \cdots K_n = \frac{[ML_n][H]}{[M][L]^n} \tag{3.6}$$

In general, $$\beta_n = \prod_{i=1}^{n} K_i \tag{3.7}$$

For a complex formation reaction occurring between a metal, **M**, and a protonated ligand, **L**, forming a complex $M_pL_qH_r$, the equilibrium process is given by the following expression,

$$pM + qL + rH \rightleftharpoons M_pL_qH_r \tag{3.8}$$

According to the law of mass action, the formation constant for $M_pL_qH_r$ is given by the following equation;

$$\beta_{pqr} = \frac{[M_pL_qH_r]}{[M]^p[L]^q[H]^r} \tag{3.9}$$

and the concentration of each species $M_pL_qH_r$ in the k^{th} point is given by

$$[M_pL_qH_r]_k = \beta_{pqr}[M]_k^p[L]_k^q[H]_k^r \tag{3.10}$$

where β_{pqr} is the formation constant of the species under consideration, $[M]_k$, $[L]_k$ and $[H]_k$ are concentrations of the free metal, free ligand and hydrogen ion, while **p**, **q** and **r** are stoichiometric coefficients for metal, ligand and proton respectively. While **r** can be any negative number, when **r** = -1, the proton is either removed from a water molecule (which in principle, is the same as coordination of a hydroxide ligand to the metal ion) or from the ligand molecule occurring only in the complex, like the peptide-NH.

The equilibrium conditions together with the mass balance conditions for the three components are given in the general case for the k^{th} point as follows;

$$T_{k,M} = [M]_k + \sum_{i=1}^{N} p\beta_{pqr}[M]_k^p[L]_k^q[H]_k^r \quad (3.11)$$

$$T_{k,L} = [L]_k + \sum_{i=1}^{N} q\beta_{pqr}[M]_k^p[L]_k^q[H]_k^r \quad (3.12)$$

$$T_{k,H} = [H]_k + \sum_{i=1}^{N} r\beta_{pqr}[M]_k^p[L]_k^q[H]_k^r \quad (3.13)$$

where $T_{k,M}$, $T_{k,L}$ and $T_{k,H}$ are the analytical concentrations of metal ion, ligand and hydrogen ion respectively. These mass balance equations are non-linear in the unknowns $[M]_k$, $[L]_k$ and β_{pqr} and the value $[H]_k$ is obtained from the potentiometric measurement. The complex $M_pL_qH_r$ may be considered to be formed by the reaction,

$$pM + qLH_n \rightleftharpoons M_pL_qH_r + (qn - r)H \quad (3.14)$$

The formation constant of this reaction denoted by ${}^{*}\beta_{pqr}$ can be transformed into β_{pqr} and vice versa with the aid of K_W, the autoprotolysis constant of water in experimental [8].

For the quantitative evaluation of data [9] the Nernst equation is used between the experimental electromotive force values **(E)** and the equilibrium hydrogen ion concentrations $[H^+]$ delivered by a glass electrode. Glass electrodes in general, are found experimentally to exhibit a Nernstian response over a wide range of concentration [10].

An electrochemical cell consisting of a test solution surrounding a glass electrode in electrical contact with a reference electrode through a salt bridge can be represented as follows [11];

first reference half-cell (in glass electrode)		second reference half-cell (external)
	test solution	
g		**l**

The measured emf of the cell is given by the following equation,

$$E_{cell} = E_r + E_l + E_g \quad (3.15)$$

where, E_r is a fixed combined potential arising from the reference electrodes, E_l is potential difference generated across boundary **l** and E_g is potential difference generated across boundary **g**. The Nernst equation is thus stated as follows;

$$E_{cell} = E_r + E_l + E_g^{\circ} + \frac{RT}{F} \ln\{H^+\} \quad (3.16)$$

where E_{cell} is measured e.m.f, E° is standard glass-electrode potential of hydrogen ions at unit activity, **R** is the universal gas constant, **T** is the absolute temperature, **F** is the Faraday constant and $\{H^+\}$ is the hydrogen ion activity. As long as the ionic strength of the test solution remains constant, the free hydrogen ion activity, $\{H^+\}$ can be expressed in terms of concentration. This is the case in practice and it conveniently allows the hydrogen ion activity to be expressed as a concentration. By putting $s = \frac{2.303RT}{F}$ and collecting all the constants together including the hydrogen-ion activity coefficient and factors arising from it as E_{const}, the Nernst equation becomes,

$$E_{cell} = E_{const} + s \log[H^+] \quad (3.17)$$

The activity of the hydrogen ion is defined with respect to concentration and the two are related by the following equation;

$$a_i = f_i c_i \quad (3.18)$$

where, f_i is the activity coefficient of ion **"i"** and c_i is the concentration of ionic species **"i"**. The departure of activity from concentration for charged species is a function of the ionic strength **I** of the solution, given by the following equation;

$$I = \frac{1}{2} \sum c_i z_i^2 \quad (3.19)$$

where c_i is the concentration of ionic species **"i"** and z_i is charge on that ion. The activity coefficient f_i, can be estimated from the ionic strength using equations developed from the Debye-Hückel theory [12]. Various relationships have been derived depending on whether ions are considered point charges in solution or are assigned certain radii for their hydrated spheres [13]. With the point-charge approximation, an assumption is that ions do not interact in solution, a reasonable approximation for $I < 0.01$, and a solvent of water at 25 ^{0}C, the Debye-Hückel limiting law can be used to estimate f_i as follows;

$$-\log f_i = 0.5 z_i^2 I^{\frac{1}{2}} \tag{3.20}$$

For solutions of higher ionic strength, the form below provides a better estimate.

$$-\log f_i = \frac{0.5 z_i^2 I^{\frac{1}{2}}}{1 + I^{\frac{1}{2}}} \tag{3.21}$$

It must be noted that only as ionic strength approaches zero, the experimentally unreachable "infinite dilution" point, is the Debye-Hückel theory rigorous, with the estimates worsening as the ionic strength increases.

The thermodynamic definition of activity is given by the following equation;

$$G = G^{\theta} + RT \ln a \tag{3.22}$$

where G is the Gibbs free energy or chemical potential of solute, G^{θ} is the value of G when the solute is in a specified standard reference state and R and T have their usual meaning as defined earlier. The conventionally chosen standard state is when the solute has unity activity, and strictly, the equation would be expressed as,

$$G = G^{\theta} + RT \ln \frac{a}{a_{ref}} \tag{3.23}$$

with a_{ref} having the value 1, and the following equation results;

$$G = G^{\theta} + RT \ln \gamma m \tag{3.24}$$

The expression (3.25) becomes more valid as solution becomes more dilute.

$$G = G^{\theta} + RT \ln m \tag{3.25}$$

3.2 Equilibrium Simulation for Titration Analysis (ESTA)

ESTA [14] is an acronym for Equilibrium Simulation for Titration Analysis. This is a computer program used for simulation of simple equilibrium distributions of chemical species and analysis of potentiometric titration. The main calculations are done by two types of program modules, namely, simulation module (**ESTA1**) and optimization module (**ESTA2**). The simulation module produces results on a point by point basis while an optimization module determine the best values based on a least squares procedure over a whole system of titrations. The other program modules are error propagation module (**ESTA3**) which performs a Monte Carlo error propagation analysis, the interactive data preparation module (**ESTA8**) providing access to an extensive on-line help facility.

In ESTA, a Gauss-Newton method is used to minimize the objective function, $\mathbf{U}_{obj}$, while the mass balance equations are solved in an iterative Newton-Raphson manner. This objective function is optimized by the task OBJE (optimization with respect to the observed emf) within the ESTA2 module. Depending on the chemical systems being investigated, like ligand, the binary and tenary systems, the functions are defined differently. They are the formation functions (Z-bar) and deprotonation function (Q-bar) calculated by tasks ZBAR and QBAR respectively within the ESTA1 module. A correct model is assumed if there is a satisfactory fit between the observed and calculated functions as well as reasonably low standard deviations in log β_{pqr}'s and Hamilton R-factor.

ESTA program library also incorporates the task SPEC within the ESTA1 module, and this calculates the distribution of species taking part in an equilibrium system as a function of pH of the solution.

3.2.1 The Objective function (U_{obj})

The objective function [15, 16] is described as the summation of all the squared residuals of the real parameter values from the calculated values. In the optimization section a Gauss-Newton least squares method is used to minimize the objective function, $\mathbf{U_{obj}}$, given by the following equation;

$$\mathbf{U_{obj}} = (\mathbf{N} - \mathbf{n_p})^{-1} \sum_{n=1}^{N} \mathbf{n_e^{-1}} \sum_{i=1}^{n_e} \mathbf{w_{ni}} (\mathbf{y_{ni}^{obs}} - \mathbf{y_{ni}^{cal}})^2 \qquad (3.26)$$

where $\mathbf{N}$ is the total number of experimental titration points, $\mathbf{n_p}$ is the number of parameters being optimised, $\mathbf{n_e}$ is the total number of electrodes (one in this study), and $\mathbf{w_{ni}}$ is the weight of $\mathbf{i^{th}}$ residual at $\mathbf{n^{th}}$ point, while $\mathbf{y_{ni}}$ is electrode emf of $\mathbf{i}$ at the $\mathbf{n^{th}}$ titration point.

The objective function assumes that the function is quadratic with respect to all the parameters, hence $\mathbf{U_{obj}}$ can be expressed as in the following equation;

$$\mathbf{U_{obj}} = \mathbf{a} + \mathbf{p^t b} + \frac{(\mathbf{p^t H p})}{2} \qquad (3.27)$$

where $\mathbf{H}$, the Hessian, is given by $\mathbf{H_{sr}} = \left\{ \frac{\partial^2 \mathbf{U_{obj}}}{\delta \mathbf{p_s} \delta \mathbf{p_r}} \right\}$

3.2.2 Formation function (Z_M-bar) and deprotonation function (Q_M-bar)

Analysis of data is achieved by extensive use of features within the ESTA suite of programs. Some of these features are fairly novel and they would need to be explained.

The complex formation function, Z_M-bar, defines the average number of ligands bound per metal ion and this is given by the following equation;

$$\mathbf{Z_M\text{-bar}} = \frac{(\mathbf{T_L} - [\mathbf{L}])}{\mathbf{T_M}} \qquad (3.28)$$

where, T_L, T_M and L are the total ligand, total metal and free ligand respectively. The Z_M-bar function applies only to mononuclear binary complexes. A plot of this function against -log [L], defined as pL gives a pictorial representation of the equilibria. If only mononuclear binary species are present in solution, then titrations performed under different conditions of concentrations and ratios of metal to ligand should give overlapping curves. Any deviation from this is an indication that there are species other than mononuclear binary complexes present.

On the other hand the deprotonation function, Q_M-bar is the average number of protons released per metal ion, as a result of complexation, and is defined according to equation (3.29). Thus,

$$\mathbf{Q_M\text{-}bar} = \frac{(T_H^* - T_H)}{T_M} \tag{3.29}$$

where T_H is total proton and T_H^* is the calculated total concentration of protons that would be necessary to give rise to the observed pH if no complexation took place, and is defined as follows;

$$T_H^* = [H^+] - [OH^-] + \sum r\beta_{0qr}[L]^q[H]^r \tag{3.30}$$

In order to evaluate T_H^* it is first necessary to solve for the free ligand concentration using equation (3.12) with p = 0.

If a formation function for a ligand subsystem is defined as follows,

$$n_{bar} = \frac{(T_H^* - [H^+] + [OH^-])}{T_L} \tag{3.31}$$

then the average number of dissociable protons in a complex would be given as in the following equation,

$$F = qn_{bar} - Q_{bar}p \tag{3.32}$$

where n_{bar} is the average number of protons which would be bound to the ligand in the absence of metal complexation, and the other terms are as defined earlier.

The selected and refined model generates a set of theoretical titration data. The agreement between the experimental plot and the theoretical plot is

an indication of the validity of the proposed chemical model, a process termed pseudo-plotting [3].

3.2.3 Standard deviations and Hamilton R-factors

The standard deviations are the errors estimated for the parameters being optimized by the method of least-squares. The standard deviations may be calculated as follows;

$$\sigma_r = \left[\frac{U \times G_{rr}}{N - n_p} \right]^{0.5} \tag{3.33}$$

where G is the reciprocal of the Hessian, $G = H^{-1}$.

An important quantity which has been used in non-linear estimation situations is the Hamilton R-factor, (R_f^H), defined in the following equation;

$$R_f^H = \left[\frac{U}{\sum n_e^{-1} \sum w_{ni} (y_{ni}^{obs})^2} \right]^{\frac{1}{2}} \tag{3.34}$$

This is compared with its limit (R_{lim}^H), calculated from the following expression;

$$R_{lim}^H = \left[\frac{N}{\sum n_e^{-1} \sum w_{ni} (y_{ni}^{obs})^2} \right]^{\frac{1}{2}} \tag{3.35}$$

where the symbols have their usual meaning as outlined in section 3.2.1. R_{lim}^H is the lowest possible R value based on the error in the analytical data and number of variables. The closer R_f^H is to R_{lim}^H the better the fit between the experimental and theoretical data. Because of the analytical errors, a value of $R_f^H < R_{lim}^H$ is not statistically significant.

3.3 Results and Discussion

The protonation constants for H^+-L equilibria were evaluated in the pH range 2.00 - 11.00 where the ligands were found to take up one to three protons. In order to examine the experimental data, the protonation curves of the ligands and species distribution graphs have been calculated, and the results presented in Figures 3.1 - 3.4 below. Protonation constants for the four ligands [555-N], [H(555)-N], [H_2(5555)-N] and [H_2(556)-N] are given in Table 3.1, as log β_{0qr}.

3.3.1 H^+-[555-N] system

Figure 3.1(a) shows the average number of protons on [555-N], Z_H-bar, as a function of pH.

There is an inflection in the curve at pH 6.50, Z_H-bar = 2.0, and then the curve rises to 3.0. This indicates that there are 3 dissociable protons in the ligand, and that pK_{a1} is very different from pK_{a2} and pK_{a3} which are very similar.

The excellent agreement between the theoretical (solid lines) and experimental (symbols) curves in Figure 3.1(a) at different total ligand concentrations as well as low standard deviations in log β_{0qr} and Hamilton R factors lends confidence to the model. The calculated speciation diagrams of [555-N] (Figure 3.1(b)), confirms that the di-protonated species, [555-N]H_2^{2+} dominates in the pH range 5.30 - 6.80.

Figure 3.1: (a) Experimental ($[L]_T = 1.2\times10^{-3}$ (□), 6.0×10^{-4} (◇) *mol dm* $^{-3}$) and theoretical (line) protonation curves and (b) calculated species distribution curves for the $[555\text{-}N]H^{n+}$ system plotted as a function of pH.

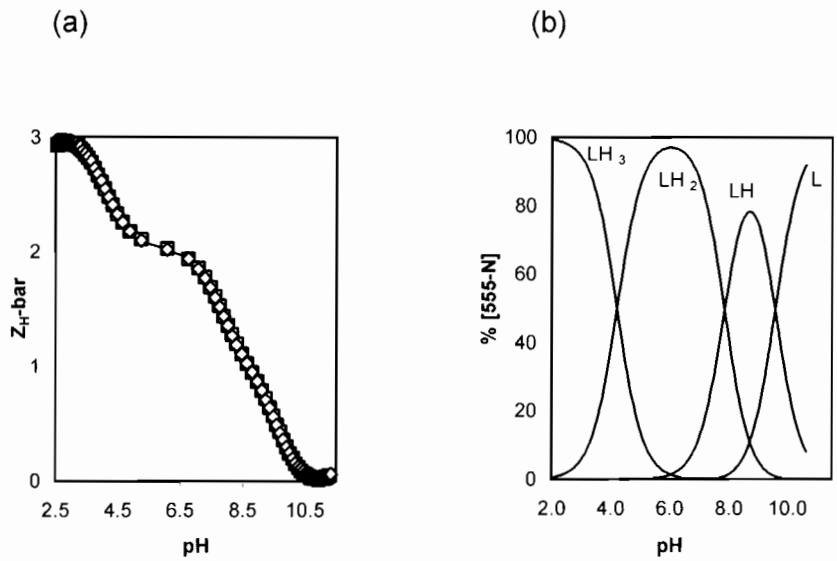

3.3.2 H^+-[H(555)-N] system

The Z_H-bar function given in Figure 3.2(a) represent variation of the mean number of protons bound to the ligand for [H(555)-N] as a function of pH. Like [555-N], at high pH (pH > 10.50) the function levels off at zero indicating that the last proton is lost at this pH. Below pH 5.00 the function rises and levels off at a Z_H-bar value of 2.0, indicating that two protons have been added to the ligand making it di-protonated at low pH. Thus [H(555)-N] exhibits two measurable acid dissociation constants and these have been determined in this study. The plateau at Z_H-bar value of 1.0 in the pH range 7.10 - 8.90 indicates that the mono-protonated species of [H(555)-N], ($[H(555)\text{-}N]H^+$) is the dominating species at physiological pH.

Figure 3.2: (a) Experimental ($[L]_T=1.8\times10^{-3}$ (□), 9.0×10^{-4} (◇) *mol dm* $^{-3}$) and theoretical (line) protonation curves and (b) calculated species distribution curves for the $[H(555)\text{-}N]H^{n+}$ system plotted as a function of pH.

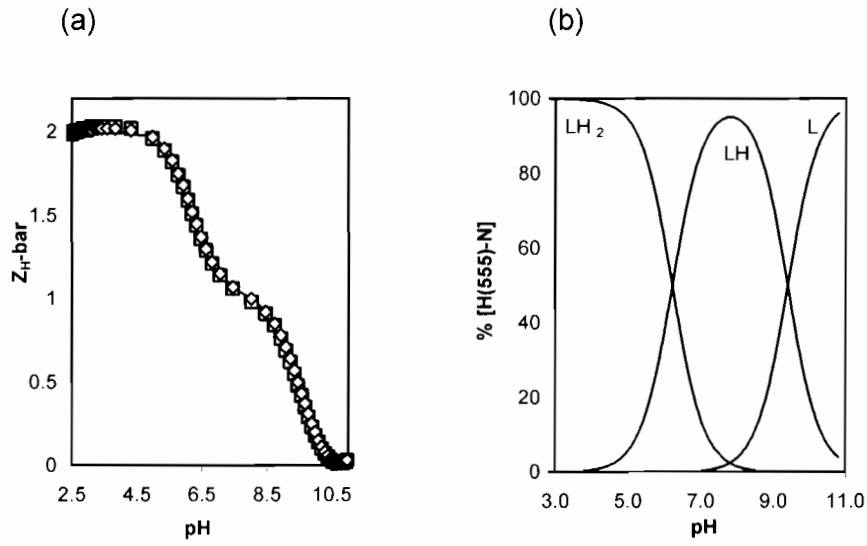

The agreement between the theoretical (solid lines) and experimental (symbols) data in Figure 3.2(a) at different total ligand concentrations is good and this lends confidence to the model. The calculated speciation diagrams of [H(555)-N] (Figure 3.2(b)), confirms that the species $[H(555)\text{-}N]H^+$ dominates in the pH range 7.10 - 8.90. If neutral ligand is denoted by [H(555)-N], then the species [H(555)-N], $[H(555)\text{-}N]H^+$ and $[H(555)\text{-}N]H_2^{2+}$ are predominant at pH > 10.00, between pH 7.10 and 8.90 and below pH 5.00 respectively, in aqueous solution of this ligand.

3.3.3 H^+-$[H_2(5555)\text{-}N]$ system

Figure 3.3(a) indicates that $[H_2(5555)\text{-}N]$ contains one measurable protonation site as revealed by the levelling off of the Z_H-bar function at 1.0.

Figure 3.3: (a) Experimental ($[L]_T=2.0\times10^{-3}$ (□), 1.0×10^{-3} (◇) *mol dm* $^{-3}$) and theoretical (line) protonation curves and (b) calculated species distribution curves for the $[H_2(5555)\text{-}N]H^{n+}$ system plotted as a function of pH.

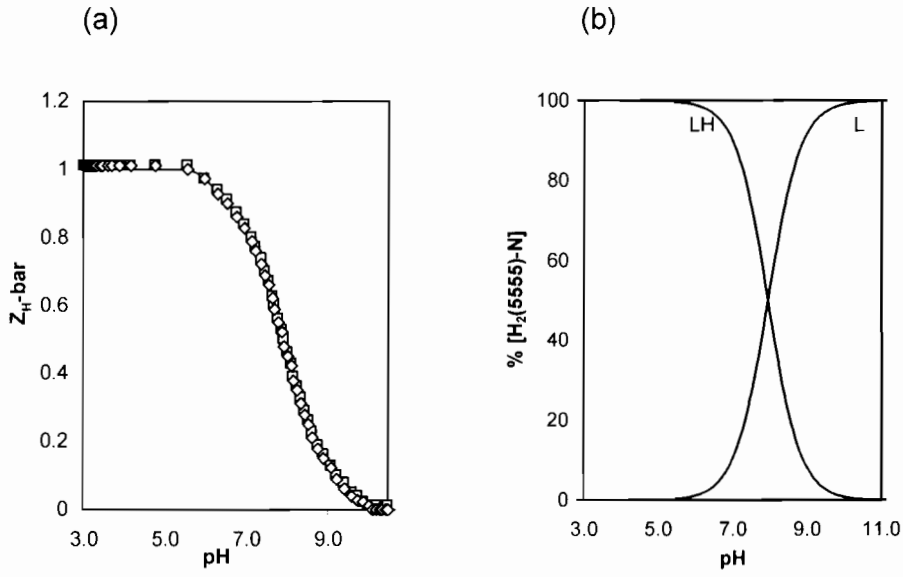

The function levels to zero at a high pH of 10.00, indicating that the single proton has been lost at this pH. Below pH of 5.50 the function levels off at a Z_H-bar value of 1.0, indicating that one proton was added to the ligand, resulting in a mono-protonated ligand at low pH. This is the single protonation constant that has been determined for $[H_2(5555)\text{-}N]$. The species $[H_2(5555)\text{-}N]$ and $[H_2(5555)\text{-}N]H^+$ are predominant above and below pH 7.90 respectively in aqueous solution of the ligand. These two species are also confirmed by the calculated species distribution diagram in Figure 3.3(b). An excellent agreement between theoretical and experimental functions supports the $[H_2(5555)\text{-}N]$ protonation model.

3.3.4 H^+-$[H_2(556)\text{-}N]$ system

rises and levels off at 2.0 indicating that just like [H(555)-N], [H_2(556)-N] also has two measurable acid dissociation constants.

Figure 3.4: (a) Experimental ($[L]_T$=1.1×10^{-3} (□), 5.2×10^{-4} (◇) *mol dm*$^{-3}$) and theoretical (line) protonation curves and (b) calculated species distribution curves for the [H_2(556)-N]H^{n+} system plotted as a function of pH.

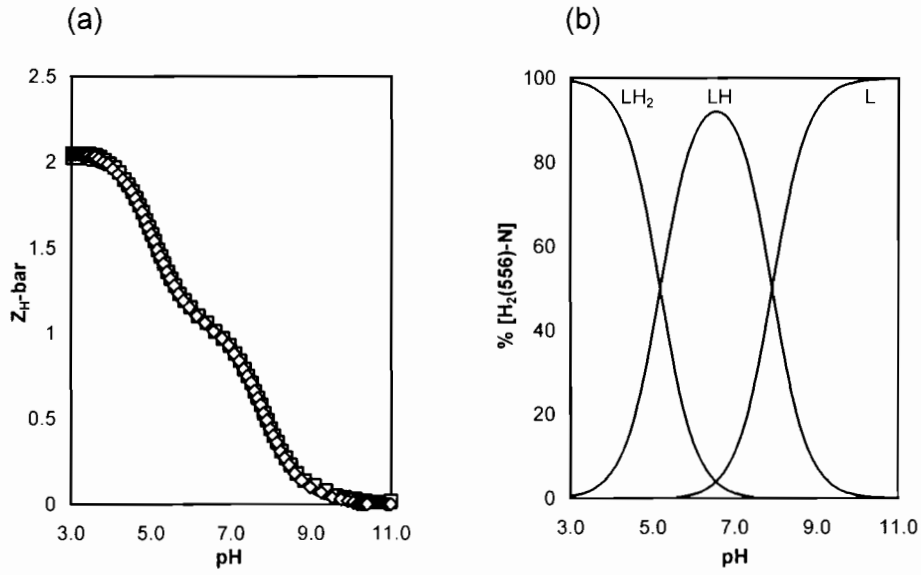

At high pH (pH > 9.50) the curve levels off at zero. This indicates that the last proton is lost at this pH. Below a pH of 4.00 the curve levels off at 2.0, indicating that two protons have been added to the ligand, making it di-protonated at low pH. These two protonation constants have been determined for [H_2(556)-N] in this study. The speciation diagrams (Figure 3.4(b)) confirm that [H_2(556)-N]H^+ dominates in the pH range 6.00 - 7.50.

The superimposability of theoretical and experimental Z_H-bar curves at different [H_2(556)-N] concentrations confirms the validity of the proposed protonation model.

Table 3.1: Log β_{pqr} 's of [555-N], [H(555)-N], [H_2(5555)-N] and [H_2(556)-N] determined at 25 °C and I = 0.15 *mol dm*$^{-3}$ NaCl. σ_{pqr} denotes the standard deviation in log β_{pqr}; R_f^H is the Hamiltonian R-factor and R_{lim}^H is its limit, n_T and n_P are the number of titrations and points respectively. The general formula of a complex is $M_pL_qH_r$ denoted by the stoichiometric coefficients p q r where p = 0.

L	p q r	log β_{pqr}	σ_{pqr}	R_f^H	R_{lim}^H	n_T (n_P)
[555-N]	0 1 1 0 1 2 0 1 3	9.573 17.480 21.642	0.003 0.004 0.005	0.004	0.009	4 (340)
[H(555)-N]	0 1 1 0 1 2	9.404 15.627	0.004 0.005	0.004	0.009	3(315)
[H_2(5555)-N]	0 1 1	7.940	0.009	0.020	0.012	3 (279)
[H_2(556)-N]	0 1 1 0 1 2	7.910 13.091	0.004 0.005	0.007	0.011	3(453)

3.3.5 Protonation constants

Results presented in Table 3.1 show that protonation constants were measurable for all the available amines except for the pyridyl and amide nitrogens. The pyridyl nitrogens are acidic and amide nitrogens are very basic and their protonation occurs outside the reliable pH range of our glass electrode. Several workers [17, 18, 19, 20] have estimated the pK_a value of the amide hydrogen to be ~15 which is outside the upper pH limit of our measurements. In fact, the deprotonation of the amide protons can only be facilitated by the presence of a metal ion such as Cu(II) [21]. However failure to measure the protonation constants for the pyridyl nitrogens in [H(555)-N] and [H_2(5555)-N] is at variance with what has been reported in literature [22]. Protonation constants for similar pyridyl nitrogens ($pK_{py,1}$ and $pK_{py,2}$) in potentially hexadentate N_6 and N_4O_2 ligands have been reported (Table 3.2).

pyridyl nitrogen in [H_2(556)-N] (pK_{py} = 5.81) with an ethylenic group adjacent to the pyridyl nitrogen. In this case the inductive effects seem to override the expected base-weakening effect of two CONH-groups [23] present in [H_2(556)-N].

Table 3.2: Protonation constants (pK_{py} values) for pyridyl nitrogens in ligands with different side chains (R); I = 1 mol dm^{-3} (KNO_3); 20 °C.

Ligand	R	pK_{py} $pK_{py,1}$	$pK_{py,2}$	Reference
pyctrien	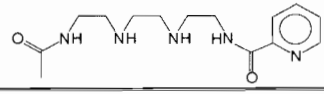	1.60	2.19	21
pycdpnen	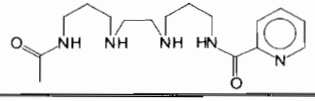	1.87	2.35	22
pycdado	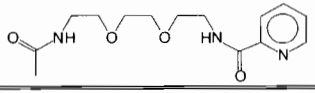	1.73	2.57	22
[555-N]	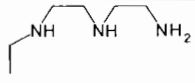	-		This work
[H(555)-N]	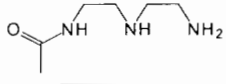	-		This work
[H_2(5555)-N]	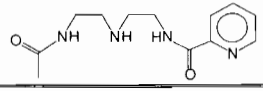	-	-	This work
[H_2(556)-N]	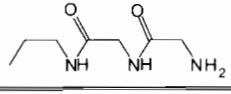	5.18		This work

Note that $pK_{py,1}$ and $pK_{py,2}$ in this Table refer to protonation constant(s) of pyridyl nitrogen(s) in a ligand system.

However electronic repulsion effects or strong coulombic interactions seem to be responsible for the pyridyl nitrogen acidity in [555-N] with a

and second protonation constant is large (from 7.91 to 4.16) because the third proton is also subjected to a great deal of coulombic charge. The fourth protonation constant would be extremely small, and a very high proton concentration would be required for protonation. The protonation constant of pyridyl nitrogen in 2-methylpicoline [24] reduces by half from log β_{011} = 5.95 to 2.73 in N-2-picolylethylenediamine [25] under the same conditions, clearly illustrating the role of electronic repulsion as the charge on the ligand increases from a single charged species to a doubly charged species. Thus it would be expected for the pyridyl protonation constant in [555-N] to decrease further when an extra amine is present resulting in a triply charged species.

The protonation constants for all the four ligands show low standard deviations while their Hamilton R-factors which are either close or smaller than their corresponding limits indicate the correctness or validity of the protonation model. For these four ligands the log β_{011} value is similar for [555-N] and [H(555)-N] (9.573; 9.404) as well as for [H_2(5555)-N] and [H_2(556)-N] (7.940; 7.910), but decreases from [555-N] to [H_2(556)-N] (9.573; 9.404; 7.940; 7.910). The log β_{011} value decreases as the number of amidic groups are introduced in a particular ligand. This result is in complete accordance with the base-weakening effect of the CONH-group [23].

The value of log β_{011} for [555-N] (9.573) and [H(555)-N] (9.404) are reasonably close to each other differing by only 0.2 log units whereas values for log β_{012} (17.480; 15.627) are much further apart, differing by 1.8 log units. This suggests that the secondary nitrogen donor atoms are protonated during the first stage of the protonation process in [555-N] and [H(555)-N], while the primary nitrogen atoms are protonated in the second protonation step (Scheme 3.1). Secondary nitrogen donor atoms are more basic sites in these two systems due to inductive effects of two ethylene groups as opposed to one ethylene for the primary amine. In this case the inductive effects override

protonation of diethylenetriaminepentaacetic acid (DTPA) [26]. The fact that there is a significant difference between the log β_{012} values in the two systems is due to increased repulsion between ligand and proton indicating that the proton is being added to a nitrogen adjacent to an already protonated nitrogen in [H(555)-N]. In [555-N] $pK_{a,1}$ is significantly lower than $pK_{a,2}$ whereas $pK_{a,2}$ is closer to $pK_{a,3}$. This is expected on the basis of both statistical factors [27] and electronic repulsion between the hydrogen ion and the protonated ligand. Proton addition to the second and third amine of an already protonated ligand is difficult compared to protonation of the neutral ligand. The protonation mechanism in [555-N] (Scheme 3.1) and [H(555)-N] is consistent with the gas-phase pattern where prediction is based on inductive effects rather than changes in solvation as is usually the case in aqueous solution [28, 29].

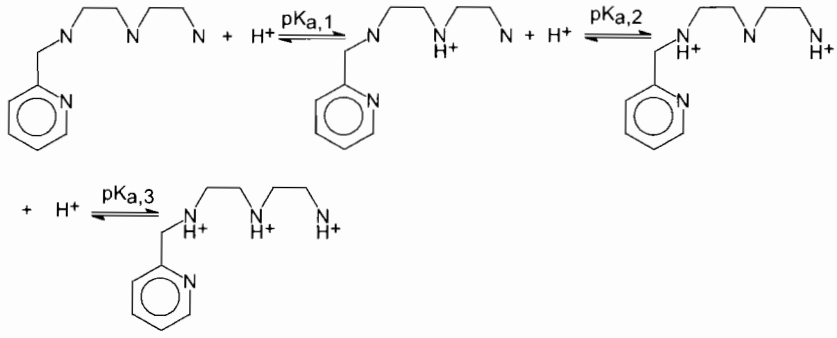

Scheme 3.1: Proposed protonation mechanism for [555-N].

The fact that $pK_{a,1}$ value is significantly lower than $pK_{a,2}$ indicates that the protonation stages in [555-N] involves non-equivalent nitrogen atoms, a secondary and a primary amine respectively. Thus for [555-N], a $pK_{a,3}$ value of 9.573 is assigned to protonation of a seconadry amino group while a $pK_{a,2}$ value of 7.907 is assigned to equilibrium involving protonation of a secondary and primary amine with $pK_{a,1}$ value of 4.162 assigned to protonation of a secondary amine in a doubly protonated ligand. In the case of [H(555)-N] log β_{011} ($pK_{a,2}$) value of 9.404 is assigned to protonation of the secondary amino

5.181 corresponding to the subsequent protonation of the pyridyl nitrogen in the pyridine ring.

The amino groups of [H(555)-N] which are protonated in the pH range 2.00 -11.00 are observed to be less basic than the nitrogen donor atoms of 1,2-diaminoethane ($pK_{a,1}$ = 7.08; $pK_{a,2}$ = 9.89) [30], while the amino groups of [555-N] are observed to be less basic than the nitrogen donor atoms of diethylenetriamine ($pK_{a,1}$ = 4.23; $pK_{a,2}$ = 9.02; $pK_{a,3}$ = 9.84) [30]. This decrease in basicity is expected as a result of steric hindrance and solvation effects, which seem to override the positive inductive effect of the carbon chain in these ligands. For [H(555)-N], the base weakening effect has also been attributed to the electron-withdrawing properties of the amide CONH-group [23]. However the basicity of the amino group in [H_2(556)-N] compares well with that of glycylglycylglycine ($pK_{a,1}$ = 7.89), a related peptide [31]. Reduced basicity in the pyridyl nitrogen of [H_2(556)-N] as compared to that in 2-ethyl pyridine ($pK_{a,1}$ = 6.07) can also be attributed to the electron-withdrawing properties of the two CONH-groups present in the ligand.

3.4 Complexation formation and deprotonation functions

Two functions [11, 15, 32], which are derived from the experimental data and are quantitatively related to the log β_{pqr} 's were used to investigate the reproducibility of the experimental data and the reliability of evaluated β_{pqr} values. The complex formation function, Z_M-bar, measures the average number of ligands bound per metal ion due to complexation. This function is plotted against the negative logarithm of the free ligand concentration (pL).

On the other hand the deprotonation function, Q-bar, indicates the average number of protons released due to complexation and is plotted against the pH of the solution. Q-bar is evaluated in conjunction with the n-bar

These two functions serve two purposes. Firstly they give one a visual check on the experimental data and secondly their shape gives one an idea of the speciation model applicable to the systems. If the Z_M-bar curves at different metal to ligand ratios are superimposable then simple stepwise complexation is indicated. Non superimposability indicates polynuclear species are present. Fanning back of Z_M-bar curves indicates the presence of hydroxo and/or mixed hydroxo species [33].

3.4.1 Cu-L systems

3.4.1.1 [555-N]

Theoretically, the complex formation function is only defined for simple, stepwise complexation. Ideally, this function should rise and level off towards a Z_M-bar limiting value of 1.0 for mononuclear ML species formation indicating the presence of ML as a major species. This was observed to be the case for the Cu(II)-[555-N] system as shown in Figure 3.5(a) and it is independent of component ratios and concentrations, suggesting a complex stoichiometry of 1:1. As the titration continues, the curves rise steeply and fan back indicating the formation of hydroxo and/or mixed-hydroxo complex species. de Witt et al. [34] have reported a similar phenomenon for related ligands.

The deprotonation function in Figure 3.5(b) shows that at the start of the titration, at a pH of approximately 2.00, Q-bar is greater than zero indicating that complexation has already commenced. The function then increases rapidly in the pH range 2.00 - 3.50 to a maximum value of 2.7 indicating the release of approximately three protons due to complex formation. The n-bar curve shows that at pH 3.50 there are essentially three protons to be displaced from the ligand while Q-bar indicates that at this pH these protons have already been displaced by the metal ion, ie an ML species has been formed.

Figure 3.5: Experimental (1:2 (◇), 1:3(o) and 1:4 (□)) and theoretical (line) (a) formation and (b) deprotonation curves for the Cu(II)-[555-N] system.

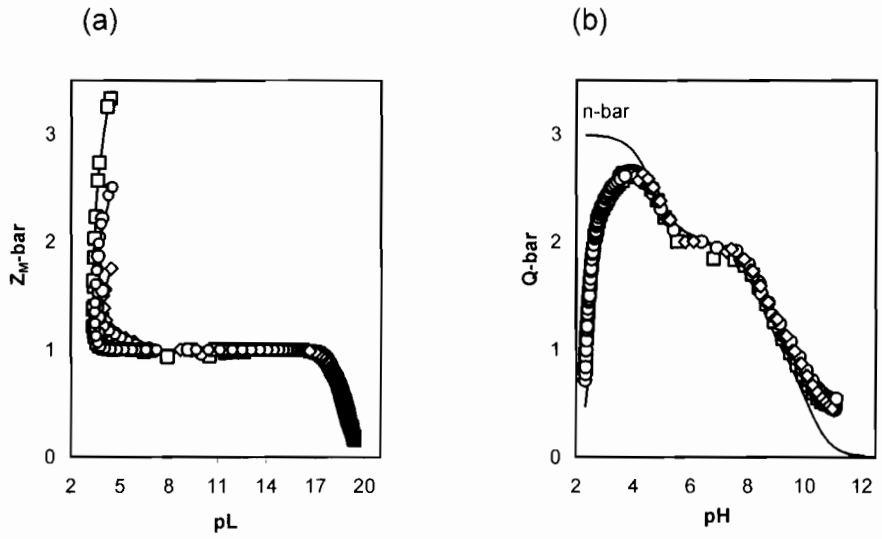

Between pH 4.00 - 10.50 Q-bar coincides with the n-bar indicating that no further complexation takes place in this pH range. At pH > 10.50 Q-bar curve rises above the n-bar curve, which indicates hydrolysis of the metal ion forming an MLH_{-1} species for this Cu(II)-[(555)-N] system.

The metal-ligand formation constants obtained by analysis of the potentiometric data using the ESTA suite of programs [14, 15, 16] are given in Table 3.3. Several different possible species were tried in the model selection, but they were rejected by the optimization process.

Table 3.3: Log β_{pqr} 's of [555-N], [H(555)-N], [H_2(5555)-N] and [H_2(556)-N] with Cu(II), Ni(II), Ca(II) and Zn(II) determined at 25 °C and **I** = 0.15 *mol dm*$^{-3}$ NaCl. The other symbols have their usual meaning as defined in Table 3.1.

L	Metal ion	p q r	log β_{pqr}	σ_{pqr}	R_f^H	R_{lim}^H	n_T (n_p)
[555-N]	Cu(II)	1 1 0	18.620	0.076	0.009	0.009	8 (569)
		1 1 -1	7.967	0.079			
	Ni(II)	1 1 1	20.622	0.153	0.033	0.010	9 (994)
		1 1 0	17.204	0.155			
		1 1 -1	9.384	0.156			
	Ca(II)	1 1 1	12.980	0.031	0.013	0.010	6 (786)
		1 1 0	3.923	0.028			
		1 1 -1	-7.165	0.036			
	Zn(II)	1 1 1	16.629	0.008	0.007	0.010	6 (906)
		1 1 0	11.513	0.007			
		1 1 -1	2.493	0.012			
[H(555)-N]	Cu(II)	1 1 0	11.513	0.018	0.009	0.009	6 (778)
		1 1 -1	7.978	0.010			
	Ni(II)	1 1 0	6.981	0.042	0.016	0.012	6 (906)
		1 1 -1	1.951	0.010			
		1 1 -2	-9.327	0.026			
	Ca(II)	1 1 1	12.351	0.013	0.008	0.010	6 (966)
		1 1 0	3.245	0.012			
		1 1 -1	-8.026	0.017			
	Zn(II)	1 1 0	5.546	0.021	0.0127	0.013	6 (886)
		1 1 -1	-1.000	0.008			
		1 1 -2	-10.364	0.011			
		1 1 -3	-22.242	0.045			
[H_2(5555)-N]	Cu(II)	1 1 -1	2.832	0.015	0.025	0.009	8 (808)
		1 1 -2	-5.929	0.022			
	Ni(II)	1 1 0	5.008	0.015	0.015	0.012	6 (906)
		1 1 -1	-1.485	0.014			
		1 1 -2	-8.199	0.012			
	Zn(II)	1 1 0	3.987	0.031	0.018	0.011	6 (906)
		1 1 -1	-3.524	0.023			
		1 1 -2	-11.521	0.016			
		1 1 -3	-22.809	0.031			
[H_2(556)-N]	Cu(II)	1 1 0	5.848	0.009	0.011	0.027	6(906)
		1 1 -2	-4.094	0.004			
		1 1 -3	-12.593	0.030			
	Ni(II)	1 1 1	10.907	0.018	0.022	0.022	6 (906)
		1 1 0	4.404	0.016			
		1 1 -2	-10.157	0.019			
		1 1 -3	-18.094	0.037			

The calculated formation constants in Table 3.3 have reasonably low standard deviations and Hamilton R^H-factors indicating that the model is a good description of the equilibria occurring in solution. The agreement between the theoretical and experimental formation and deprotonation functions as well as the reproducibility of repeat titrations at different metal: ligand ratios also lends confidence to the model.

3.4.1.2 [H(555)-N]

Unlike the Cu(II)-[555-N] system, the Z_M-bar for the Cu(II)-[H(555)-N] system shown in Figure 3.6(a) levels off at 1.5. This indicates that ML is not the predominant species in solution. In fact the predominant species in this system is an MLH_{-1} as confirmed by the species distribution graph for this system shown in Figure 3.7(b). This species reaches 100 % formation at pH 6.00 while an ML reaches 38.8 % formation at pH 3.50. For higher metal to ligand ratios the curves fan back to indicate the loss of an amide proton upon metal ion coordination [35, 36, 37].

Figure 3.6: Experimental (1:2 (◇), 1:3(o) and 1:4 (□)) and theoretical (line) (a) formation and (b) deprotonation curves for the Cu(II)-[H(555)-N] system.

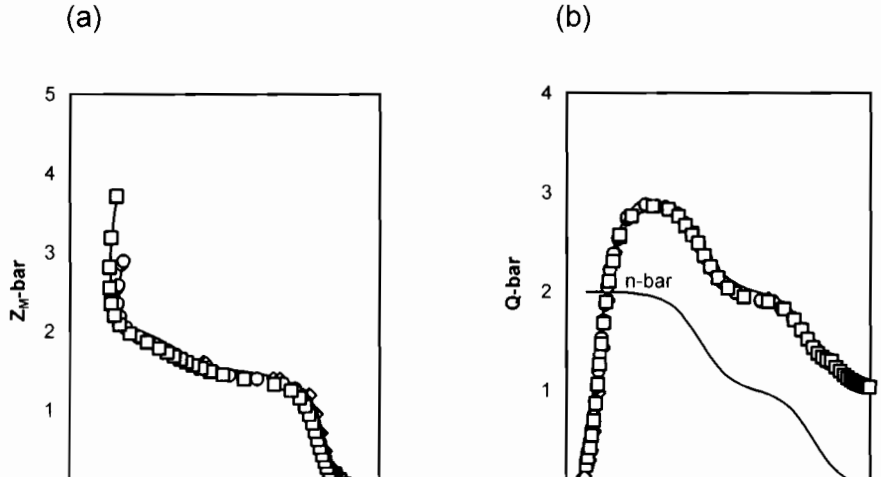

As can be seen, the deprotonation function Q-bar rapidly moves up to intersect the protonation curve n-bar at pH of 3.60, reaching a maximum value of about 2.9 indicating the release of approximately three protons due to complex formation at pH 4.90. Since at this pH the ligand only has two protons (n-bar = 2), the MLH_{-1} species must be formed. From pH 4.90 onwards the Q-bar curves run parallel to the protonation curve indicating no further detectable complexation takes place. At pH 10.50 the Q-bar level off at a value of 1.0.

Figure 3.7: Calculated speciation of (a) Cu(II) (1.1×10^{-3} *mol dm*$^{-3}$)-[(555)-N] (1.2×10^{-3} *mol dm*$^{-3}$) and (b) Cu(II) (4.1×10^{-4} *mol dm*$^{-3}$)-[H(555)-N] (1.8×10^{-3} *mol dm*$^{-3}$) systems as a function of pH.

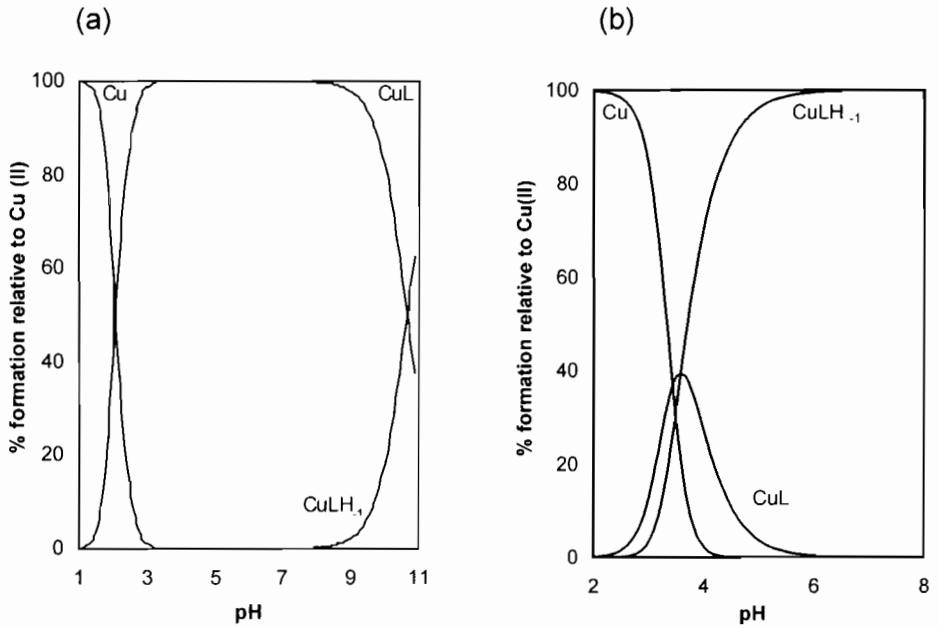

The calculated species distribution graph given in Figure 3.7(a) indicates the presence of an ML mononuclear species as the predominant species reaching 100 % formation in the pH range 3.00 - 9.00 for the Cu(II)-[555-N] system. A noticeable feature about the speciation diagrams is the significant reduction in the amount of ML species for the Cu(II)-[H(555)-N] system compared to ML for the Cu(II)-[555-N] system as the amide groups are introduced into the ligand. This suggests that the base weakening effect of

the CONH-group in [H(555)-N] plays a role in determining the coordination ability of donor atoms in this ligand system.

The analysis of the potentiometric data by ESTA suite of programs for the Cu(II)-[H(555)-N system, as shown in Figure 3.6, generates theoretical and experimental formation and deprotonation functions with excellent agreement and reproducibility of repeat titrations at different metal to ligand ratios. Moreover the calculated formation constants for this system given in Table 3.3 have very low standard deviations and Hamilton R^H-factors. This lends confidence to the model selected.

3.4.1.3 [H_2(556)-N]

The complex formation function given in Figure 3.8(a) does not level off at a value of 1.0, clearly indicating that an ML species in the Cu(II)-[H_2(556)-N] system is not predominant in solution. Extensive fanning back of the curves is exhibited by curves corresponding to lower metal to ligand concentration ratios. This indicates loss of the amide protons in this ligand system upon metal ion co-ordination [35, 36, 37].

Figure 3.8: Experimental (1:2 (◇), 1:3(o) and 1:4 (□)) and theoretical (line) (a) formation and (b) deprotonation curves for the Cu(II)-[H_2(556)-N] system.

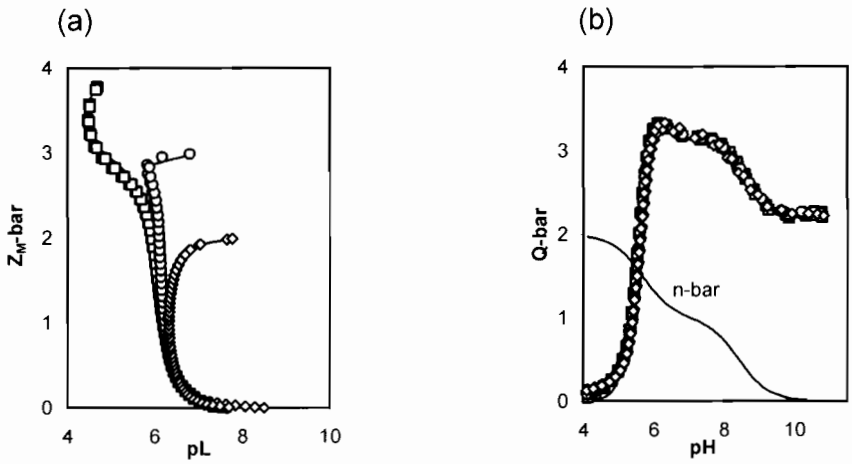

At pH values less than 4.00 the deprotonation function Q-bar of zero indicates that no protons have been displaced due to complexation. The protonation function n-bar has a value of 2.0 at this pH confirming that the ligand is still diprotonated at low pH. For pH values above 4.00 the deprotonation function Q-bar rapidly rises to intersect the protonation curve, n-bar, at a pH of 5.00, reaching a maximum value of about 3.30 at pH 5.60. From here on the Q-bar curves run parallel to the protonation curve and then level off at a value of 2.0 in the strongly alkaline region. This means that from a pH of $\approx$ 5.60 onwards two additional protons have been displaced per metal ion from the ligand, resulting in the ligand losing a total of four protons.

A problem that occurs commonly in the computational analysis of potentiometric data arises when two or more models describe the experimental data equally well as far as the statistical criteria are concerned. This problem was found to occur with the Cu(II)-[H_2(556)-N] system. Five models comprising the sets of species MLH, ML, MLH_{-1}, MLH_{-2} and MLH_{-3} were generated from analysis of the potentiometric data for the Cu(II)-[H_2(556)-N] system using the ESTA suite of programs. These models are given in Table 3.4. Since it was difficult to distinguish and decide between the various models based on statistics or the shape of the formation (Z_M-bars) and deprotonation curves (Q_M-bars), the selection of the model(s) presented in Table 3.3 and those used to postulate the structures of various species for the Cu(II)-[H_2(556)-N] system was based on chemical grounds and Okham's razor. Okham's razor is a very old phenomenon based on consideration of the simplest explanation whenever available data cannot distinguish between two or more models. Consequently, the choice of the chemical model(s) for this system became a matter of personal judgement [3]. Model 1 was dismissed on chemical grounds. Coordination of a pyridyl nitrogen only while the amine is still protonated resulting in an MLH species in the Cu(II)-[H_2(556)-N] system is unlikely due to the chelate effect. Coordination via two (pyridyl and carbonyl) or three (pyridyl and two carbonyls) donors is not favourable due to formation of unstable 8 and 7,8 membered chelate ring systems respectively as shown in Figure 3.25c. Model 3 was presented in Table 3.3 as well as

used to generate the complexation and deprotonation functions given in Figure 3.8. Models 2, 3, 4 and 5 were all considered to postulate structure formation and relative stability in section 3.4.5.

Table 3.4: Possible models generated from potentiometric analysis of data for the Cu(II)-[H_2(556)-N] system using ESTA suite of programs.

Model	p q r	log β_{pqr}	σ_{pqr}	R^H_f	R^H_{lim}	n_T / n_p
1	1 1 1 1 1 0 1 1 -2	10.972 5.747 -3.896	0.088 0.063 0.024	0.010	0.022	6 / 339
2	1 1 0 1 1 -2	5.846 -4.094	0.011 0.004	0.014	0.027	6 / 339
3	1 1 0 1 1 -2 1 1 -3	5.848 -4.094 -12.593	0.009 0.004 0.028	0.011	0.027	6 / 339
4	1 1 0 1 1 -1 1 1 -2	5.818 -0.388 -4.099	0.021 0.263 0.006	0.013	0.027	6 / 339
5	1 1 0 1 1 -1 1 1 -2 1 1 -3	5.802 -0.186 -4.104 -12.595	0.018 0.135 0.028 0.028	0.011	0.027	6 / 339

Despite the difficulty experienced in selecting a single model that best describe the solution equilibria for the Cu(II)-[H_2(556)-N] system, these models generated the same theoretical and experimental formation and deprotonation functions with excellent agreement and reproducibility of repeat titrations at different metal to ligand ratios, as shown in Figure 3.8. A noticeable feature about the models given in Table 3.4 is that the calculated formation constants for models 2 - 5 have reasonably low standard deviations and Hamilton R^H-factors. This lends the same confidence to these 4 models with respect to their description of the equilibria occurring in solution for the Cu(II)-[H_2(556)-N] system.

Figure 3.9: Calculated speciation of (a) Cu(II) (4.8×10^{-4} *mol* dm^{-3})-[H_2(5555)-N] (1.9×10^{-3} *mol* dm^{-3}) system and (b) Cu(II) (3.8×10^{-4} *mol* dm^{-3})-[H_2(556)-N] (1.5×10^{-3} *mol* dm^{-3}) system for model 3 as a function of pH.

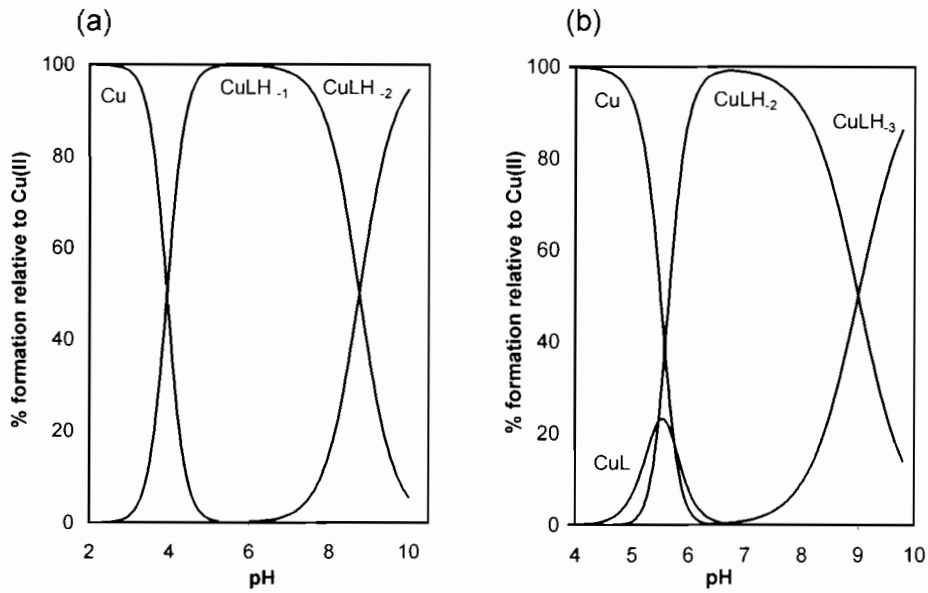

Figure 3.10: Calculated speciation of Cu(II) (3.8×10^{-4} *mol* dm^{-3})-[H_2(556)-N] (1.5×10^{-3} *mol* dm^{-3}) system for models (a) 4 and (b) 5 as a function of pH

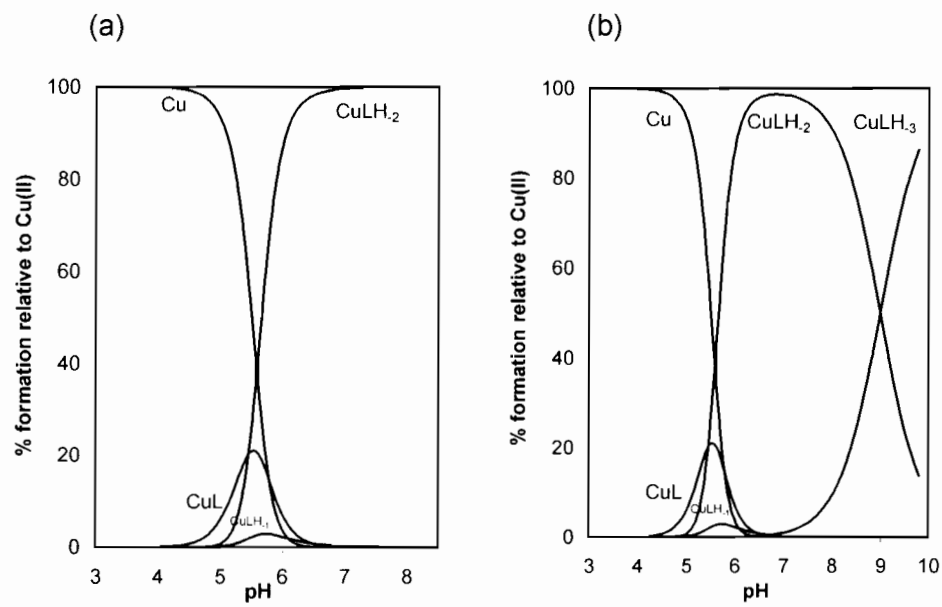

The speciation diagram for the Cu(II)-[H_2(556)-N] system calculated using model 3 in Figure 3.9(b) shows that the ML species reaches 24 % formation at pH 5.00. The MLH_{-2} species account for at least 50 % of bound Cu(II) in the pH range of 6.00 - 8.00, while it reaches 99 % formation at pH 6.50, with the MLH_{-3} species becoming increasingly important at pH values above 9.00. Thus the calculated species distribution based on the formation constants indicates that the neutral MLH_{-2} complex species predominate at physiological pH (7.40). Since more than one model could describe the experimental data equally, as will be discussed in section 3.4.5, the species distribution for models 4 and 5 have also been given in Figure 3.10. A noticeable feature about these species distribution graphs is the insignificant amount of MLH_{-1} (3%) indicating that this species is in the minority in the equilibrium system under the conditions used for this system.

Unlike the species distribution graphs for the Cu(II)-[H_2(556)-N] system shown in Figure 3.9(b) and 3.10, the species distribution diagram for the Cu(II)-[H_2(5555)-N] system, as given in Figure 3.9(a) indicates that the predominant species MLH_{-1} exist under physiological pH. The neutral species MLH_{-2} of this system becomes increasingly important under alkaline conditions, accounting for more than 50 % of the bound Cu(II) at a pH of 9.00 and above.

3.4.2 Ni-L systems

The experimental data for Ni(II) with [555-N], [H(555)-N], [H_2(5555-N] and [H_2(556)-N] ligand systems are given in Figures 3.11 - 3.15 respectively. The data were analysed with ESTA suite of programs and the results are given in Table 3.3.

Figure 3.11: Experimental (1:2 (◇), 1:3(o) and 1:4 (□)) and theoretical (line) (a) formation and (b) deprotonation curves for the Ni(II)-[H(555)-N] system.

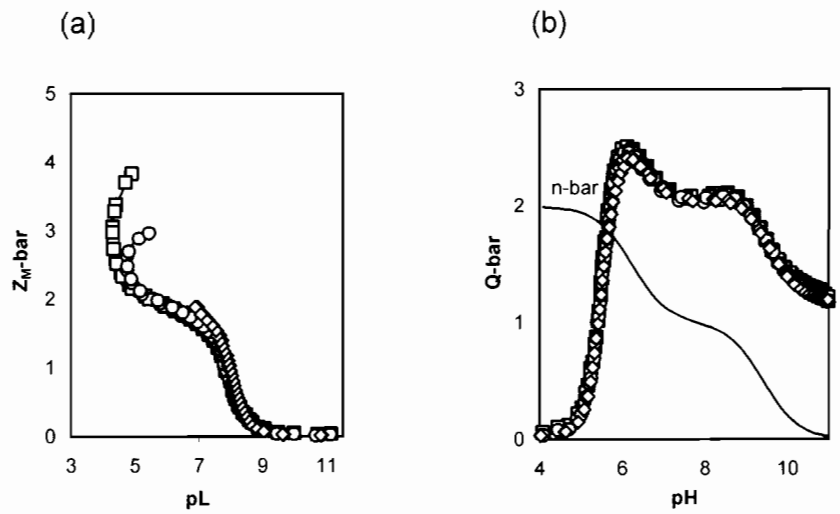

Figure 3.12: Experimental (1:2 (◇), 1:3 (o) and 1:4 (□)) and theoretical (line) (a) formation and (b) deprotonation curves for the Ni(II)-[H_2(5555)-N] system.

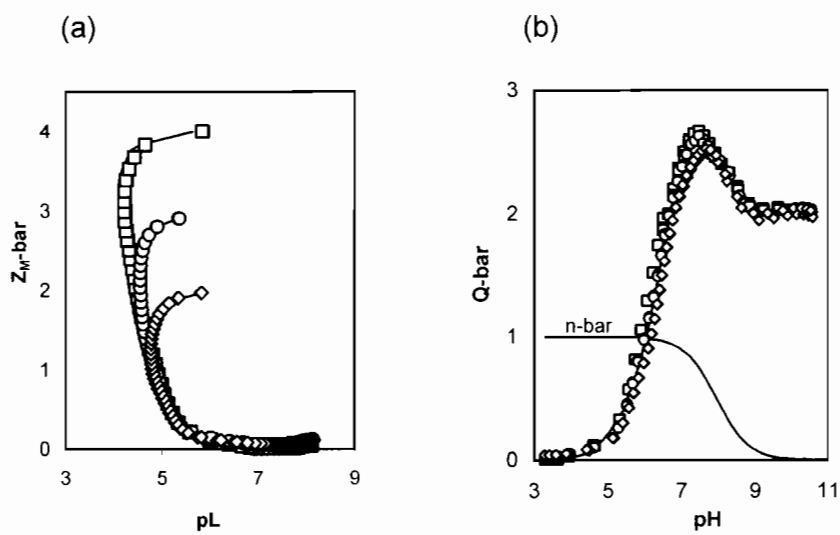

Figure 3.13: Experimental (1:2 (◇), 1:3 (o) and 1:4 (□)) and theoretical (line) (a) formation and (b) deprotonation curves for the Ni(II)-[H_2(556)-N] system.

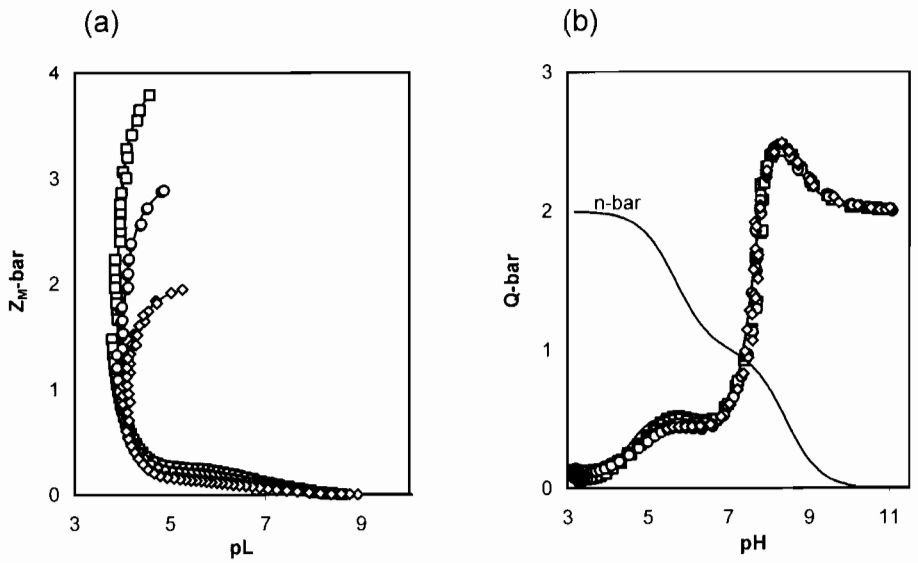

Unlike both the Ni(II)-[H(555)-N] and Ni(II)-[H_2(5555)-N] systems, slow kinetics was observed in the Ni(II)-[H_2(556)-N] system. Despite the known limitations associated with slow kinetics, there is an excellent agreement between the experimental and theoretical complexation and deprotonation functions as well as reproducibility of repeat titrations as shown in Figure 3.13.

Q-bar for the Ni(II)-[H_2(556)-N] system shown in Figure 3.13(b) initially rises and levels to a value of 0.5 within a pH range of 4.70 - 6.40 before rapidly rising to a maximum value of 2.5. Levelling of Q-bar at a value of 0.5 under mildly acidic conditions indicates release of a proton in solution due to the deprotonation of an MLH species. This species is also present in the model for the Ni(II)-[H_2(556)-N] system given in Table 3.3. Moreover, the MLH species is shown to be one of the predominant species in the speciation diagram given in Figure 3.15(b). The calculated species distribution diagram shows that this species is present within a pH range of 4.00 - 8.00 with a maximum of 54 % of the species formed at pH 6.00.

Figure 3.14: Calculated speciation of (a) Ni(II) (2.6×10^{-4} *mol* dm^{-3})-[555-N] (1.0×10^{-3} *mol* dm^{-3}) and (b) Ni(II) (4.6×10^{-4} *mol* dm^{-3})-[H(555)-N] (1.8×10^{-3} *mol* dm^{-3}) system as a function of pH.

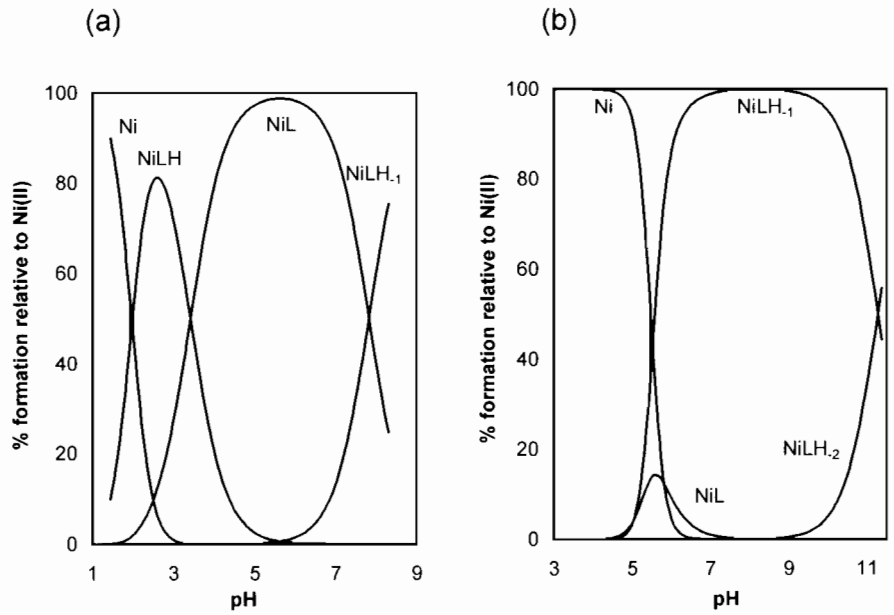

Figure 3.15: Calculated speciation of (a) Ni(II) (5.3×10^{-4} *mol* dm^{-3})-[H_2(5555)-N] (2.1×10^{-3} *mol* dm^{-3}) and (b) Ni(II) (3.7×10^{-4} *mol* dm^{-3})-[H_2(556)-N] (1.5×10^{-3} *mol* dm^{-3}) systems as a function of pH.

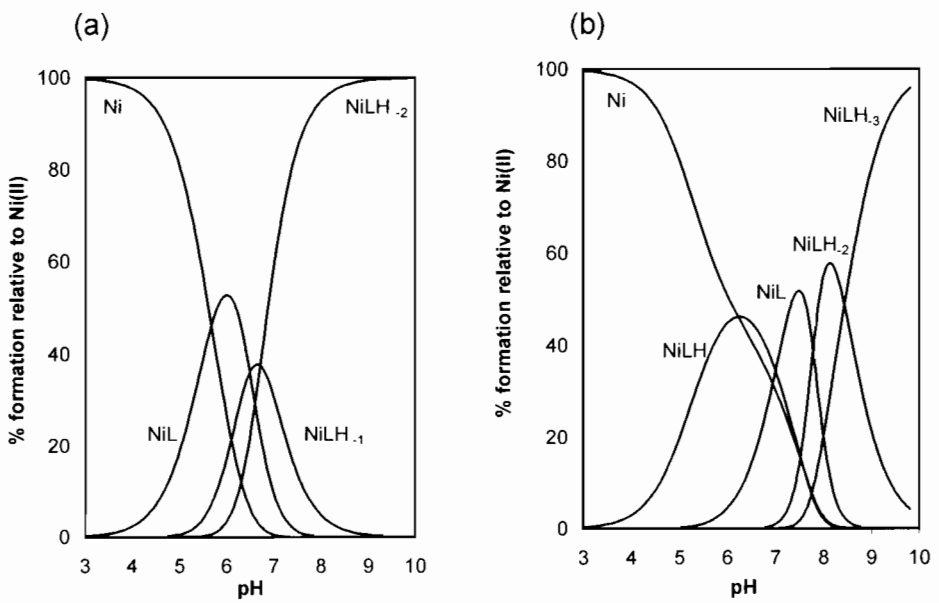

The calculated species distribution diagram given in Figure 3.14 above, illustrates that the ML species of the Ni(II)-[555-N] system predominates while that of the Ni(II)-[H(555)-N] system is remarkably reduced. The metal ion does not exceed 20 % in the ML species of the Ni(II)-[H(555)-N] system, indicating that this species is in the minority and therefore relatively insignificant. On the other hand the ML species of the Ni(II)-[555-N] system reaches almost 100 % formation at a pH of 5.60 as shown in Figure 3.14(a). The MLH_{-1} species in the Ni(II)-[H(555)-N] system predominates and reaches 100 % formation in the pH range 7.30 - 9.30, while the MLH_{-2} becomes significant above pH 10.00, reaching only 50 % formation at pH 11.00. A noticeable feature about the two distribution diagrams is the presence of MLH species and the absence of MLH_{-2} in the Ni(II)-[555-N] system. For the Ni(II)-[H(555)-N] system, a minor ML and a major MLH_{-1} species are present.

The ML species in the Ni(II)-[555-N] system (β = 17.20) forms at the start of the titration whereas that of the Ni-[H(555)-N] system (β = 6.98) is only formed at higher pH. At this pH, as soon as the ML species is formed, the complex can rearrange and with metal-assisted amide deprotonation forms the MLH_{-1} species. Thus in the Ni(II)-[H(555)-N] system (Figure 3.14b) the two protons of the ligand are lost in practically one step as indicated by the formation of $NiLH_{-1}$ taking place parallel with NiL.

3.4.3 Zn-L systems

Figures 3.16 - 3.20 show the complexation and deprotonation functions as well as the speciation distribution diagrams for the Zn(II)-ligand systems. These diagrams were analysed as before using ESTA suite of programs and the results are given in Table 3.3. The complexation function in Figure 3.16(a) for the Zn(II)-[555-N] system levelling to a value of 1.0 clearly indicates the formation of a mononuclear ML species of ratio 1:1. In the other Zn(II)-ligand systems studied the ML species is never dominant and hence the Z_M-bar curves do not level off at 1.0.

Figure 3.16: Experimental (1:2 (◇), 1:3 (o) and 1:4 (□)) and theoretical (line) (a) formation and (b) deprotonation curves for the Zn(II)-[555-N] system.

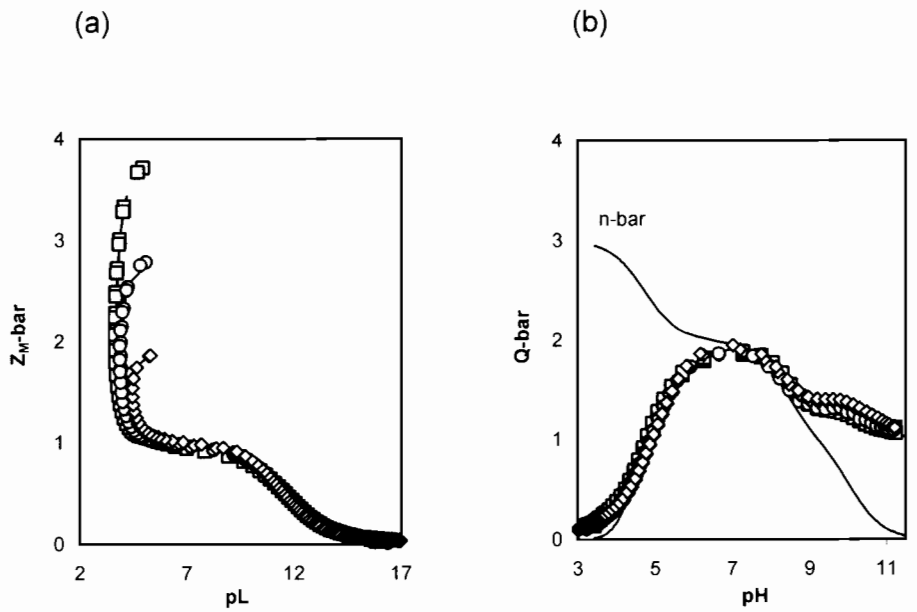

Figure 3.17: Experimental (1:2 (◇), 1:3 (o) and 1:4 (□)) and theoretical (line) (a) formation and (b) deprotonation curves for the Zn(II)-[H(555)-N] system.

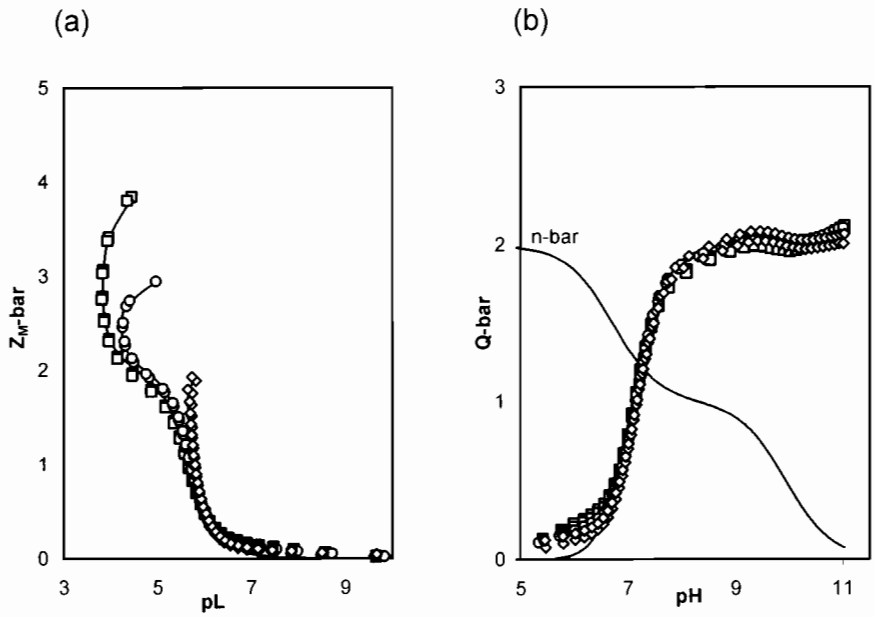

Figure 3.18: Experimental (1:2 (◇), 1:3 (o) and 1:4 (□)) and theoretical (line) (a) formation and (b) deprotonation curves for the Zn(II)-[H_2(5555)-N] system.

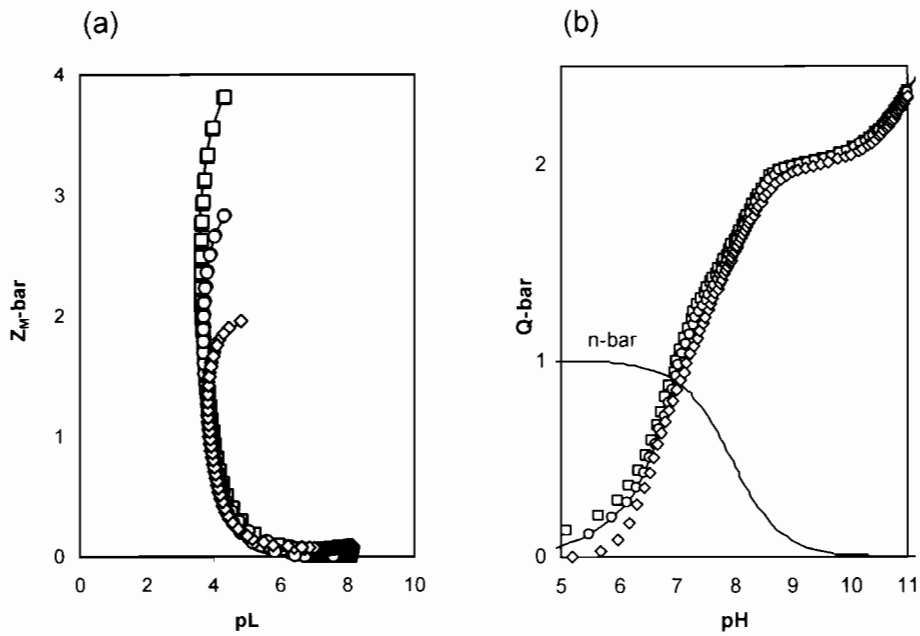

Figure 3.19: Calculated speciation of (a) Zn(II) (3.1×10^{-4} *mol* dm^{-3})-[555-N] (1.2×10^{-3} *mol* dm^{-3}) and (b) Zn(II) (4.6×10^{-4} *mol* dm^{-3})-[H(555)-N] (1.9×10^{-3} *mol* dm^{-3}) systems as a function of pH.

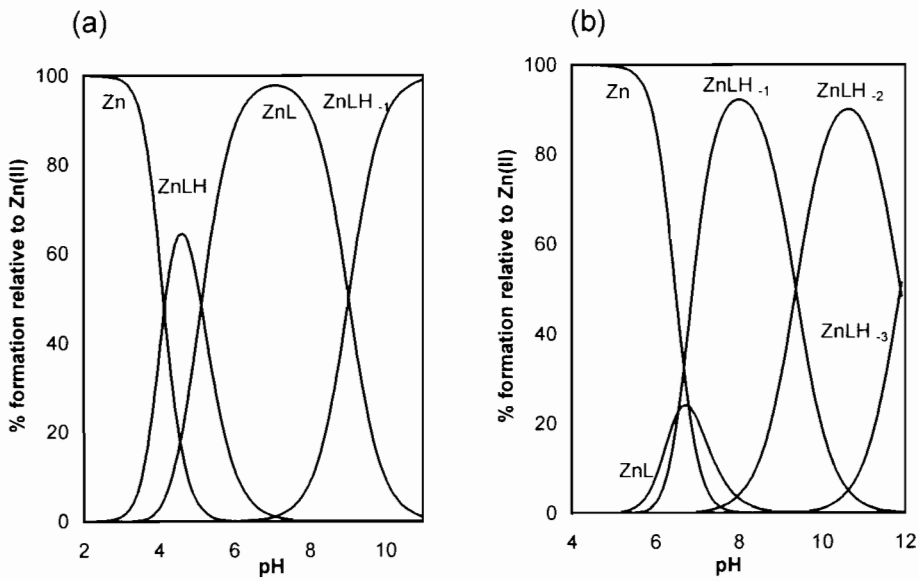

Figure 3.20: Calculated speciation of (a) Zn(II) (5.0×10^{-4} *mol* dm^{-3})-[H_2(5555)-N] (2.0×10^{-3} *mol* dm^{-3}) and (b) Zn(II) (3.8×10^{-4} *mol* dm^{-3})-[H_2(556)-N] (1.5×10^{-3} *mol* dm^{-3}) systems as a function of pH.

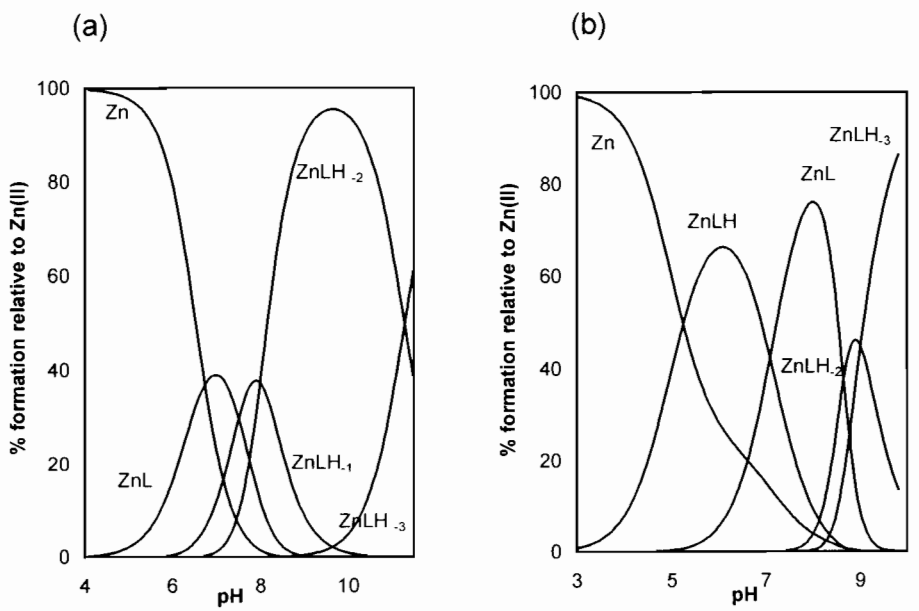

3.4.4 Ca-L systems

Inspection of the complexation and deporotonation functions for the Ca(II)-[555-N] and Ca(II)-[H(555)-N] systems showed that there were a number of similarities in their behaviour. Therefore the analysis for these systems is described together. Figures 3.21 - 3.23 show the complexation and deprotonation functions as well as the speciation distribution diagrams for the Ca(II)-ligand systems. These diagrams were analysed in the same way as the Cu(II)-ligand systems already described in section 3.4.1 and the results are given in Table 3.3.

Ca(II) demonstrated a low, but measurable affinity for the donor atoms of the ligands, [555-N] and [H(555)-N]. The complex formation functions in Figures 3.21(a) and 3.22(a) confirm this observation for the Ca(II)-[555-N] and Ca(II)-[H(555)-N] systems respectively, remaining at zero until pH > 7.00.

The Q-bar curves in Figures 3.21(b) and 3.22(b) also remain close to zero and never rise to the expected value of 3.0. This indicates weak complexation by Ca(II) and makes the analysis of the data difficult. Several models were tried in the ESTA analysis of the data with the final models being given in Table 3.3. The statistics are excellent with low standard deviation being obtained for all the log β_{pqr} 's and a final Hamilton R^H_f of 0.01 and 0.008 for the Ca(II)-[555-N] and Ca(II)-[H(555)-N] systems respectively. From this we see that an MLH species is formed above pH 5.00. This species was found in some of the other systems studied, but there it was a minor species whereas for Ca(II) it is a major species. Unfortunately Z_M-bar and Q-bar are not very sensitive to the formation of protonated species and hence the difficulty of identifying this species from these curves. However, the difference in Q-bar and n-bar in both Figures 3.21b and 3.22b changes indicating complex formation, although Q-bars are not significantly changing. Moreover, the standard deviations for the various betas are reasonably small while more than 80% of species are formed above pH 5.00 as shown in Figure 3.23.

Figure 3.21: Experimental (1:2 (◇), 1:3 (o) and 1:4 (□)) and theoretical (line) (a) formation and (b) deprotonation curves for the Ca(II)-[555-N] system.

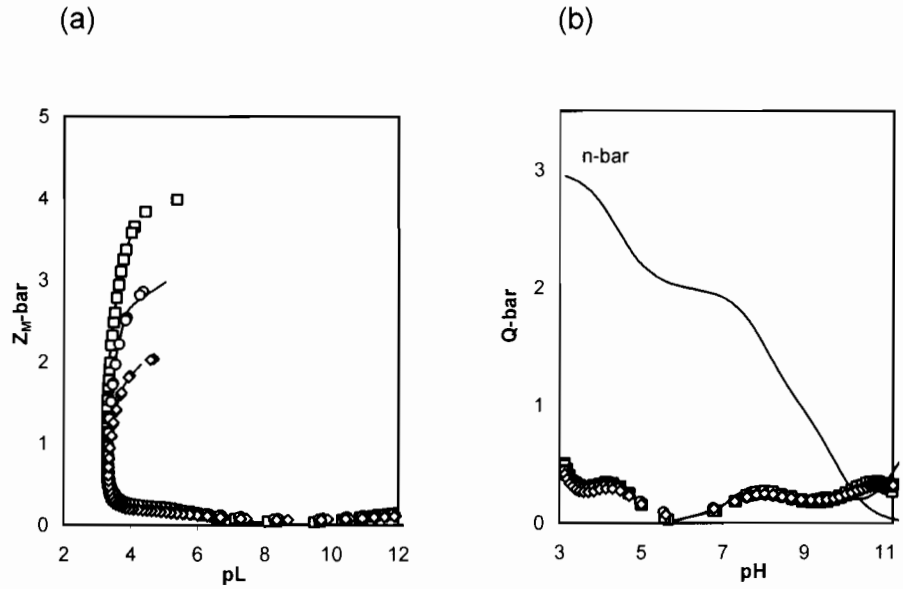

Figure 3.22: Experimental (1:2 (◇), 1:3(o) and 1:4 (□)) and theoretical (line) (a) formation and (b) deprotonation curves for the Ca(II)-[H(555)-N] system.

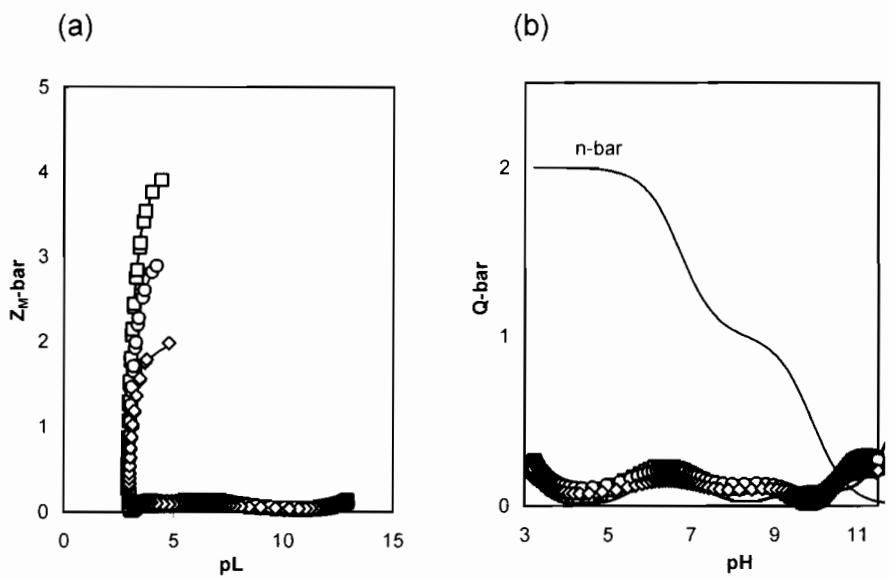

For the Ca(II)-[H_2(5555)-N] and Ca(II)-[H_2(556)-N] systems no complexation could be detected under the conditions of this study.

Figure 3.23: Calculated speciation of (a) Ca(II) (2.6×10^{-4} *mol* dm^{-3})-[555-N] (1.0×10^{-3} *mol* dm^{-3}) and (b) Ca(II) (4.6×10^{-4} *mol* dm^{-3})-[H(555)-N] (1.9×10^{-3} *mol* dm^{-3}) systems as a function of pH.

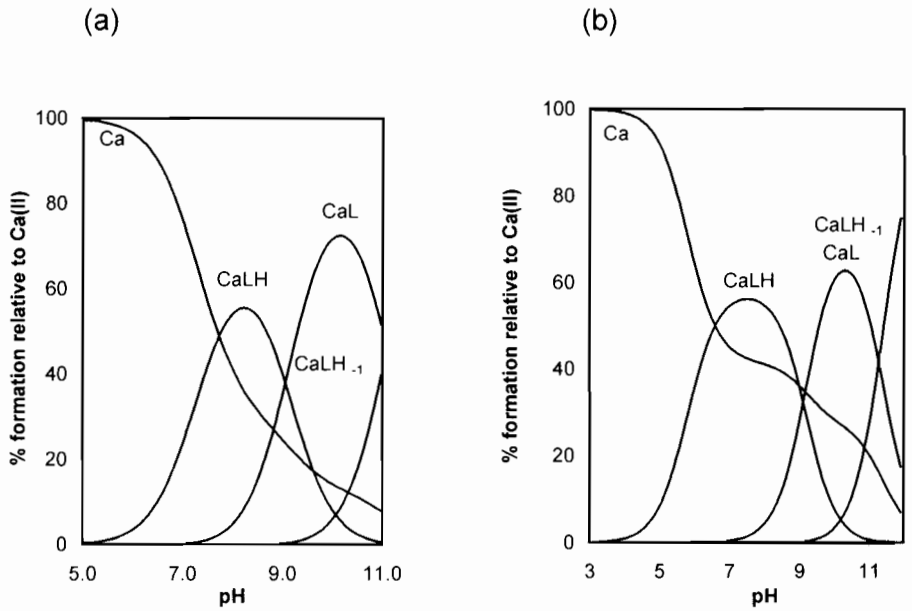

The calculated species distribution diagrams given in Figure 3.23(a) and (b) illustrates that the two systems are characterised by the formation of protonated species at physiological pH. Moreover such species dominate a wider pH range from 6.00 - 10.00 for both the Ca(II)-[555-N] and Ca(II)-[H(555)-N] systems. This inability of Ca(II) to readily deprotonate these ligand systems demonstrate the metal ion's reduced affinity for complexation.

3.4.5 Structure and stability

Possible structures for the various species found in this study have been postulated and are given in Figures 3.24 and 3.25.

Comparison of formation constants for the mononuclear binary ML species of [555-N], [H(555)-N] and [H_2(556)-N] with Cu(II) shows that the ML

species of the Cu(II)-[555-N] system is the most stable, with stability decreasing as amidic groups are introduced into a particular ligand. Thus the value of log β_{110} for the Cu(II) complex of [555-N] (18.6) is about 7 log units higher than the corresponding constant for [H(555)-N] (11.5), which in turn is 5 log units higher than the corresponding constant for [H_2(556)-N] (5.85).

Figure 3.24: Possible structures for M(II)-L systems [M(II)=Cu(II), Ni(II), Zn(II), Ca(II)].

M(II)-[555-N] system

MLH a (i) (ii)

ML b (i) (ii) MLH_{-1} c(i) (ii)

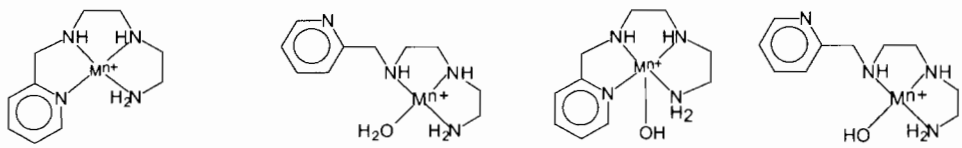

M(II)-[H(555)-N] system

ML d (i) (ii) (iii) (iv)

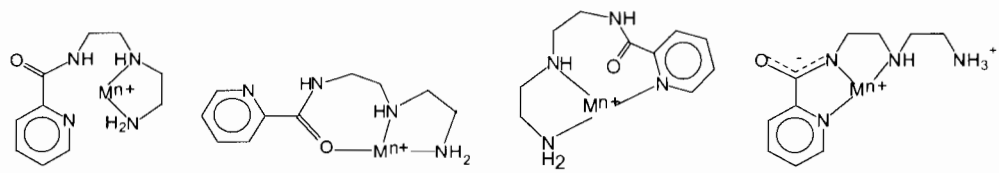

MLH_{-1} e (i) (ii)

One possible explanation for the significant higher stability of an ML species in the Cu(II)-[555-N] system is the formation of a tetradentate 5,5,5 chelate complex (Figure 3.24b(i)) as opposed to a less stable tridentate 5,7 chelate complex formed in the Cu(II)-[H(555)-N] system (Figure 3.24d(ii)). The presence of amidic groups in the ligands [H(555)-N] and [H_2(556)-N] also lowers the stability of the complexes formed with these systems as this would involve interaction of a hard amide ligand and a border line metal ion. Moreover amidic groups have electron-withdrawing properties making the donor atoms less basic. This result is not unexpected as it is in complete accordance with the base-weakening effect of the CONH-group [23].

Table 3.5 below, presents the protonation (pK_a) and Cu(II)-L formation constants for [555-N], [H(555)-N] [This work], ethylenediamine (en), diethylenetriamine (dien) and triethylenetetraamine (trien) [30].

Table 3.5: Protonation (pK_a) and Cu(II)-L formation (log β_{110}) constants for [555-N], [H(555)-N], ethylenediamine (en), diethylenetriamine (dien) and triethylenetetraamine (trien).

	$pK_{a,1}$	$pK_{a,2}$	$pK_{a,3}$	β_{110}	Reference
[555-N]	4.1	7.9	9.6	18.6	This work
[H(555)-N]	6.2	9.4	-	11.5	This work
en	7.1	9.9	-	10.5	30
dien	4.2	9.0	9.8	15.9	30
trien	6.4	8.9	8.7	19.4	30

Comparison of log β_{110} values for [555-N] (18.6) and dien (15.9) shows that log β_{110} ([555-N]) is greater than log β_{110} (dien) by almost 3 log units. However the three pK_a values for dien (4.2; 9.0; 9.8) are higher than those for [555-N] (4.1; 7.9; 9.6). This indicates that the pyridyl group is bound to the metal ion in the ML species of the Cu(II)-[555-N] system giving this complex

species extra stability over the ML for [Cu(II)dien] due to one more bound nitrogen, resulting in the formation of three stable membered chelate rings. This greater stability of an ML for the Cu(II)[555-N] complex is consistent with the structure given in 3.24b(i) which has three chelate rings in contrast with the two chelate rings of the complex sketched in 3.24b(ii). The fact that log β_{110} value for an ML species in the Cu(II)[555-N] system (18.6) is smaller than log β_{110} for an ML species for the [Cu(II)trien] system (19.4) by only 0.8 log units indicates that the pyridyl nitrogen is not as strong a base as an amino ($-NH_2$) group.

The calculated Cu(II) assisted deprotonation constant ($pk^{ML}_{MLH_{-1}}$) associated with the formation of an MLH_{-1} for the Cu(II)-[H(555)-N] system is calculated from the difference between log β_{110} and log β_{11-1}. The last deprotonation at the alkaline end of the pH range investigated converts the ML species into MLH_{-1} for both the Cu(II)-[555-N] and Cu(II)-[H_2(555)-N] systems. The pK_a value determined for the Cu(II)-[555-N] system ($pK^{Cu[555-N]}_{Cu[555-N]H_{-1}}$ = 10.65) is assigned to deprotonation of an axial water molecule. This pK_a is higher than the pK_a of [$Cu(H_2O)_6$] (8.00), but this is ascribed to the fact that in [$Cu(H_2O)_6$] an equatorial water proton is deprotonated rather than an axial water. This would therefore suggests the structure shown in Figure 3.24c(i) as the postulated structure for the MLH_{-1} complex species.

The calculated $pK^{Cu[H(555)-N]}_{Cu[H(555)-N]H_{-1}}$ value of 3.53 for the Cu(II)-[H(555)-N] system is in the range expected for metal assisted deprotonation of the amide proton [21, 38, 39, 40], rather than a water molecule from the coordination sphere of the complex. Moreover the log β_{110} value for an ML in the Cu(II)[H(555)-N] (11.5) is observed to be much less than the log β_{110} value for an ML for the [Cu(II)dien] system (15.9) by 4 log units. This is consistent with a structure in which the amide group is not coordinated suggesting 3.24d(i), (ii) and (iii) as possible structures for the ML species of the Cu(II)[H(555)-N] system. However the fact that the log β_{110} value for the Cu(II)[H(555)-N] (11.5) is greater than the log β_{110} value for the [Cu(II)en] system (10.5) by only 1 log

unit implies that there is an extra weak binding in this complex species. Such weak binding could be due to either a pyridyl nitrogen or carbonyl oxygen present in this ligand system as shown in structures 3.24d(ii) and (iii). We believe, however that the size of the chelate ring argues against structure 3.24d(iii). We therefore favour structure 3.24d(ii), based on the following arguments. First, coordination through a carbonyl group is feasible, as has been demonstrated in the Cu(II)-glycinamide and -β-alaninamide systems [31]. With the latter two ligands Cu(II) ions form a chelate ring with the metal coordinated to both the amine and the carbonyl groups. Upon proton loss from the Cu(II)-gycinamide complex, rearrangement of the chelate ring takes place such that co-ordination switches from carbonyl to the amide nitrogen, yielding structures similar to those shown in Figure 3.24e. This then suggests that in the ML species the ligand is coordinated to the metal ion through two nitrogen and one oxygen donor atoms excluding the amide nitrogen with the postulated structure for the ML species illustrated as sketched in Figure 3.24d(ii). The MLH_{-1} species in this system therefore results from loss of an amide proton from a tri-coordinated ligand with the most likely structures for MLH_{-1} species in this system given in Figure 3.24e. As can be seen, these essentially differ according to the number of nitrogen atoms co-ordinated to the metal ion. Thus, in this MLH_{-1} complex species of the Cu(II)[H(555)-N] system, the ligand is postulated to coordinate to Cu(II) ion through three or four nitrogen donor atoms leaving two axial sites occupied by water molecules. The structure given in Figure 3.24e(i) is however favoured because of formation of three chelate rings in contrast with the two chelate rings of structure 3.24e(ii).

In the pH range in which the ML species for the Cu(II)[H(555)-N] system forms, any uncoordinated amine would be protonated. Thus if the ML species for the Cu(II)-[H(555)-N] system is represented by the structure given in 3.24d(iv), where the amide is deprotonated and the amine protonated to give an overall neutral ML species in the Cu(II)-[H(555)-N] system, then formation of the MLH_{-1} species could arise from deprotonation of this amine. The $pK^{Cu[H(555)-N]}_{Cu[H(555)-N]H_{-1}}$ value of 3.53 corresponding to this deprotonation is

comparable with $pK_{a,1}$ of 4.1 for [555-N] and would therefore support this suggestion. This presents a rather paradoxical situation.

The ligand [H_2(5555)-N] exhibit the lowest coordination to Cu(II) as compared to the other ligand systems with log β_{pqr} values of 2.83 and -5.93 for the MLH_{-1} and MLH_{-2} species respectively. The presence of more electron withdrawing CONH-groups in [H_2(5555)-N] could be responsible for such behaviour. Moreover the two pyridyl groups present in [H_2(5555)-N] are less basic groups. A noticeable feature about the complexation behaviour of Cu(II) with this ligand is the absence of an ML species. A complexation model involving this species resulted in failure in the optimization of the objective function. This species could have already been formed at low pH as demonstrated by the acidic nature of the pyridyl nitrogen donors in [H_2(5555)-N] and this therefore rendered the complex formation process not measurable by potentiometry. The ligand however demonstrates an ability to form MLH_{-1} and MLH_{-2} species with Cu(II), with structures given in Figure 3.25(a) and (b), where one or both amide moieties are deprotonated, as possible structures for the species. The feasibility of formation the species MLH_{-1} and MLH_{-2} for this Cu(II)-[H_2(5555)-N] system is due to the remarkable ability of Cu(II) to readily deprotonate the ligand and form bonds to amide nitrogens in their ionized state [41]. Direct evidence for the amide proton dissociation on complexation has been obtained from aqueous (D_2O) infrared studies [42, 43, 44] for Cu(II) complexes in solution. The result of X-ray crystallographic studies [45] have also shown unequivocally that the amide proton displacement takes place in the solid and the coordination of the resulting negative amide groups occur to the metal ion.

The analysis of the Cu(II)-[H_2(556)-N] system using ESTA suite of programs in section 3.4.1 revealed that five models described the solution equlibria equally. Model 1 was dismissed on chemical grounds. The possible MLH species generated from this model are given in Figure 3.25c.

Figure 3.25: Possible structures for M(II)-L systems [M(II)=Cu(II), Ni(II), Zn(II)].

M(II)-[H_2(5555)-N] system

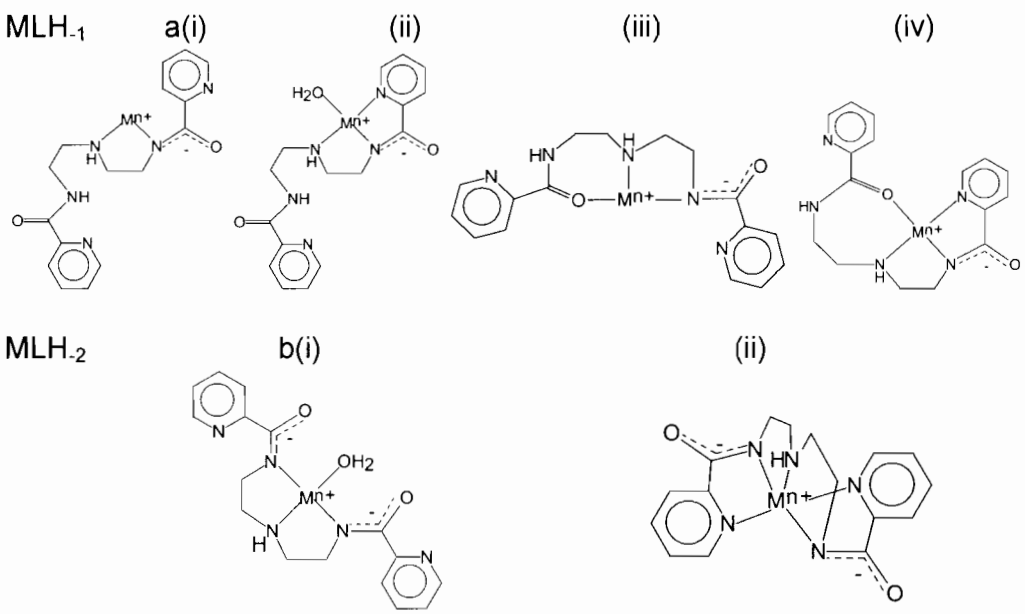

M(II)-[H_2(556)-N] system

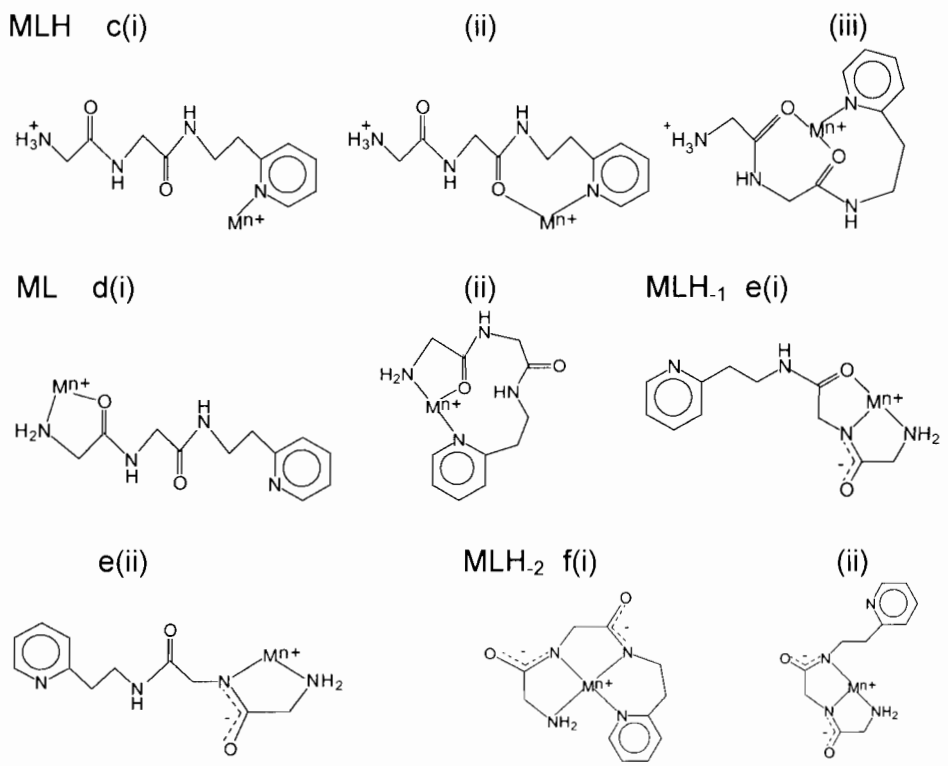

Coordination of a pyridyl nitrogen to Cu(II) while the amine is protonated as given in Figure 3.25c(i) is unlikely due to the chelate effect. Moreover log K^{LH}_{MLH} of 3.06 from model 1 differs significantly by 1.76 log units from the log β_{110} (1.3) of the [Cu(II)-Mepy] system. Surpisingly, the pK_{a1} of Methylpyridine (5.95) is larger than the pK_{a1} of [H_2(556)-N] (5.20). This therefore rules out the protonated complex, with the structures given in Figure 3.25c(ii) and (iii) remaining as possible structures for this MLH species. The fact that log β_{110} (10.5) for the [Cu(II)en] system where two donors are present, is 0.47 log units lower than log β_{111} (10.97) for the Cu(II)-[H_2(556)-N] system suggests three donor atoms as opposed to only two, to be coordinated to the metal ion. This then supports the structure given in Figure 3.25c(iii), where a pyridyl nitrogen and two carbonyl oxygen donors are coordinated forming a 7,8 chelate ring system. However, the feasibility of this structure is unlikely based on the size of the chelate rings. Moreover oxygen donors are hard donors and would have lower affinity for the metal ion as compared to the protonated amino group.

Considering the significantly non-overlapping deprotonations of the pyridyl and amino groups in the free ligand, [H_2(556)-N], with pK_2 - pK_1 value of 3.0, the first metal promoted deprotonation is likely to occur at the pyridyl nitrogen and formation of two binding isomers is unlikely. This is in contrast to what has been reported for glycylglycylhistamine [46] and alanylglycylhistamine [47], two related peptides, where deprotonations of the imidazole and amino groups significantly overlap (pK_2 - pK_1 = 1.0), implying competition between the two deprotonation processes, thereby producing an alternative microprotonation pathway. In Figure 3.25, in the 2N coordinated ML complexes, all nitrogens in [H_2(556)-N] can be candidates as binding sites. However, in the case of N-acetylhistamine, even Cu(II) is not able to promote amide deprotonation; [48], with {N^-, imidazole-N^3} 6-membered chelate formation neglected. Thus a 5-membered chelate formation {NH_2, O} given in Figure 3.25d(i) seems to be more probable on thermodynamic grounds compared to an amino and pyridyl coordinated macrochelate given in Figure 3.25d(ii). The Cu(II)[H_2(556)-N] complexation starts just past pH 4.50 and

rapidly reaches a maximum value over a small pH range of less than 1.50 units. This means once the first coordination bond is formed, the chelate effect will aid in formation of the next coordination bonds to the central Cu(II) ion. Since the pyridyl group has its pK_a established at 5.20 and that of the terminal amino group at 7.91, giving a wide difference in ΔpK_a, it can be concluded that these two groups are involved in Cu(II) coordination. Thus the postulated structure for the MLH_{-2} species in the Cu(II)-[H_2(556)-N] system is the one given in Figure 3.25f(i). Structure 3.25f(i) is favoured because of formation of three chelate rings where Cu(II) has a tetragonally distorted configuration in contrast with the two chelate rings in structure 3.25f(ii).

The influence of substituents on the coordinating ability of mimicking pseudo-peptides of the serum albumin N-terminal residue has been widely reported [46, 47]. Due to the multidentate nature of [H_2(556)-N], and of all serum albumin mimicking pseudo-peptides, monomeric complexes, are formed in all systems. At physiological pH, the MLH_{-2} species in the Cu(II)-[H_2(556)-N] system predominates. However the formation constants determined in this study showed a somewhat lower coordination ability of [H_2(556)-N] in the MLH_{-2} species compared to the analogous ligands containing an imidazole ring, a methyl group, or having additional O-donor group(s) (amide and/or carboxylate), for instance glycylglycylhistamine (ggha) [46], alanylglycylhistamine (Ala-Gly-Ha) [47], Gly-Gly-His [49, 50], Gly-Gly-His-*N*-methylamide (gghma) [51] and Asp-Ala-His-*N*-methylamide (aahm) [52], where the observed formation constants have been reported as: log β_{11-2} $\approx$ -2.48; -2.86; -1.80; -0.48 and -0.55 (against -4.09 for [H_2(556)-N]). A noticeable feature about the two peptides ggha and ala-gly-ha is the stability associated with the MLH_{-1} species while this was difficult to detect for the Cu(II)-[H_2(556)-N] system. A minor complex of this MLH_{-1} species has also been suggested in the distribution curve for the Cu(II)-[H_2(556)-N] complex given in Figure 3.10(b) for Model 5. The analogous ligands bearing side chain substituents are given in Figure 3.26.

Figure 3.26: Some analogous ligands mentioned in the discussion [46, 47, 49, 51].

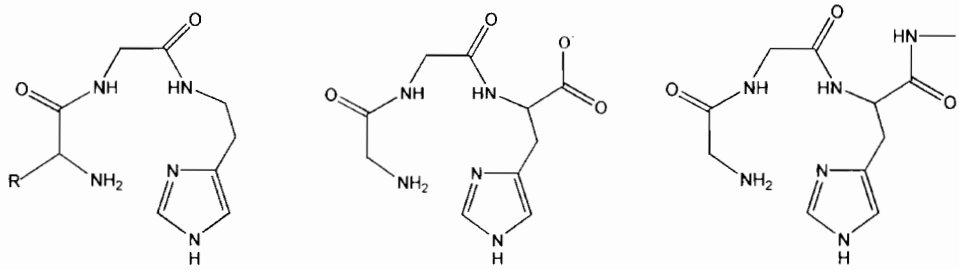

ggha (R = H) gly-gly-his gghma
ala-gly-ha (R = CH_3)

The difference can be attributed to the basicity of an imidazole and weak axial coordination of the O-donor group. However, under these conditions, the above sequence of formation constants should imply that the carboxylate end of gly-gly-his binds less strongly than the amide carbonyl oxygen of gghma (or aahma), which is unlikely on electrostatic grounds. Another piece of evidence against an additional coordination of an O-donor group comes from the observation of the same formation constants sequence (log $\beta_{11\text{-}2}$ = -10.16; -7.99; -6.93 and -5.94 for [H_2(556)-N], GGHA, gly-gly-his [53] and aahma [52] respectively) in the case of Ni(II) complexes, where, however, the $NiLH_{-2}$ species are generally reported to have a 4N coordinated square planar structure and where additional coordination is not probable. Considering these facts, the effect of the free carboxylate or of the amide side chain seems to arise from an increased acidity of the nearby peptide nitrogen, rather than from a direct coordination.

While from potentiometric results presented here it is not possible to unambiguously assign the structure of a complex, based on knowledge of the ligand and by comparison with related systems it may be possible to infer the structure of the complex. It is however clear from these results that potentiometric data alone cannot unambiguously predict the correct structure of a complex in solution. To get more evidence of the solution structures

formed between Cu(II) and these ligand systems, as well as gaining more insight into the coordination geometry of these structures, they have also been determined spectroscopically and this will be discussed in detail in Chapter four.

3.4.6 Stability comparison of Cu(II), Ni(II), Zn(II) and Ca(II)-ligand systems

Table 3.3 also lists the equilibrium constants for Ni(II), Zn(II) and Ca(II). As expected, these three metal ions form reasonably stable complexes with the two ligands [555-N] and [H(555)-N], but their stability is much lower than that of Cu(II). A noticeable feature about the complexes formed with these three metal ions is the prevalence of MLH, ML and MLH_{-1} species. The presence of stable protonated species in the Ni(II)-[555-N] (log β_{111} = 20.62), Zn(II)-[555-N] (log β_{111} = 16.63) and Ca(II)-[555-N] (log β_{111} = 12.98) systems suggests the inability of these metal ions to readily deprotonate these ligand systems. This indicates the metal ions' reduced affinity for complexation and lower binding strength of the ligand [555-N] towards Ni(II), Zn(II) and Ca(II). For the ML species, the difference in stability of some 7 - 15 log units is observed between Cu(II) and the *in vivo* competitors Zn(II) and Ca(II). One possible explanation is that the arrangement of the ligand donor atoms is such that the metal ion is constrained to adopt square planar coordination geometry. Zn(II) prefers a tetrahedral coordination geometry as observed in the majority of its simple systems [54] and in biological metallo-enzymes [55]. In such enzymes the Zn(II) ion is coordinated to three nitrogen atoms while a water molecule occupies the fourth coordination site constituting the tetrahedral arrangement of donor atoms. On the other hand, Cu(II) prefers a tetragonally distorted or square planar arrangement of ligand(s) donor atoms around the metal ion. Unlike the Ni(II)-[555-N] and Zn(II)-[555-N] systems, the Ni(II)-[H(555)-N] and Zn(II)-[H(555)-N] form ML, MLH_{-1}, MLH_{-2} and MLH_{-3} species. While the MLH_{-1} species could be attributed to deprotonation of the amide group in the [H(555)-N] ligand system, the other two species are a result of the ionisation of coordinated water molecules. High pK_a value of

11.28 for the formation of MLH_{-2} from MLH_{-1} for the Ni(II)-[H(555)-N] system and 11.88 for formation of MLH_{-3} from MLH_{-2} for the Zn(II)-[H(555)-N] system are quite consistent with the hydrolysis of the two metal ions [56].

The ligand, $[H_2(5555)\text{-}N]$, demonstrates remarkable ability to form MLH_{-1} and MLH_{-2} species with Cu(II), Ni(II) and Zn(II). This is due to the ability of these metal ions to deprotonate the amide protons above pH 7.00. For Ni(II), the calculated $pK^{Ni[H_2(5555)-N]}_{Ni[H_2(5555)-N]H_{-1}}$ and $pK^{Ni[H_2(5555)-N]H_{-1}}_{Ni[H_2(5555)-N]H_{-2}}$ values are 6.49 and 6.71 respectively. These pK_a values are 8.51 and 8.29 log units lower than the reported deprotonation constant of an amide group ($pK_a \approx 15.00$) [17, 18, 19, 20] respectively. The same pK_a values are 3.4 and 2.4 log units lower than the first and second hydrolysis constants of Ni(II) ($pK_{M\text{-}OH}$ = 9.86 & 9.14) respectively [56]. On the other hand, the calculated $pK^{Zn[H_2(5555)-N]}_{Zn[H_2(5555)-N]H_{-1}}$ value of 7.51 is 7.49 log units lower than the deprotonation constant of an amide nitrogen and 0.5 log units lower than the hydrolysis constant of the metal ion ($pK_{M\text{-}OH}$ = 8.00). This then suggests that these protons are most likely to have been released from the amide groups of $[H_2(5555)\text{-}N]$ as a result of metal-induced complexation. However the calculated $pK^{Zn[H_2(5555)-N]H_{-2}}_{Zn[H_2(5555)-N]H_{-3}}$ of 11.29 is 3.3 log units above the deprotonation constant of the ligand and closer to the hydrolysis constant of the metal ion ($pK_{M\text{-}OH}$ = 10.50), suggesting that the third deprotonation comes from a coordinated water molecule in the complex.

Although $[H_2(556)\text{-}N]$ is selective for Cu(II) the reported log β_{110} value of 5.84 is only 1.44 and 1.07 log units higher than those of Ni(II) and Zn(II) respectively. However this log β_{110} for Cu(II) is reasonably close to 5.08, a value reported for glycylglycylglycine [31], a related peptide, determined under different conditions of ionic strength. Ni(II) and Zn(II) demonstrate extensive formation of MLH species with $[H_2(556)\text{-}N]$ (log β_{111} = 10.91 and log β_{111} = 11.36) respectively. It is also observed that log β_{pqr}'s for the MLH and ML species in the Zn(II)-$[H_2(556)\text{-}N]$ system are slightly higher than those for the Ni(II)-$[H_2(556)\text{-}N]$ system (Table 3.3). This order of stability is in clear violation of the Irving-Williams series [57, 58]. Although log β_{110} for Cu(II) does not

significantly differ from those of Ni(II) and Zn(II), the presence of protonated species for Ni(II) and Zn(II) is an indication of the lower binding strength of the ligand [H_2(556)-N], towards these metal ions, as this demonstrates their inability to readily deprotonate the ligand. A noticeable feature about the complexation behaviour of [H_2(556)-N] with Cu(II) Ni(II) and Zn(II) is the absence of the MLH_{-1} species in model 3, given in Table 3.3. The presence of this species in models 4 and 5 (Table 3.4) is also insignificant as illustrated by the speciation diagrams given in Figure 3.10. This suggests that the two amides in [H_2(556)-N] are dissociated in overlapping steps. This observation is in agreement with what has been reported for N,N'-diglycyltrimethylenediamine; where Cu(II) complex has been observed to release the two peptide protons simultaneously [59]. This can be explained in terms of the pH delayed coordination of either the second amide nitrogen or both amide nitrogen donors if the terminal nitrogen donors are coordinated in the M(II)-[H_2(556)-N] system.

Unlike divalent Cu(II) and Ni(II), Zn(II) appears to deprotonate the amide nitrogens of both [H_2(5555)-N] and [H_2(556)-N] with difficulty. The low formation constants for the MLH_{-2} of the Zn(II)-[H_2[(5555)-N] and Zn(II)-[H_2(556)-N] systems are partly due to the difficulty associated with Zn(II)'s ability to deprotonate the amide moieties [40, 60] in these two ligand systems. Furthermore, it is known that Zn(II) prefers a tetrahedral geometry as observed with the majority of its simple systems [54].

Another noticeable feature about the models for the M(II)-[H_2(556)-N] system given in Table 3.3 is the presence of MLH_{-3} species. The calculated $pK^{M[H_2(556)-N]H_{-2}}_{M[H_2(556)-N]H_{-3}}$ for the Cu(II) Ni(II) and Zn(II)-[H_2(556)-N] systems are 8.50, 7.94 and 8.51 respectively. These calculated pK_a values are 6.50, 7.16 and 7.49 log units below the amide group deprotonation constant ($pK_a \approx 15.00$) and 2.00, 3.06 and 1.99 lower than the third hydrolysis constant of their metal ions ($pK_{Cu-OH} = 10.50$, $pK_{Ni-OH} = 11.00$ $pK_{Zn-OH} = 10.50$). Although this suggests metal-assisted deprotonation from the amide nitrogen, all the amide nitrogens have been deprotonated at this pH, and this third proton is likely to be

released from an equatorially coordinated water molecule in these complexes. A pK_a value of 8.00 for an equatorial water in $[Cu(H_2O)_6]$ further supports this observation.

Unlike Cu(II), Ni(II) and Zn(II), Ca(II) was observed to form weak complexes with the studied ligands. Several attempts, using different metal to ligand concentrations, failed to detect any interaction between Ca(II) and the two ligands $[H_2(5555)\text{-}N]$ and $[H_2(556)\text{-}N]$. Only weak complexes were formed between Ca(II) and [555-N] and [H(555)-N] as indicated by low log β_{110} values of 3.92 and 3.24 respectively. The significant presence of protonated species (MLH) in the solution equilibria of these two ligand systems, as mentioned earlier is a clear indication of the lower binding strength of these ligands towards Ca(II) as compared to the other metal ions. The formation of the ML species from the MLH species in both metal-ligand systems is due to an insignificant metal ion assisted deprotonation of the terminal amino group. The high pK_a values determined for the processes $pK^{Ca[555-N]}_{Ca[555-N]H_{-1}}$ = 11.09 and $pK^{Ca[H(555)-N]}_{Ca[H(555)-N]H_{-1}}$ = 11.27 resulting in the formation of MLH_{-1} species from ML species are only 1.2 and 1.3 log units less than the metal ion's hydrolysis constant ($pK_{Ca\text{-}OH}$ = 12.45). Therefore formation of the MLH_{-1} species is due to deprotonation of a water molecule in the two ligand systems, and this clearly indicates that Ca(II) cannot induce amide deprotonation in the case of the Ca(II)-[H(555)-N] system.

The weak complexes formed by these two systems may have resulted from the presence of the soft nitrogen donor atoms in [555-N] and [H(555)-N]. Similar results have been found for a majority of ligands with soft nitrogen donor atoms such as glycylglycine [31]. Generally, there are no reported constants of this metal ion with the majority of ligands containing nitrogen donor atoms [31]. This behaviour for Ca(II) which is classified as a hard Lewis acid (HSAB classification) is expected as this metal ion prefers ligands with hard donor atoms such as oxygen [61]. Thus the formation of weak complexes with [555-N] and [H(555)-N] and failure to form any complexes with $[H_2(5555)\text{-}N]$ and $[H_2(556)\text{-}N]$ is a result of such behaviour.

3.4.7 Selectivity

From the measured formation constants it is possible to calculate the selectivity of a ligand for a particular metal ion. The metal ion selectivity of a ligand is generally defined as the difference in the formation constants of the complexes formed with all metal ions likely to be present under the same conditions of pH [62]. Since selectivity is pH-dependent and in this study different types of metal-ligand species were formed at different pH, it is not possible to simply compare formation constants. For this reason, the selectivity of Cu(II) has been re-defined as the ratio of the total concentration of the competing metal ion required to effect 50 % complexation to the concentration of Cu(II). This definition can be summarised in the form of an equation as follows;

$$\text{Selectivity (S)} = \frac{[\text{M(II)}]}{[\text{Cu(II)}]} \qquad (3.36)$$

where [M(II)] is the total concentration of the competing metal, and [Cu(II)] is the total concentration of Cu(II).

Selectivity values were calculated in the pH range 2.50 - 11.00 for [555-N] and pH range 4.00 - 11.00 for [H(555)-N], [H_2(5555)-N] and [H_2(556)-N] using the ESTA suite of programs. For simplicity, the species due to the hydrolysis of the metal ions were excluded from the calculation, so the results obtained would be an estimation of selectivity.

The selectivity factors of the four ligands for Cu(II) relative to the other metal ions are given in Tables 3.6 and 3.7, while graphs of log selectivity (S) as a function of pH are presented in Figures 3.27 and 3.28.

Table 3.6: Selectivity (S) factors of [555-N] and [H(555)-N] ligand systems for Cu(II) relative to Ca(II) Ni(II) and Zn(II).

Ligands												
	[555-N]						[H(555)-N]					
	Cu(II)/Ca(II)		Cu(II)/Ni(II)		Cu(II)/Zn(II)		Cu(II)/Ca(II)		Cu(II)/Ni(II)		Cu(II)/Zn(II)	
pH	S	Log S	S	Log S	S	Log S	S	LogS	S	Log S	S	Log S
3.00	2×10^{8}	8.34	3.95	0.60	5×10^{4}	4.68	-	-	-	-	-	-
3.50	6×10^{8}	8.81	7.70	0.89	2×10^{5}	5.18	-	-	-	-	-	-
4.00	2×10^{9}	9.35	11.3	1.05	4×10^{5}	5.64	3×10^{3}	3.51	7×10^{4}	4.83	2×10^{6}	6.31
4.50	7×10^{9}	9.84	12.4	1.09	1×10^{6}	6.02	2×10^{4}	4.38	1×10^{5}	5.12	5×10^{6}	6.68
5.00	2×10^{10}	10.4	12.6	1.10	6×10^{5}	5.74	2×10^{5}	5.36	3×10^{5}	5.43	1×10^{7}	7.13
5.50	7×10^{10}	10.8	13.8	1.14	7×10^{4}	4.82	2×10^{6}	6.35	4×10^{5}	5.60	4×10^{7}	7.59
6.00	2×10^{11}	11.4	13.8	1.14	7×10^{3}	3.82	2×10^{7}	7.34	5×10^{5}	5.68	1×10^{8}	8.03
6.50	5×10^{11}	11.7	12.6	1.10	7×10^{2}	2.82	2×10^{8}	8.34	5×10^{5}	5.72	2×10^{8}	8.36
7.00	3×10^{11}	11.4	11.4	1.06	7×10^{1}	1.82	2×10^{9}	9.34	5×10^{5}	5.72	3×10^{8}	8.53
7.50	3×10^{10}	10.5	9.44	0.98	7.22	0.86	2×10^{10}	10.3	5×10^{5}	5.72	4×10^{8}	8.63
8.00	3×10^{9}	9.47	5.86	0.77	1.17	0.07	2×10^{11}	11.3	5×10^{5}	5.72	5×10^{8}	8.65
8.50	3×10^{8}	8.47	2.74	0.44	0.57	-0.25	2×10^{12}	12.2	5×10^{5}	5.72	4×10^{8}	8.62
9.00	3×10^{7}	7.51	1.38	0.14	0.52	-0.29	-	-	5×10^{5}	5.72	3×10^{8}	8.52
9.50	3×10^{6}	6.51	0.79	-0.11	0.49	-0.31	-	-	5×10^{5}	5.72	2×10^{8}	8.31
10.00	4×10^{5}	5.55	0.61	-0.21	-	-	-	-	5×10^{5}	5.72	9×10^{7}	7.94
10.50	5×10^{4}	4.72	0.56	-0.25	-	-	-	-	4×10^{5}	5.64	3×10^{7}	7.49
11.00	1×10^{4}	4.01	0.51	-0.30	-	-	-	-	3×10^{5}	5.54	9×10^{6}	6.97

Table 3.7: Selectivity (S) factors of $[H_2(5555)\text{-}N]$ and $[H_2(556)\text{-}N]$ ligand systems for Cu(II) relative to Ni(II) and Zn(II).

Ligands												
	$[H_2(5555)\text{-}N]$						$[H_2(556)\text{-}N]$					
	Cu(II)/Ca(II)		Cu(II)/Ni(II)		Cu(II)/Zn(II)		Cu(II)/Ca(II)		Cu(II)/Ni(II)		Cu(II)/Zn(II)	
pH	S	Log S	S	Log S	S	Log S	S	Log S	S	Log S	S	Log S
4.50	-	-	2×10^2	2.18	2×10^3	3.21	-	-	-	-	-	-
5.00	-	-	3×10^2	2.52	4×10^3	3.58	-	-	1.26	0.10	1.19	0.08
5.50	-	-	9×10^2	2.97	1×10^4	4.03	-	-	3.50	0.54	3.74	0.57
6.00	-	-	2×10^3	3.38	3×10^4	4.53	-	-	65	1.80	67.4	1.83
6.50	-	-	4×10^3	3.59	1×10^5	5.02	-	-	1×10^3	3.10	1×10^3	3.10
7.00	-	-	3×10^3	3.51	3×10^5	5.43	-	-	2×10^4	4.20	2×10^4	4.27
7.50	-	-	2×10^3	3.18	5×10^5	5.70	-	-	4×10^4	4.50	2×10^5	5.30
8.00	-	-	6×10^2	2.79	5×10^5	5.70	-	-	7×10^4	4.80	2×10^6	6.18
8.50	-	-	3×10^2	2.42	4×10^5	5.60	-	-	1×10^5	4.99	4×10^6	6.63
9.00	-	-	2×10^2	2.17	3×10^5	5.44	-	-	2×10^5	5.29	1×10^7	7.00
9.50	-	-	1×10^2	2.05	2×10^5	5.34	-	-	5×10^5	5.70	3×10^7	7.42
10.00	-	-	98.2	1.99	2×10^5	5.30	-	-	2×10^6	6.19	8×10^7	7.91
10.50	-	-	98.2	1.99	2×10^5	5.21	-	-	5×10^6	6.66	3×10^8	8.40
11.00	-	-	98.2	1.99	1×10^5	5.09	-	-	2×10^7	7.17	8×10^8	8.89

Figure 3.27: Log selectivity of (a) [555-N] and (b) [H(555)-N] for Cu(II) relative to Ca(II), Zn(II) and Ni(II) plotted as a function of pH.

(a) (b)

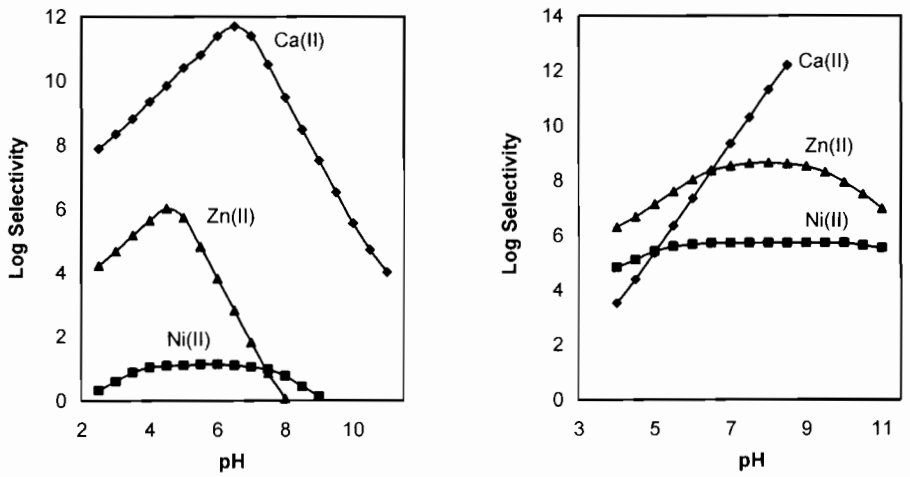

Figure 3.28: Log selectivity of (a) [H_2(5555)-N] and (b) [H_2(556)-N] for Cu(II) relative to Ca(II), Zn(II) and Ni(II) plotted as a function of pH.

(a) (b)

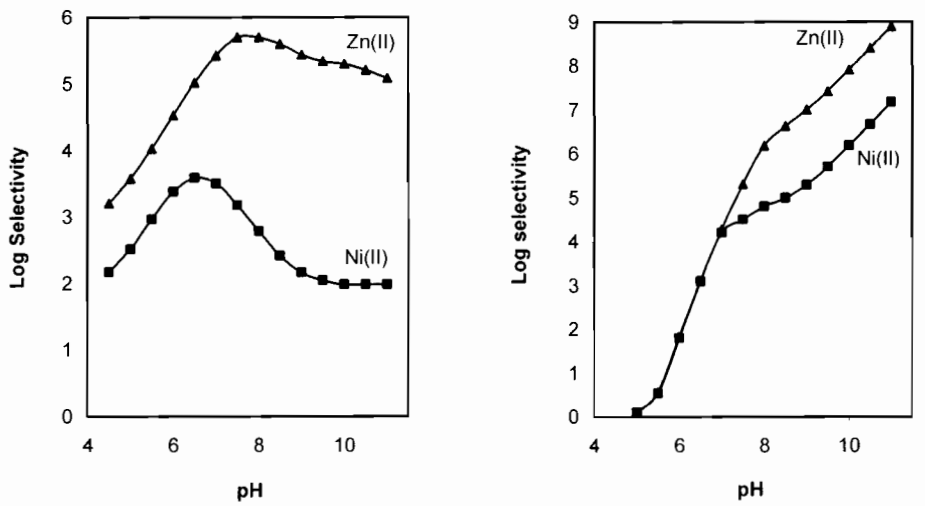

With the exception of the Ni(II)-[555-N] system, it is observed from Tables 3.6 and 3.7 that selectivity factors for Cu(II), relative to the other metal ions of several orders of magnitude are obtained for these four ligand systems. Comparable high selectivity factors for Cu(II)/Zn(II) of the order of 10^4 have been reported [41].

Figures 3.27 and 3.28 demonstrate the pH-dependence of selectivity. From these graphs, it can be observed that selectivity for Cu(II) increases generally as pH increases towards physiological pH, and then gradually decreases in the alkaline region. However, the [H_2(556)-N] ligand system is observed to be an exception to this trend, as its Cu(II) selectivity relative to both Zn(II) and Ni(II) continuously increases as pH increases. A noticeable feature about the Cu(II) selectivity factors as illustrated in Figures 3.27 and 3.28 is the following order of selectivity; Cu(II)/Ca(II) > Cu(II)/Zn(II) > Cu(II)/ Ni(II). Such an order of selectivity clearly demonstrates favourable complexation for Cu(II) by these ligand systems relative to its *in vivo* competitors, Ca(II) and Zn(II) over a wide pH range. This then suggests that the ligand systems are likely to complex Cu(II) *in vivo* under various conditions of pH despite competition from Ca(II) and Zn(II). However, the high concentrations of Ca(II) and Zn(II) *in vivo* could upset the favourable selectivity for Cu(II), so a study of an *in vivo* speciation modelling will be necessary to verify and support these selectivity results. This is the subject of detail discussion in Chapter 5.

Cu(II) selectivity is enhanced by the utilization of the ion's preference for a tetragonally distorted environment due to the ligand field Jahn-Teller distortion. This is in contrast with tetrahedral Cu(I) and Zn(II). Both these effects are exemplified by the binding site of the Cu(II) carrying plasma protein serum albumin, incorporating ionized peptide nitrogen and Cu(II) bonds in a roughly square planar, four nitrogen chelate environment [41].

3.5 Experimental

3.5.1 Introduction

The experimental procedures used in this work were similar to those used by other workers in this field [63, 64]. Generally, solutions containing different metal to ligand concentrations and ratios were titrated potentiometrically with strong base. The ionic strength of these solutions was kept as constant as possible during titration by the addition of an inert background electrolyte. The ESTA suite of programs [14] was used to analyse the resulting data to obtain the best fit of formation constants. The resulting models were used to generate theoretical formation curves which could be compared with experimental curves. The extent of the agreement between these two curves, together with the optimization statistics were used to assess the validity of the proposed model.

3.5.2 Preparation and standardisation of solutions

All the solutions used were prepared using glass-distilled or deionised water prepared by passing through a Milli-Q water purification system (Millipore Corp.) The distilled and/or purified water was boiled to remove dissolved carbon dioxide and then cooled in a container protected by a "Carbosorb" (BDH) carbon dioxide trap [5, 63, 64].

The other reagents such as $CuCl_2 \bullet 2H_2O$, $NiCl_2 \bullet 6H_2O$, $ZnCl_2$, $CaCl_2 \bullet 2H_2O$, NaCl, NaOH, HCl and EDTA (Merck) were commercially available and of analytical grade. These were used without further purification. Standard divalent metal solutions of Cu(II), Ni(II), Zn(II) and Ca(II) were prepared in calibrated volumetric flask according to Vogel's method [65] for metal standard solution preparation. Sufficient sodium chloride was added to the metal solutions to give a final ionic strength of 0.15 mol dm^{-3}. These metal solutions were standardised by direct titration against EDTA [64] which had earlier been standardised by standard Zn(II) solution prepared from carefully

weighed zinc metal. Approximately 0.02 mol dm^{-3} of each divalent cation solution (50 cm^3) prepared from the chloride salts was diluted to 100 cm^3 resulting in a solution of 0.01 mol dm^{-3}. 25 cm^3 portions of the 0.01 mol dm^{-3} divalent cation solutions were titrated with 0.01 mol dm^{-3} EDTA using the standard method of Vogel [65]. The concentrations of the metal ions ranged between 0.01917 mol dm^{-3} and 0.02060 mol dm^{-3}.

Sodium hydroxide solutions (0.100 mol dm^{-3}) were prepared under a nitrogen atmosphere from Titrisol standard ampules, with appropriate amounts of sodium chloride added to give a final ionic strength of 0.15 mol dm^{-3}. The sodium hydroxide solutions were then standardised against potassium hydrogen phthalate (KHP) using the method of Gran [66]. Hydrochloric acid solutions (0.100 mol dm^{-3}) were prepared from Titrisol standard ampules and ionic strength adjusted using sodium chloride before they were standardised against sodium tetraborate decahydrate (Borax). The sodium hydroxide solutions prepared were further standardised against standard hydrochloric acid solutions. These acid-base titrations were also used to check the carbonate content of the sodium hydroxide titrant solution using the Gran Method [66]. Ligand solutions (100 cm^3) were prepared in water and standardised by acid-base titration according to Gran's method [66]. Three buffer solutions of pH 4.00, 6.85 and 9.18 were prepared using 0.05 mol dm^{-3} potassium hydrogen phthalate, 0.01 mol dm^{-3} potassium di-hydrogen phosphate & sodium hydrogen phosphate and 0.05 mol dm^{-3} borax [65]. The solutions were used within a short period of preparation and discarded whenever signs of carbonate contamination were noticed.

3.5.3 Equipment

The potentiometric titrations were performed using a Radiometer PHM 84 research pH meter and a Metrohm Dosimat 665 piston burette, which were linked and controlled by a computer. The pH meter was equipped with a Metrohm 6.0133.100 separate glass electrode and 6.0726.100 Ag/AgCl reference electrode with a renewable liquid junction of 0.15 mol dm^{-3}. These electrodes were immersed in solutions contained in a double-walled titration

vessel thermostated at 25 ± 0.1°C by circulating water from a constant temperature Haake thermostat bath. The titrant **T** was delivered to the titrated solution **S** through an immersed capillary tip from a Metrohm Dosimat 665 piston burette using a Pascal program developed in this laboratory to monitor the electromotive force (emf) and the volume of **T** added for each titration point. These titrations were carried out at least in duplicate. Throughout the titration, the magnetically stirred solution was protected from the intrusion of atmospheric oxygen and carbon dioxide by passing a continuous flow of high purity nitrogen stream over it. The high purity nitrogen was first passed through five traps before introduced into the titration solution. These traps included the following;

- 50 % potassium hydroxide, to remove traces of carbon dioxide.
- Fierser's solution to remove traces of oxygen.
- Glass wool
- Distilled water
- Background electrolyte of 0.15 mol dm^{-3} to humidify the gas.

The last three traps were maintained at a temperature of 25 ± 0.1°C in the Haake temperature bath. A gas bubbler attached to the gas outlet from the titration vessel prevented back diffusion.

The electrode was calibrated using three buffers. The Nernstian slope over pH range 2.00 - 11.00, varied between 58.86 and 58.91. The precision calibration of the instrument was done by titration of 0.100 mol dm^{-3} sodium hydroxide from the burette against 0.100 mol dm^{-3} hydrochloric acid in the vessel and vice versa. The values of the intercept, E^o, varied from 399.6 mV to 407.6 mV, while an average pK_W value of 13.75 was determined from these acid-base titrations.

The following procedure was followed to study the reaction between each of the ligands and the divalent metal ions. Aliquots of the prepared ligand and divalent metal cation solutions were pipetted into the titration

vessel. The resulting solution was made up to 15 cm^3 using 0.15 mol dm^{-3} sodium chloride solution. This resulted in concentrations of metal ions varying from 6.25×10^{-4} to 1.22×10^{-3} mol dm^{-3}, the concentrations of the ligand from 9.33×10^{-4} to 2.43×10^{-3} mol dm^{-3} and the ratios C_L/C_M from 1.06 to 3.84. The vessel was attached to the titration apparatus, flushed with nitrogen and solution temperature stabilized at 25 °C. This was then titrated with 0.100 mol dm^{-3} sodium hydroxide solution via piston burette reading to a precision of 0.001.

3.5.4 Data analysis

The potentiometric titration data were analysed using the ESTA suite of computer programs. The collected data were imported into a preformatted data file for the purpose of calculating the electrode parameters, protonation and formation constants. The task OBJE within the ESTA2A module of the ESTA library of computer speciation modelling programs was used to calculate the required parameters. The analysis was performed by fitting these constants to the titration data, based upon minimization of the objective function, U_{obj}, with respect to emf. Since E^o, $[H^+]_{vessl}$, $[L]_{vessl}$ and $[M]_{vessl}$ were fixed, these values were not refined. Thus the required log β_{pqr}**'s** were the only values refined. Tasks ZBAR and QBAR within ESTA1 module of ESTA were used to generate complex formation and deprotonation functions from the determined log β_{pqr}**'s**. These functions served as the criteria for testing the validity of the selected potentiometric models in the data analysis. Task SPEC within the same ESTA1 module, was used to determine the species distribution diagrams as a function of pH, of all the $M_pL_qH_r$ species present in solution over the pH range of measurement.

The reproducibility and quality of the experimental data was always checked visually using the formation and deprotonation functions. In every case, repeat titrations were superimposable.

References

1. Sillién L.G., Martell A.E., (1964, Vol 1; 1971, Vol 2), Stability Constants of Metal Ion Complexes, Chemical Society Special Publications 17 and 25.
2. Beck M.T., (1972) Reaction Mechanisms in Inorganic Chemistry, Chapter 1, in International Review of Science, Inorganic Chemistry Series One, Vol 9 (ed. Tobe. M.L.). London: Butterworths.
3. Vacca A., Sabatini A., Gristina M.A., (1972), *Coord. Chem. Rev.*, **8**, 45.
4. Martell A.E., Motekaitis R.J., (1988), The determination and use of Stability Constants, VCH Publishers Inc. New York.
5. Hartley F.R., Burgess C., Alcock R.M., (1980), Solution Equilibria, Ellis Horwood Limited, Chichester, John Wiley & Sons, pp. 147-169.
6. Rossotti F.J.C., Rossotti H., (1961), The Determination of Stability Constants, New York: McGraw-Hill, pp. 127.
7. Meloun M., Havel j., Högfeldt E., (1988), Computation of Solution Equilibria, A guide to Methods in Potentiometry, Extraction and Spectrophotometry, Ellis Horwood Limited, Chichester.
8. Högfeldt E., (1982), Stability Constants of Metal-ion Complexes, Part A. Inorganic Ligands, Pergamon, New York, pp. 32.
9. Gajda T., Nagy L., Burger K., (1990), *J. Chem. Soc., Dalton Trans.*, 3155.
10. Rossotti H., (1978), The study of Ionic Equilibria, Longmans, London.
11. May P.M., Williams D.R., Linder P.W., Torrington R.G., (1982), *Talanta*, **29**, 249 -256.
12. Atkins P.W., Physical Chemistry, (1999), 6th ed., Oxford University Press: Oxford, Chapter 10.
13. Laitinen H.A., Harris W.E., (1975), Chemical Analysis, 2nd ed. New York: McGraw-Hill, pp. 5-17.
14. Murray K. May P.M., (1984), *ESTA*, "Equilibrium Simulation for Titration Analysis" UWIST, Cardiff.
15. May P.M., Murray K., Williams D.R., (1985), *Talanta*, **35**, 825.

16. May P.M., Murray K., Williams D.R., (1988), *Talanta*, **35**, 927.
17. Molday R.B., Kallen R.G., (1972), *J. Am. Chem. Soc.* **94**, 6739.
18. Martin R.B., (1972) *J. Chem. Soc. Chem. Commun.* 793.
19. Martin R.B., Hutton W.C., (1971), *J. Am. Chem. Soc.* **93**, 4752.
20. Fersht A.R., (1971), *J. Am. Chem. Soc.* **93**, 3504.
21. Jubert C., Mohamadou A., Gerard C., Brandes S., Tobard A., Bardier J.P., (2002) *J. Chem. Soc., Dalton Trans.*, 2660.
22. Jubert C., Mohamadou A., Gerard C., Brandes S., Tobard A., Bardier J.P., (2003) *Inorg. Chem. Commun.*, **6**, 900.
23. Clark J., Perrin., D.D., (1964), *Quart. Rev. Chem. Soc.*, **18**, 295.
24. Eriksen J., Monsted L., Monsted O., (1990), *Acta. Chem. Scand.*, **44**, 561.
25. Donatsch P., Gerber K.H., Zuberbuhler A., Fallab S., (1970), *Helv. Chim. Acta.*, **53**, 262.
26. Letkeman P., (1979), *J. Chem. Edu.*, **56**, 5, 348.
27. Chung C.S., (1979), *Inorg. Chem.*, **18**, 1318.
28. Purcell K.F., Kotz J.C., (1977), Inorganic Chemistry, W.B. Saunders Company, London.
29. Kramer-Schnabel U., Linder P.W., (1991), *Inorg. Chem.*, **30**, 1248.
30. Martell A.E., Smith R.M., (1975), Critical stability constants, Vol 2, Plenum Press. New York and London.
31. Martell A.E., Smith R.M., (1975) *Critical Stability Constants*, Vol 1, Plenum Press. New York and London.
32. Sabatini A., Vacca A., Gans P., (1974) *Talanta*, **21**, 53.
33. Nomkoko E.T., Jackson G.E., Nakani B.S., Bourne S.A., (2004), *J. Chem. Soc., Dalton Transactions*, 1789.
34. de Witt G.C., May P.M., Webb J., Hefter G., (1998), *Inorg. Chim. Acta.*, **275-276**, 37.
35. Zuberbühler A. Kaden Th. (1968), *Helv. Chim. Acta.*, **51**, 1805.
36. Ojima H., Nonoyama K., (1988), *Coord. Chem. Rev.*, **921**, 857.
37. Kodama M., Yatsunami T., Kimura E., (1979), *J. Chem. Soc., Dalton Trans*,. 1783.
38. Motekaitis R.J., Sun Y., Martell A.E., and Welch M.J., (1999) *Inorg. Chim. Acta*, **77**, 614.

39. Chen D., Sun Y., Martell A.E., Welch M.J., (2002), *Inorg. Chim. Acta.*, **335**, 119.
40. Santos M.A., Gaspar M., Amorim M.T., (1999), *Inorg. Chim. Acta.*, **284**, 20.
41. Frausto da Silva J.J.R., Williams R.J.P., (1991), The Biological Chemistry of the Elements. Clarendon Press, Oxford.
42. Kim M.K., Martell A.E., (1964), *Biochemistry*, **3**, 1169.
43. Kim M.K., Martell A.E., (1966), *J. Am., Chem., Soc.*, **88**, 914.
44. Kim M.K., Martell A.E., (1967), *ibid.*, **89**, 5138.
45. Freeman H.C., (1966) in: "The Biochemistry of Copper". J. Peisach, P. Aisen and W.E., Blumberg, Ed., Academic Press, New York, N.Y.
46. Gajda T., Henry B., Aubry A., Delpuech J.J., (1996), *Inorg. Chem.*, **35**, 586.
47. Gizzi P., HenryB., Rubini P., Giroux S., Wenger E., (2005), *J. Inorg. Biochem.*, **99**, 1182.
48. Sovago I., Hartman B., Gergely A., (1986), *J. Chem. Soc., Dalton Trans.*, 235.
49. Kruck T.P.A., Sarkar B., (1975), *Inorg. Chem.*, **14**, 10, 2383.
50. Lau S., Sarkar B., (1981), *J. Chem. Soc., Dalton Trans.* 491.
51. Kruck T.P.A., Lau S., Sarkar B., (1976), *Can. J. Chem.*, **54**, 1300.
52. Iyer K.S.; Lau S.; Laurie S.H.; Sarkar B.; (1978), *Biochem. J.*, 169.
53. Glennon J.D.; Sarkar B.; (1982), *Biochem. J.*, **203**, 15.
54. Koike T. and Kimura E., (1991), *J. Am. Chem. Soc.*, **113**, 8935.
55. Koike T., Kimura E., Shiota T., Koike T., Shiro M. and Kodama M., (1990), *J. Am. Chem. Soc.*, **112**, 5805.
56. Baes C.F., Jr., Mesmer R.E., (1976), The Hydrolysis of Cations, A Wiley-Interscience Publication, 137.
57. Irvine H., Williams J.P.R., (1948), *Nature*, **162**, 746.
58. Irvine H., Williams J.P.R., (1953), *J. Chem. Soc.*, 3192.
59. Zuberbuehler A., Fallab S., (1967), *Helv. Chim. Acta.*, **50**, 889.
60. Bu X.H., An D.L., Cao X.C., Zhang R.H., Clifford T., Kimura E., (1998), *J. Chem. Soc., Dalton Trans.* 2247.
61. Pearson R.G., (1985), *J. Am. Chem. Soc.*, **107**, 6801.

62. Comba P., Hambley T.W., (1995), Molecular Modeling of Inorganic Compounds; VCH: Weinheim.

63. Jackson G.E., Kelly M.J., (1989), *J. Chem. Soc., Dalton Trans.*, 2429.

64. Jackson G.E., Nakani B.S., (1996), *J. Chem. Soc., Dalton Trans.*, 1373.

65. Furniss B.S., Hannaford A.J., Smith P.W.G., Tatchell A.R., (1989), Vogel's Practical Organic Chemistry, 5th edn., Longman Scientific & Technical.

66. Gran G., (1952), *Analyst*, **77**, 661.

CHAPTER FOUR

Ancillary studies

4.1 UV-Visible Spectroscopy

4.1.1 Introduction

The interaction of electromagnetic radiation of wavelength in the UV-Visible region with transition metal chelates gives rise to UV-Visible spectra of these complexes. Electronic spectroscopy is concerned with electronic transitions between orbitals of different energy in transition metal chelates. A common transition is one where an electron is promoted from the occupied orbital of highest energy to the vacant orbital of lowest energy. The absorption bands caused by the promotion of an electron from a lower to a higher d orbital of the metal ion are labelled as d $\rightarrow$ d bands. The energy difference between such orbitals in organic and inorganic molecules lies between 1.5×10^5 and 6.0×10^5 J mol $^{-1}$ [1], and the corresponding transition gives rise to absorption in the ultraviolet and visible regions of the electromagnetic spectrum [2]. Thus spectra of complexes of transition metal ions exhibit absorption bands in the visible region of the spectrum and the complexes are highly coloured. A study of electronic spectra for such complexes gives information about the electronic structure of molecules and often allow structural aspects of the complexes to be determined [3].

4.1.2 Theory

In a free, gaseous transition metal ion the five d orbitals have the same energy, ie., they are degenerate. The degeneracy of the metal d orbitals is lost when the transition metal ion is surrounded by a field of negative charge in the form of ligand presence. For an octahedral complex the ligands are located at the corners of an octahedron, with the metal ion located at the centre of the complex experiencing a non-spherical field. Thus the electron density of the ligands is oriented directly along the x, y and z axes, resulting in greater electron repulsion between electrons of the metal ion and the electrons of the ligand for orbital oriented along the axes than those oriented in between the axes. As a consequence, the d orbitals are split into two sets

of different energy: a doubly degenerate set (e_g) of higher energy and a triply degenerate set (t_{2g}) of lower energy. The difference in energy between these sets of orbitals is termed the ligand field splitting and is represented by the symbol Δ or 10Dq. When an octahedral complex is formed the energy of each of the e_g orbitals is raised by 6Dq ($3/5\Delta$) relative to their energy in the spherical field while the corresponding decrease in energy for the t_{2g} orbitals is 4Dq ($2/5\Delta$).

The following selection rules are pertinent to electronic absorption spectroscopy:

(i) Transitions between states of different multiplicity are multiplicity forbidden, ie., electronic transitions in which the spin of an electron changes are forbidden.

(ii) In a molecule which has a centre of symmetry, transitions between two gerade or two ungerade states (ie., g $\rightarrow$ g or u $\rightarrow$ u) are Laporte forbidden. The allowed transitions are g $\rightarrow$ u and u $\rightarrow$ g.

As a result of rule number (ii), d $\rightarrow$ d transitions in octahedral complexes are Laporte forbidden and therefore many complexes will be colourless. However, most ions do not have perfect symmetry, and are distorted so that the centre of symmetry is destroyed, resulting in mixing (hybridization) of d and p orbitals.

UV-Visible spectroscopy measures the wavelength of maximum absorption of each species in solution, i.e., λ_{max}. This wavelength is related to the energy of the absorbed radiation by the following well-known expression,

$$\mathbf{E} = \mathbf{h\nu} = \frac{\mathbf{hc}}{\boldsymbol{\lambda}} \qquad (4.1)$$

where h is Planck's constant and c is the speed of light. Equation (4.1) gives a measure of the ligand field stabilization energy. This does not however give a direct measure of the strength of bonding, but only the amount by which the degenerate d-orbitals of the metal ion have been split due to the crystal field,

or more precisely the ligand field experienced by the central metal ion in solution.

The nature of the ligands in a complex affect the energy of the d $\rightarrow$ d transitions for a particular transition metal ion. It has been found that the following ligands can be arranged in a series I^-, Br^-, SCN^-, Cl^-, NO_3^-, F^-, OH^-, H_2O, NH_3 and CN^-, where on moving from left to right along the series the effect on the absorption maximum of the d $\rightarrow$ d band is to move it to shorter wavelength, ie the 10Dq value of the ligand increases on moving from left to right. This effect can be illustrated for the ligands NH_3 and H_2O by substituting NH_3 for H_2O in the complex $[Cu(H_2O)_6]^{2+}$ where it has been found that the absorption maximum for the d $\rightarrow$ d band in the complex $[Cu(H_2O)_{6-n}(NH_3)_n]^{2+}$ [4] shifts progressively to the blue as n is changed from 0 to 4.

The concentration of species in a system may be determined by measurement of the absorption of radiation by the species. A relationship relating concentration and absorption is the Beer-Lambert law, which can be expressed in the following form;

$$\log_{10}\frac{I_o}{I} = \epsilon\, c\, b \qquad (4.2)$$

where I_0 and I are the intensities of incident and transmitted radiation respectively, c is the molar concentration of absorbing species, b is the thickness of absorbing layer and ϵ is the extinction coefficient. The term $\log\frac{I_o}{I}$ is called the absorbance and is represented by the symbol A, with this law becoming, $A = \epsilon\, c\, b$. For electronic absorption spectra of solutions containing more than one absorbing species the Beer-Lambert Law can be expanded to give a linear combination of terms for each individual species, as follows,

$$A^{\lambda} = b(\epsilon_1^{\lambda} c_1 + \epsilon_2^{\lambda} c_2 + \ldots\ldots \epsilon_i^{\lambda} c_i) = b\sum \epsilon_i^{\lambda} c_i \qquad (4.3)$$

where all the terms are as defined earlier. The molar absorptivities or extinction coefficients are characteristics of the molecular electronic spectra and they should be positive, smooth when plotted as a function of wavelength, with no sharp discontinuities present and prediction of isosbestic points should be borne out by experiment [5].

Observed spectra in a typical M(II) chelate, consist of a series of crystal field bands, which depend on donor atoms of the ligand system and metal ion [6]. The Ni(II) ion (d^8) exhibits a variety of coordination geometries giving different electronic spectra characteristic of these geometries. The most common geometry for this metal ion is an octahedral arrangement of donor atoms around the central metal ion, with the degeneracy of E and T terms partially or wholly lifted. Ni(II) chelates are normally green in colour and they exhibit three spin-allowed crystal field bands corresponding to $v_1 = {}^3T_{2g}(F) \leftarrow {}^3A_{2g}(F)$, $v_2 = {}^3T_{1g}(F) \leftarrow {}^3A_{2g}(F)$ and $v_3 = {}^3T_{1g}(P) \leftarrow {}^3A_{2g}(F)$ as would be expected in an octahedral field [6]. These absorption bands (v_1, v_2 & v_3) generally fall within the ranges 7, 000 - 13, 000; 11, 000 - 20, 000 and 19, 000 - 27, 000 cm^{-1} respectively, with intensities less than 30 $dm^3 mol^{-1} cm^{-1}$ in a regular octahedral system. In addition to these three spin-allowed absorption bands, two spin-forbidden bands are often observed, and these correspond to transition to the ${}^1E_g$ and ${}^1T_{2g}$. Generally square planar complexes differ from those given above in that absorption below 10, 000 cm^{-1} is not seen because the ligand field strength in these complexes is very high [6].

Unlike Ni(II), the colour of Cu(II) complexes are generally blue or green due to a broad absorption band in the 540 - 800 nm region of the spectrum. The envelop of this band encompasses several overlapping transitions but definitive resolution of the sub-bands with correct locations is difficult due to the large half-width [6]. In a tetragonally distorted octahedral system, these sub-bands correspond to the spin-allowed ${}^2A_{2g} \leftarrow {}^2B_{1g}$, ${}^2B_{2g} \leftarrow {}^2B_{1g}$ and ${}^2E_g \leftarrow {}^2B_{1g}$ transitions. These transitions can only be resolved unambiguously

when polarised spectra of single crystals have been measured [6]. Like Ni(II), Cu(II) systems with close to or square planar coordination, will not have electronic absorption below 10 000 cm^{-1} due to the very high ligand field strength in these complexes [6]. The square planar Cu(II) complexes are generally brown or reddish in colour. For other weak field systems these colours are due to the strong charge transfer bands in the ultra violet region tailing off into the blue end of the visible spectrum [6].

Tetrahedral geometry is not common for Cu(II) and Ni(II) as compared to the square planar geometry. This geometry is usually stabilised by π-donor ligands (weak field ligands) such as halides while π-acceptor ligands (strong field ligands) such as PR_3 and CN^- promote square planar geometries. Tetrahedral Ni(II) complexes are generally highly coloured (blue or green) with three expected d $\rightarrow$ d transitions, ie $v_1 = {}^3T_2(F) \leftarrow {}^3T_1(F)$, $v_2 = {}^3A_2(F) \leftarrow {}^3T_1$ and $v_3 = {}^3T_1(P) \leftarrow {}^3T_1(F)$. However the observed spectra tend to be complicated by spin-orbit coupling effects [6].

Billo [7] has proposed a method for calculating v_{max} (λ_{max}) for a tetragonally distorted Cu(II) complex, with axially coordinated water molecules. The v_{max} of the d $\rightarrow$ d band of the Cu(II) complex in an aqueous solution spectra can be expressed as the sum of individual ligand-field contributions from the four donor atoms which, with Cu(II), define the square planar. This is given in equation 4.4 where $v_i(10^3 cm^{-1})$ is the contribution of each of the four coordinating groups make to the calculated absorption frequency.

$$\mathbf{v}_{calc} = \sum \mathbf{v}_i \qquad (4.4)$$

According to Billo [7], the contribution of an amino group, $v_N = (4.53 \pm 0.07) \times 10^3$ cm^{-1}, and a peptide group $v_N = (4.85 \pm 0.04) \times 10^3$ cm^{-1}, while that for carbonyl, H_2O and OH^-, $v_O = (3.01 \pm 0.03) \times 10^3$ cm^{-1}. Although Billo's equation (4.4) can predict v_{max} (λ_{max}) of several of these types of complexes with good accuracy, the equation cannot predict absorption maxima of

mixtures which are likely to be present in solutions containing axially coordinating solvent molecules such as water.

4.1.3 Cu-L systems

Distinct colour changes were observed as the potentiometric titrations progressed for all the Cu(II)-[555-N], [H(555)-N], [H_2(5555)-N] and [H_2(556)-N] systems. This was a result of the changing speciation of the solution with pH, forming different complex species with different absorption spectra. Therefore aqueous electronic absorption spectra were measured for these Cu(II)-ligand systems in the pH range 2.00 - 11.00 and wavelength region 400 - 800 nm.

4.1.3.1 [555-N]

Figure 4.1 shows the UV-Visible electronic spectra of the Cu(II)-[555-N] system as a function of pH.

Figure 4.1: Electronic spectra for solutions containing Cu(II) (5.3×10^{-4} *mol dm*$^{-3}$) and [555-N] (1.1×10^{-3}*mol dm*$^{-3}$).

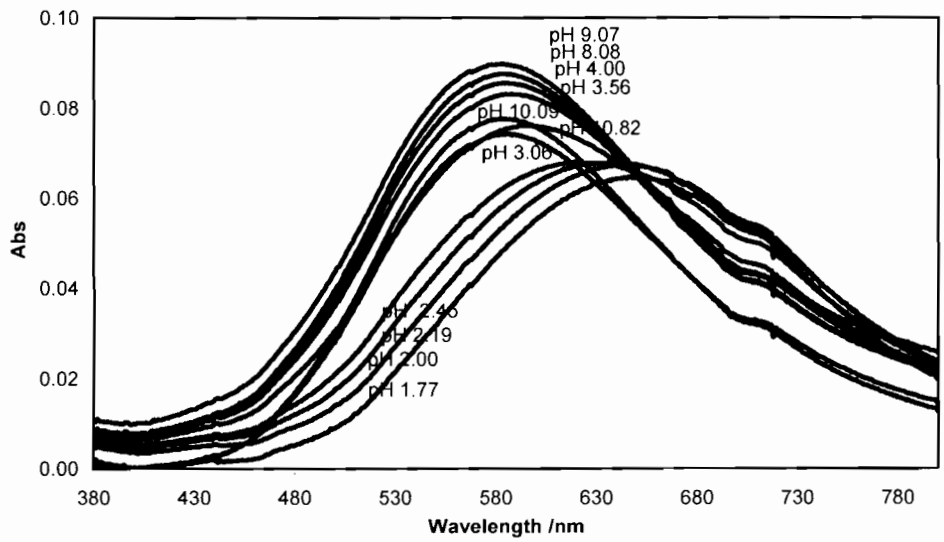

Before titration of base, complex formation has already taken place (curves for pH 1.77, 2.00 & 2.19) and the dominant complex species is that of CuN_2 with maximum absorption at 641 nm instead of CuO_6, with H_2O as ligands which normally forms under such low pH. As pH is increased, the band maximum shifts to shorter wavelengths and increases in intensity up to a pH value of 9.07, above which the intensity decreases with a slight red shift in wavelength. The curves at pH values in the range 1.77 - 2.45 exhibit a maximum absorbance at a wavelength of 644 nm. Beyond a pH value of 2.45, the curve maximum displaces by about 60 nm to a wavelength of 580 nm. Such typical blue shift in wavelength is characteristic of increase in the coordination of donor atoms around the metal ion. The MLH_{-1} species of this system has a reduced absorbance at a λ_{max} value of 580 nm. From the potentiometric results we have proposed that this species is derived from the ML species by hydrolysis of a coordinated water molecule. It is well known that increased axial coordination decreases the energy of the three spin-allowed Cu(II) d $\rightarrow$ d transitions [8].

4.1.3.2 [H(555)-N]

Figure 4.2 shows the UV-Visible electronic spectra of the Cu(II)-[H(555)-N] system as a function of pH. At low pH before titration of base, little complex formation takes place (curve for pH = 3.10) and the dominant complex is that of CuO_6, with H_2O as ligands. Thus the wavelength absorption maximum (λ_{max}) at 760 nm at this acidic pH range is easily seen in this Cu(II)-[H(555)-N] system. This absorption is due to the predominant uncomplexed octahedral $[Cu(OH_2)_6]^{2+}$ complex species since for such a complex the separation of the t_{2g} - e_g orbitals is about 770 nm for CuO_6 as opposed to 550 nm observed for CuN_4 [6].

Figure 4.2: Electronic spectra for solutions containing Cu(II) (8.5×10^{-4} *mol dm*$^{-3}$) and [H(555)-N] (1.8×10^{-3}*mol dm*$^{-3}$).

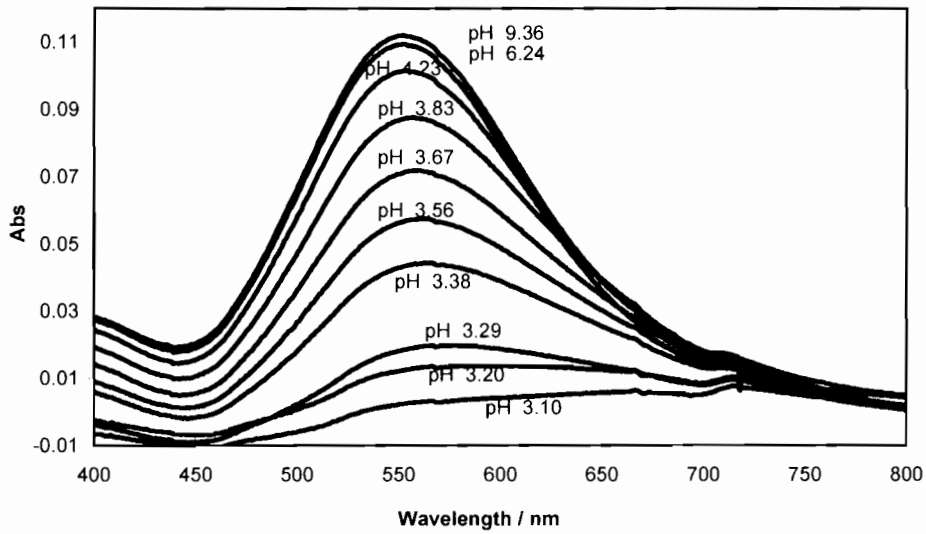

As the pH increases, the band maximum increases in intensity (curves for pH 3.20; 3.29 and 3.38). Further increase in pH (curves for pH 3.56; 3.67; 3.83; 4.23 and 6.24) causes the absorption band to shift to shorter wavelengths due to the Cu-O to Cu-N bond rearrangements as Cu(II) complexes of the type CuN_4 are formed and the deprotonation reaction at the amide site occurs. No further changes were observed when the hydroxide ion was added after formation of the MLH_{-1} species in this system.

4.1.3.3 [H_2(5555)-N]

The electronic absorption spectra for the Cu(II)-[H_2(5555)-N] system are shown in Figure 4.3. At low pH (curves for pH 3.18 and 3.41), the spectrum is the same as that of $[Cu(OH_2)_6]^{2+}$. As pH increases the band maximum increases in intensity (curves for pH 3.80; 4.00; 4.21) with a slight shift to shorter wavelength. Above pH 4.21 the band maximum increases in intensity with no further blue shift observed until a pH of 8.00.

Figure 4.3: Electronic spectra for solutions containing Cu(II) (9.7×10^{-4} *mol* dm^{-3}) and [H_2(5555)-N] (2.1×10^{-3}*mol* dm^{-3}).

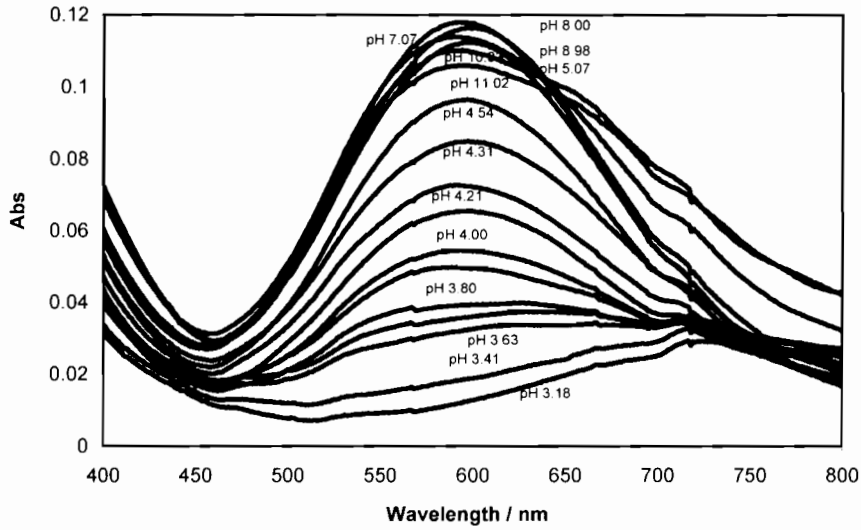

4.1.3.4 [H_2(556)-N]

Figure 4.4 shows the UV-Visible electronic spectra of the Cu(II)-[H_2(556)-N] system as a function of pH. Like the other two latter systems above before addition of base, practically no complex formation takes place (curve for pH 3.05). As base concentration is increased, the absorption bands shift slightly towards shorter wavelength with increase in intensity (curves for pH 4.67; 4.90; 5.90; 5.13). A noticeable feature about the absorption bands is that they remain the same in the pH range 8.20 - 10.33 when the hydroxide ion was added after formation of the MLH_{-2} species. This result suggests that there is no further reaction between this species with the base above pH 8.20.

Figure 4.4: Electronic spectra for solutions containing Cu(II) (7.5×10^{-4} *mol dm*$^{-3}$) and [H_2(556)-N] (1.5×10^{-3}*mol dm*$^{-3}$).

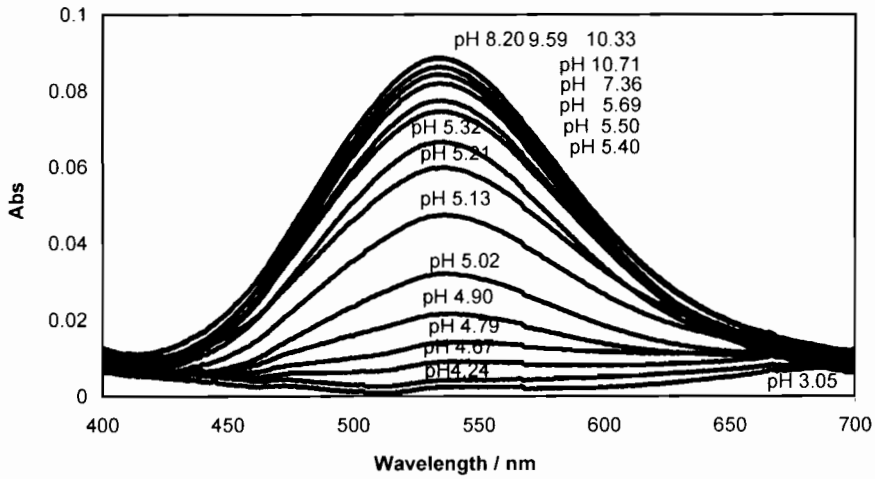

Generally large shift of λ_{max} is indicative of a re-arrangement of the ligands positioned in the coordination sphere of the Cu(II) ion. If the amide nitrogen donors are coordinated to Cu(II), besides the α-NH_2 nitrogen, then a λ_{max} less than 600 nm should be observed. Work reported by Hartzell and Gurd [9], Bryce and Gurd [10] shows the relationship of resulting visible light absorption as a function of coordination bonds involved in Cu(II)-peptide complexes. Characteristic absorption bands have been established [9, 10] for complex species in which the α-NH_2 and subsequent peptide nitrogen donors are involved. These characteristic absorptions are stated below as;

α-NH_2+1 peptide amide nitrogen, λ_{max} = 660 nm;
α-NH_2+2 peptide amide nitrogen, λ_{max} = 575 nm;
α-NH_2+3 peptide amide nitrogen, λ_{max} = 515 nm.

A λ_{max} value of 530 nm observed for the MLH_{-1} species of the Cu(II)[H_2(556)-N] system is therefore consistent with the presence of an amino nitrogen, two peptide nitrogens and a pyridyl nitrogen in the coordination sphere of the Cu(II) ion.

4.1.3.5 Calculated spectra

To gain more insight into the coordination geometries of the complexes present within the pH range studied, individual species spectra have been calculated by analysis of the UV-Visible data using a local BASIC program [11] to solve the expanded Beer-Lambert Law equation. The electronic spectra computed from the spectrophotometric titrations and formation constants of the different Cu(II) complexes with [555-N], [H(555)-N], [H_2(5555)-N] and [H_2(556)-N] for the individual species are shown in Figure 4.5 while Table 4.1 shows the wavelength and molar extinction coefficient values corresponding to maximum absorption of the Cu(II) species formed in solution with these ligands. Calculated absorption spectra using Billo's method as well as those of $[Cu(NH_3)_n(H_2O)_{6-n}]^{2+}$ [4] have also been included in Table 4.1 for comparison.

The smoothness of the deconvoluted spectra lends confidence to the analysis. This is in further support of the potentiometric model, as it has been reported before that the use of an incorrect potentiometric model in the analysis of the data gives rise to disjointed electronic spectra [12]. Also the $[Cu(H_2O)_6]^{2+}$ curve is accurately predicted and reproduced. Each metal species shows a single absorption band corresponding to three overlapping spin-allowed transitions $^2A_{2g} \leftarrow {}^2B_{1g}$, $^2B_{2g} \leftarrow {}^2B_{1g}$, $^2E_g \leftarrow {}^2B_{1g}$, characteristic of a d^9 tetragonally distorted Cu(II) complex [6, 13]. Since this is a d^9 system, the crystal-field splitting is in turn affected by the coordination sphere of the metal ion and, hence λ_{max} affords a measure of the solution structure of the complex.

The wavelength absorption maximum (λ_{max}) at 760 nm with a low molar extinction coefficient in acidic pH range 2.50 - 3.00 is observed for the Cu(II)-[H(555)-N]/[H_2(5555)-N]/[H_2(556)-N] systems. This absorption is due to the predominant uncomplexed octahedral $[Cu(OH_2)_6]^+$ (ML) complex species with a molar extinction coefficient of 29.5 $dm^3\ mol^{-1}\ cm^{-1}$ [6]. Pure aqua ion of

Figure 4.5: Calculated visible spectra for Cu(II) complexes of [555-N] (L^1), [H(555)-N] (L^2), [H_2(5555)-N] (L^3) and [H_2(556)-N] (L^4).

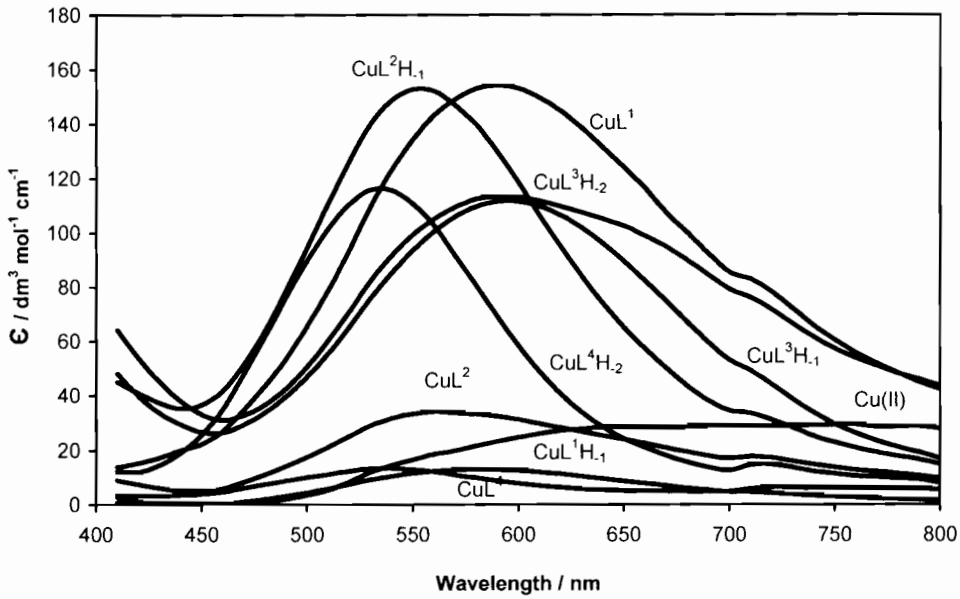

Cu(II) have been reported to have an extinction coefficient value of 12 dm^3 mol^{-1} cm^{-1} at a λ_{max} of 810 nm [14]. With the exception of [555-N] the presence of these hydrated complexes partly indicates the lower affinity of the donor atoms of these ligands towards Cu(II) ions at low pH. This may be viewed as the lack of the necessary orientation of the ligands' nitrogen lone pair electrons towards the metal ion to enhance complexation under acidic conditions.

Billo [7] has proposed a method for calculating ν_{max} (λ_{max}) for a tetragonally distorted Cu(II) complex with axially coordinated water molecules. This was given in equation 4.4. However Billo [7] does not report a value for ν_N (pyridyl nitrogen) and this was estimated from the visible spectrums of the MLH_{-1} species for the Cu(II)-[555-N], [H(555)-N], [H_2(5555)-N] systems and MLH_{-2} species for the Cu(II)-[H_2(556)-N] system. A value of 4.16×10^3 cm^{-1} was estimated and assumed for the pyridyl nitrogen.

Table 4.1: Wavelength (nm) and molar extinction coefficients values (dm^3 mol^{-1} cm^{-1}) in brackets, corresponding to the maximum absorption of the various Cu(II) species formed in solution with [555-N], [H(555)-N], [H_2(5555)-N] and [H_2(556)-N]. For comparison calculated absorption spectra using Billo's method have been included.

Ligand	M	ML	MLH_{-1}	MLH_{-2}
[555-N]	760 (29.5)	590 (154.2)	580 (13.1)	-
[H(555)-N]	760 (29.5)	560 (34.1)	550 (152.8)	-
[H_2(5555)-N]	760 (29.5)	-	590 (111.7)	590 (113.5)
[H_2(556)-N]	760 (29.5)	540 (19.2)	540 (4.13)	530 (115.9)
Calculated	-	563 (Cu[555-N])	563 (Cu[555-N]H_{-1})	580 (Cu[H_2(5555)-N]H_{-2})
Calculated	-	663(Cu[H(555)-N]	553 (Cu[H(555)-N]H_{-1})	544 (Cu[H_2(556)-N]H_{-2})
Calculated	-	-	591 (Cu[H_2(5555)-N]H_{-1})	
NH_3 in $[Cu(NH_3)_n(H_2O)_{6-N}]^+$	790 (n=0)	745 (n=1)	680 (n=2) 645 (n=3)	590 (n=4)

Since a pyridyl nitrogen has been observed to exhibit poor basicity in this work, this value appeared to be a consistent and reasonable estimate given that it is greater than that of CO but less than the one for an amine. The structural elucidation was therefore made by comparing the spectra of Figure 4.5 with the calculated [7] absorption spectra of the Cu(II) complexes. To clarify the comparison, the λ_{max} values for the complexes of this study together with those calculated as well as those of $[Cu(NH_3)_n(H_2O)_{6-n}]^{2+}$ [4] have been given in Table 4.1, while the proposed structures for the various species have already been given in Chapter three (Figures 3.24 & 3.25).

Figure 4.5 and Table 4.1 indicate that the ML species for the four ligands investigated with Cu(II) have λ_{max} values of 590 ([555-N]), 650 nm ([H(555)-N]) and 540 nm ([H_2(556)-N]) while the MLH_{-1} species have λ_{max} values of 580 ([555-N]), 550 nm ([H(555)-N]), 590 nm ([H_2(5555)-N]) and 540 nm ([H_2(556)-N]. The MLH_{-2} species which were only detected for the Cu(II)-[H_2(5555)-N] and the Cu(II)-[H_2(556)-N] systems have λ_{max} values of 590 nm and 530 nm respectively. The λ_{max} values for ML species of the Cu(II)-[555-N] system, MLH_{-1} species of the Cu(II)-[H(555)-N] system and MLH_{-2} species of the Cu(II)-[H_2(556)-N] system are similar to those for $[Cu(NH_3)_4(H_2O)_2]^{2+}$, indicating the presence of four nitrogen donor atoms in the coordination sphere of the Cu(II) ion of these species. Further support for this conclusion arises from the absence of M(HL) species in the potentiometric studies for these systems. For instance, in the pH range in which ML species predominates, for the Cu(II)-[555-N] system (2.00 -10.00) and the Cu(II)-[H(555)-N]) system (3.00 -5.00) any uncoordinated amino group would be protonated. Absence of M(HL), then implies binding of all the amino nitrogen donors in the three ligand systems. Furthermore, the relatively high stability of the ML species, particularly for the Cu(II)[555-N] system (log β_{110} = 18.6) implies a denticity of four.

At pH values as low as 2.00, the Cu(II)-[555-N] complex exists as the ML species with a λ_{max} at 590 nm. As the pH increases the coordination number of the metal ion increases until all the four nitrogen donor atoms are coordinated to the metal centre. A molar extinction coefficient value of 154.2 $dm^3\ mol^{-1}\ cm^{-1}$ for the ML species of this system suggests typical tetragonally-distorted environment of donor atoms. There is a drop in the molar extinction coefficient when an MLH_{-1} species is formed without any reasonable red shift observed as is usually expected when loss of a proton from coordinated water occurs [15]. However a drop in the extinction coefficient value suggests that the loss of this proton is from an axially coordinated water molecule, an observation consistent with the potentiometric results.

In the pH range 3.30 - 9.40, the λ_{max} value for the Cu(II)-[H(555)-N] system shifts to an absorption maximum of 550 nm due to the predominance of MLH_{-1} complex species of MN_4 coordination. A blue shift of 10 nm observed from ML to MLH_{-1} λ_{max} is due to rearrangement from O to N binding with extra nitrogen donor atom coordinated to the metal ion resulting in a square planar geometry. An increase of $\in_{max}$ from 60.5 dm^3 mol^{-1} cm^{-1} to 152.8 dm^3 mol^{-1} cm^{-1} is in support of this change in coordination [6]. A λ_{max} of 564 nm is calculated for the MLH_{-1} species of the Cu(II)[H(555)-N] system with structure given in 3.24e(i) postulated. This is in good agreement with the experimental λ_{max} of 550 nm observed for an MLH_{-1} species of the Cu(II)-[H(555)-N] system, and this lends support to the proposed structure. Moreover, the calculated λ_{max} for the ML species of the Cu(II)-[H(555)-N] system (663 nm) proposed from the potentiomeric results as given in Figure 3.24d(ii) do agree with the observed λ_{max} of 650 nm, while calculated λ_{max} for the ML (575 nm) and MLH_{-1} (575 nm) species of the Cu(II)-[555-N] system are reasonably close to the experimental values of 590 and 580 nm respectively.

The $[H_2(5555)-N]$ ligand system, is a nucleating O_2N_5 type ligand capable of donating five nitrogen atoms, two aromatic, two amidic and one secondary amine. It also includes two carbonyl oxygen atoms which can serve as potential donor atoms. An absorption maximum of 590 nm is observed for both the MLH_{-1} and MLH_{-2} species of the Cu(II)-$[H_2(5555)-N]$ system. The calculated absorption spectra for these two species differ only by a marginal 11 nm, and are given in Table 4.1 as 591 and 580 nm respectively. Such close agreement in the λ_{max} values for these two species suggests that the metal ion is coordinated by the same number of donor atoms in the two species. From Figure 4.5, it can be observed that the maximum absorbance value for the MLH_{-1} species is slightly lower than that of the MLH_{-2} species. This then suggests that although both the MLH_{-1} and MLH_{-2} species have the same number of donor atoms, the nature of the donor atoms in these species is different. A λ_{max} value of 590 nm would be consistent with the structure given in Figure 3.25b(i) for the MLH_{-2} species for this system. The structure given in Figure 3.25b(ii) with five donor atoms would be expected to have

much lower value for λ_{max}. Moreover coordination of both pyridyl nitrogen donors is likely to result in a highly strained structure. The fact that reduced absorbance is observed for the MLH_{-1} species suggest that one of the three donor atoms in this species is an oxygen donor. This is then consistent with the structure given in Figure 3.25a(iii). Nonoyama [16], Mascharak and co-workers [17] have described an octahedral complex with a structure like the one given in Figure 3.25b(ii) for this pentadentate ligand. In their description the sixth site is achieved by the fixation of a water molecule to the axial site. However experimental evidence in this current work is at variance with these findings, suggesting coordination of three nitrogen donors in both the solution MLH_{-1} and MLH_{-2} species for the Cu(II)-[H_2(5555)-N] system. The currently proposed structures for the two species are more feasible as opposed to the penta-coordinated system given in Figure 3.25b(ii) due to ligand strain around the amide-N atoms for such a complex structure. By using molecular mechanics minimum energy structures can be obtained and used to give some insight in the relative stability of these structures in terms of internal energy. This will be the subject of discussion in section 4.4.

A λ_{max} of 530 nm for the MLH_{-2} species in Cu(II)-[H_2(556)-N] system clearly indicates presence of four nitrogen atoms in the coordination sphere of the Cu(II) ion in a square-planar arrangement. A high extinction coefficient value of 115.9 $dm^3\ mol^{-1}\ cm^{-1}$ supports such geometry. Calculated absorption spectra of 544 nm as given in Table 4.1 confirms the experimental results. Thus the ligand is postulated to coordinate the metal ion as shown in the structure given in Figure 3.25(f)(i) as earlier suggested by the potentiometric data.

Any slight discrepancy between the calculated and the experimental λ_{max} values given above could be due to failure of Billo's method [7] for solution mixtures containing axially coordinating solvent molecules such as water. However, these results predict the same structures as proposed from the potentiometric results and no other possibilities give as good agreement with the observed λ_{max}.

4.1.4 Ni-L systems

Distinct colour changes were only observed for the Ni(II)-[H_2(556)-N] system, while the Ni(II)-[555-N], [H(555)-N] and [H_2(5555)-N] systems remained clear during the potentiometric titrations. Therefore reasonable absorption spectra were obtained with the former metal-ligand system while the later metal-ligand systems generated absorption spectra similar to the non coordinated ligand system. Generally, in this study, the Ni(II) spectrophotometric spectra are less informative than the Cu(II) spectra.

4.1.4.1 [H_2(556)-N]

The absorption spectra and electronic spectra for individual species of the Ni(II)-[H_2(556)-N] system as a function of pH are given in Figure 4.6. Before addition of base, practically no complex formation takes place (curve for pH 2.47). As the base concentration is increased the intensities of the absorption bands, one centred at 301 nm and the other at 430 nm, increases (curves for pH 6.72, 7.00 and 7.23). The absorption bands centred at 301 nm increases in intensity more significantly as compared to the band centred at 430 nm. At pH values below 2.50 the solution is made up of the hydrated $[Ni(OH_2)_6]^+$ species with molar extinction coefficient less than 10 $dm^3\ mol^{-1}\ cm^{-1}$. The presence of absorption bands on the longer wavelength side (430 nm) indicate the presence in this solution of a species with a geometry different from the octahedral ML species for the Ni(II)[H_2(556)-N] system. As titration progresses formation of the MLH_{-2} species becomes apparent, and the presence of such a species influence the band maximum at λ = 430 nm, with a square planar yellow species formed at pH 9.69. The MLH_{-2} species for alanylglycylhistamine, a related peptide has been reported [18] to give an absorption band at λ = 417 nm at pH 6.30. Most Ni(II) complexes coordinated with deprotonated acid amide-nitrogen atoms have been reported to be diamagnetic and square-planar [19, 20]. The two deprotonated amide groups provide a strong ligand field leading to singlet ground state Ni(II).

Figure 4.6: (a) Electronic spectra and (b) individual species absorption spectra of solutions containing Ni(II) ($3.7 \times 10^{-4} mol\ dm^{-3}$) and [$H_2$(556)-N] ($1.5 \times 10^{-3} mol\ dm^{-3}$).

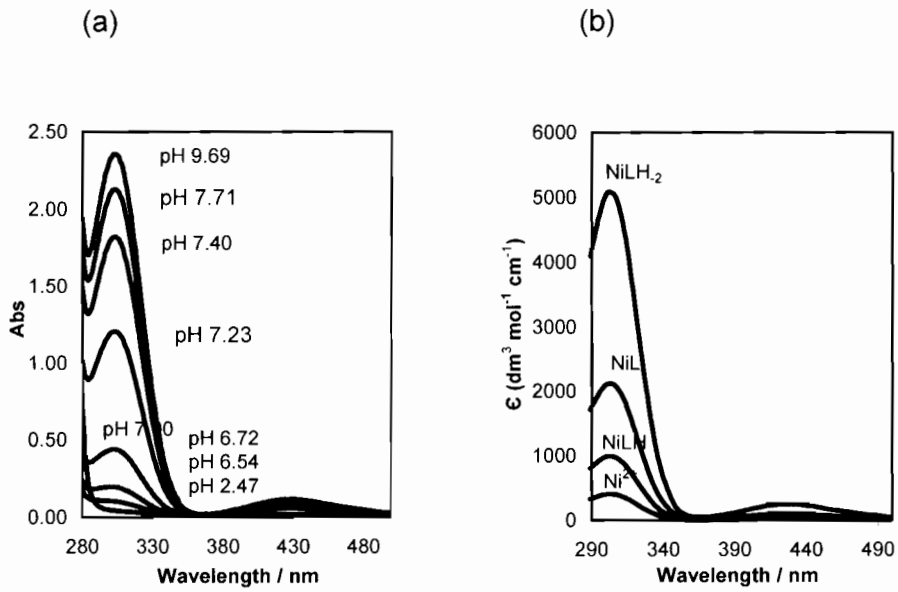

The two absorption bands seen in the spectra at 301 nm and 430 nm are a result of the transitions, $^3T_{1g}(P) \leftarrow {}^3A_{2g}$ and $^3T_{1g}(F) \leftarrow {}^3A_{2g}$ respectively. The former absorption band however, is obscured by a ligand to metal charge transfer (LMCT) band. The two transitions with low molar extinction coefficients are typical of Ni(II) in an octahedral environment in the acidic pH range, where this metal ion is unable to bind to the ligand donor atoms. Above pH 2.47, the band centred at 301 nm becomes more intense. This is an LMCT transition originating from the carbonyl oxygen and deprotonated amide nitrogen to the vacant $^1A_{2g}$ orbital of the metal ion. The molar extinction coefficient of such a band for the MLH, ML and MLH_{-2} species as given in Figure 4.7(b) is in the range of 1000 to 5000 $mol^{-1}\ dm^3\ cm^{-1}$ indicating the CT character of the system.

Three O^-, N^- and $NH_2 \rightarrow Cu^{2+}$ CT transitions have been proposed [21] to lie at 385, 327 and 277 nm respectively. The intra-ligand $\pi \rightarrow \pi^*$ transition has also been reported to occur around 250 nm [6]. It seems the

transition centred at 301 nm is probably due to NH_2 or $N^- \rightarrow Ni^{2+}$ CT transition, since the ligand system contains both coordinated amino and deprotonated amide groups. The fact that Ni(II) has been observed to be capable of deprotonating the amide groups of the [H_2(556)-N] ligand system (Chapter 3), it is highly likely that this LMCT band is due to a electron transition from the deprotonated amide nitrogen (N^-) to the vacant $^1A_{2g}$ orbital of the metal ion. In that regard, the $O^- \rightarrow Ni^{2+}$ electronic transition band is unlikely.

A worthy noting feature about this system is that increasing Ni(II) and ligand concentration does not lead to better elucidation of the d $\rightarrow$ d transition due to higher molar extinction of LMCT band. As a result, this charge transfer band dominates the electronic spectrum of this Ni(II)-[H_2(556)-N] system.

4.1.5 Experimental

UV-Visible electronic spectra of a 3.00 cm^3 aqueous solution containing a 1:4 ratio of Cu(II):ligand, in a cuvette, were taken over the pH range 2.00 - 11.00. Small amounts of 0.100 mol dm^{-3} NaOH and HCl were used to adjust the pH during the titration. The temperature of the solutions was kept at 25.0 $\pm$ 0.1 ^oC. Spectrophotometric measurements were taken automatically at 10 nm intervals in the wavelength range 400 - 800 nm. The electronic spectra in aqueous solution were recorded in 1.00-cm quarts cells using a Varian Cary 100 Ultraviolet Spectrophotometer equipped with a temperature-controlled cell holder with slit and band widths set at 0.4 nm and 1.2 nm, respectively.

4.2 Dermal absorption studies

4.2.1 Introduction

Cu(II) complexes can be administered orally and by injection intravenously or intraperitoneally. Although these two methods allows easy

drug administration so as to increase the available Cu(II), it is difficult to move the coordinated metal across body compartments without protein binding [22]. As a result, of all the various classical ways of drug administration percutaneous absorption offers the advantage of being a less painful method, and therefore tolerable to patients. However this method's usefulness in drug administration depends on the lipophilicity and molecular weight of the drug [23, 24].

Partition coefficients measurements can be used as extra-thermodynamic reference parameters for "hydrophobic bonding" in biochemical and pharmacological systems. Hydrophobicity is one of the most important physiochemical parameter governing transport, distribution, and fate of chemicals in biological systems. The octanol/water partition coefficient (log $P_{oct/aq}$) is a quantitative measure of the hydrophobicity of a substance. It can be used in the estimation of bioaccumulation in animals and plants [25, 26] and in the prediction of toxicity and drug absorption [27]. Studies on skin permeability have shown that paracellular diffusion through the lipid lamellae is the most likely route for passive diffusion through the stratum corneum [28].

4.2.2 Cu(II)- [555-N] and [H(555)-N] systems

Figure 4.7 shows the partition coefficients (log $P_{oct/aq}$) of (a) Cu(II)-[555-N] and (b) Cu(II)-[H(555)-N] systems plotted as a function of pH. These log $P_{oct/aq}$ values were determined at 25°C and an ionic strength of 0.15 mol dm^{-3} (Cl^-). For a drug to be reasonably lipophilic, the log $P_{oct/aq}$ value must be at least 0.6.

A noticeable feature about Figure 4.7 is that all log $P_{oct/aq}$ values are negative. Negative values of log $P_{oct/aq}$ indicate that these complexes are largely hydrophilic. The low log $P_{oct/aq}$ values in the acidic pH range for the complex species in both systems indicate that the hydrated $[Cu(OH_2)_6]^{2+}$ species predominates in this pH region. Although complex formation in the Cu(II)-[555-N] system begins at low pH, Figure 3.7(a) shows that at a pH of

1.50 there is only 10 % complex formation suggesting abundance of the hydrated $[Cu(OH_2)_6]^{2+}$ species at low pH. Moreover the complex formed is positively charged, a factor that could enhance its association with the aqueous solution. At pH values above 4.00, complex formation begins to take place in the Cu(II)-[H(555)-N] system through the coordination of both the amino and deprotonated amide group leading to the formation of an MLH_{-1} species.

The log $P_{oct/aq}$ values for the two systems at physiological pH (7.40) are -1.29 and -1.39 respectively. These are approximated as the values for the ML and MLH_{-1} species for the Cu(II)-[555-N] and Cu(II)-[H(555)-N] systems respectively as these are the predominant species present at this pH. There is an increase in log $P_{oct/aq}$ values above pH 10.00 for both systems, with maximum values of -1.09 and -1.14 for an ML species in the Cu(II)-[555-N] system and MLH_{-1} species in the Cu(II)-[H(555)-N] respectively. This is due to the formation of a predominantly single-charged MLH_{-1} species for both systems in this alkaline region. Aqueous partitioning of a charged species resulting in negative octanol/water partition coefficient values would be expected in these systems considering the ability of water to stabilize charges. However Green and co-workers have reported positive octanol/water partition coefficients for positively charged compounds [29, 30], indicating that electrostatic interactions are not the sole factors governing octanol/water partition.

The relative hydrophilic nature of these two ligands, in addition to the charge distributions, explains the complexes' exclusive preference for the aqueous layer, resulting in negative values of log $P_{oct/aq}$. The calculated speciation diagrams given in Figure 3.7 indicate that Cu(II) is 100 % present as the ML and MLH_{-1} species in the Cu(II)-[555-N] and Cu(II)-[H(555)-N] systems respectively for the two ligand systems at physiological pH.

Figure 4.7: Log $P_{oct/aq}$ of (a) Cu(II)-[555-N] (◇) and (b) Cu(II)-[H(555)-N] (♦) complexes plotted as a function of pH.

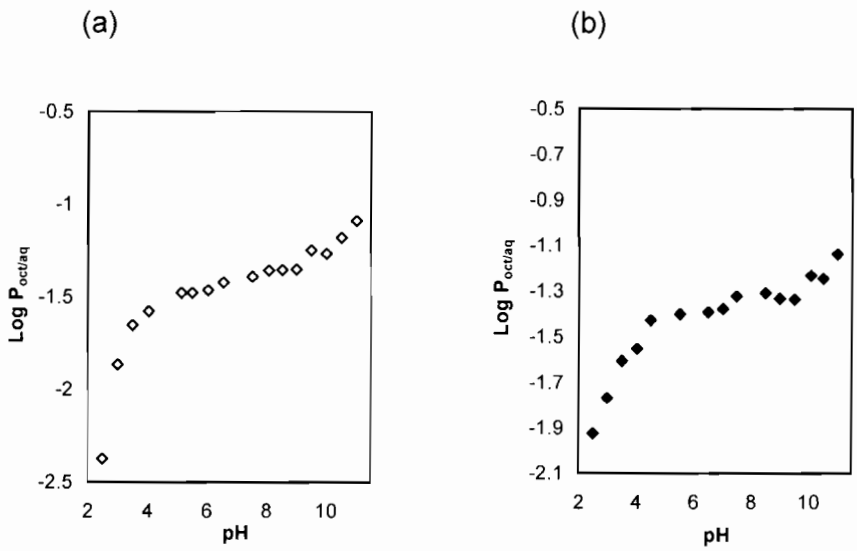

While it is not possible to calculate partition coefficients for the individual Cu(II) species, our results do indicate that the partition coefficients are higher for MLH_{-1} species than ML. Although these complexes are relatively hydrophilic by virtue of having negative log $P_{oct/aq}$, they are more lipophilic than Cu(II)-N,N'-bis(hydroxyiminopropionyl) propane-1,3-diamine recently reported [31] to have a log $P_{oct/aq}$ value of -1.73 and compares reasonably well with Cu(II)-3,3,9,9-tetramethyl-4,8-diazaundecane-2,10-dione dioxime with a reported log $P_{oct/aq}$ of -1.26 at physiological pH [32]. These complexes are also more lipophilic than bis(diethyldithiocarbamate)Cu(II) with a reported log $P_{oct/aq}$ value of -2.88 [33]. Despite their charged nature, the improved partition coefficients in these Cu(II)-[555-N]/[H(555)-N] systems compared to neutral species is due to the presence of bulky groups, and this suggest the essential role of such groups in percutaneous drug administration. The ^{67}Cu(II) and ^{64}Cu(II)-labelled [N(2-pyridylmethyl-N1-(salicylaldimino)-1,3-propanediamine] and pyruvaldehydebis(N^4-methylthio-semicarbazone) derivatives studied by Green and co-workers [34, 35] seem to be the only Cu(II) containing complexes to have high positive values, with reported log $P_{oct/aq}$ values in the range 1.97 to 3.61.

Our results show that, although the Cu(II) complexes of the two systems are relatively hydrophilic, at least 4.07 % of the Cu(II)-[555-N] and 5.13 % of the Cu(II)-[H(555)-N] complexes is extracted into the organic phase of octanol/water mixture used as a bio-phase model of membrane. Four key factors contribute to the hydrophilicity of these complexes, and these are;

- the presence of coordinated water molecules,
- hydrogen bonding between charged groups in these species and the solvent molecules.
- the overall charge of the ML and MLH_{-1} complex species, and
- hydrogen bonding interactions between the carbonyl oxygen atom in [H(555)-N] and bulk water molecules.

In general, only neutral molecules take part in the partition equilibrium between the aqueous and organic phases, while the charged complexes remain in the aqueous phase.

A predictive model for skin permeation rate in which partition coefficients are used to predict the maximal trans-dermal flux of permeation has been developed by Michaels et al. [36, 37]. It requires a mineral oil-water partition coefficient and water solubility of penetration molecules to be multiplied by the normalized flux to generate a predicted maximum permeation rate through human epidermis *in vitro*. By using this model trans-dermal fluxes of 3.98×10^{-5} and 5.01×10^{-5} cm h^{-1} are predicted for Cu(II) complexes of [555-N] and [H(555)-N] respectively. These values are encouraging considering that they are higher than the absorption rates recently reported by other workers [31] and a patented remedy previously reported for topical treatment of RA [38].

4.2.3 Cu(II)-[H_2(5555)-N] and [H_2(556)-N] systems

Figure 4.8 shows the partition coefficients (log $P_{oct/aq}$) of Cu(II) complexes for the two ligand systems [H_2(5555)-N] and [H_2(556)-N] plotted as

a function of pH. Low log $P_{oct/aq}$ values (Figure 4.8) are observed at low pH range of 2.00 - 4.00. This indicates the presence of the hydrated Cu(II) as the major species at such low pH. Unlike the two systems discussed above, a general increase in partition coefficients is observed as pH increases for both the Cu(II)-[H_2(5555)-N] and Cu(II)-[H_2(556)-N] systems.

Figure 4.8: Log $P_{oct/aq}$ of (a) Cu(II)-[H_2(5555)-N] (•) and (b) Cu(II)-[H_2(556)-N] (o) complexes plotted as a function of pH.

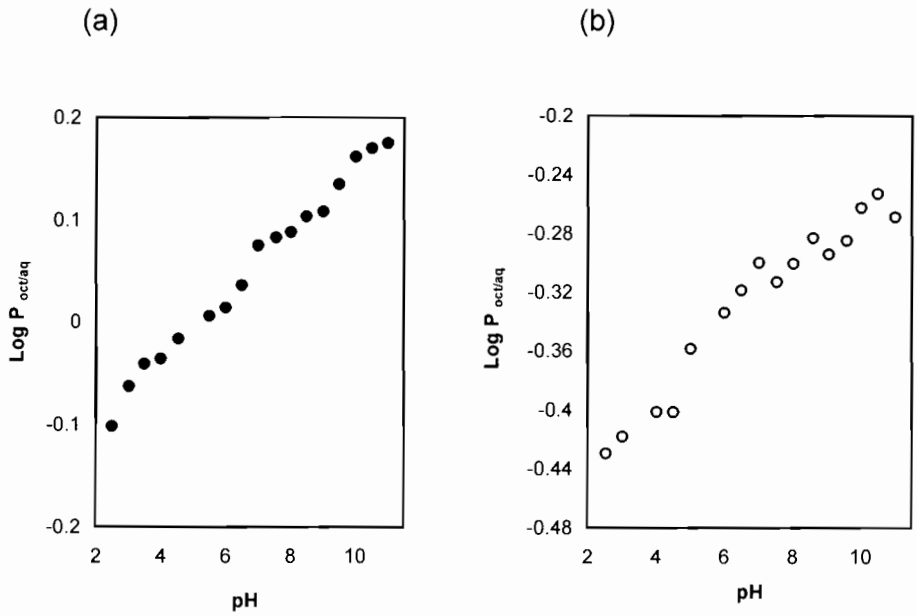

At physiological pH log $P_{oct/aq}$ values of 0.083 and -0.313 are recorded for the Cu(II)-[H_2(5555)-N] and Cu(II)-[H_2(556)-N] systems while maximum values are recorded at pH 11.00 (0.175) and 10.50 (-0.253) respectively. The calculated speciation diagrams given in Figure 3.9 indicate that Cu(II) is 100 % present as the MLH_{-1} and MLH_{-2} for the Cu(II)-[H_2(5555)-N] and Cu(II)-[H_2(556)-N] systems respectively at physiological pH. The same speciation diagrams show that 95 % of Cu(II) is present as the MLH_{-2} and MLH_{-3} species for the Cu(II)-[H_2(5555)-N] and Cu(II)-[H_2(556)-N] respectively above pH 10.00.

Cu(II) complexes with a benzyl moiety have been found to have improved lipophilicity [39]. Thus the presence of pyridyl moieties in the [H_2(5555)-N] and [H_2(556)-N] ligand systems is expected to enhance the

lipophilicity of their Cu(II) complexes and promote their extraction into the organic phase. Naturally [H_2(5555)-N], with two pyridyl moieties is expected to extract more than [H_2(556)-N] with one pyridyl moiety, and the log $P_{oct/aq}$ value reported in this study confirms this. In general the presence of alkyl and benzyl groups as part of the backbone structure of a ligand or as substituents to it do increase its lipophilicity, and therefore these bulky groups would play an essential role in percutaneous drug administration. Thus the presence of pyridyl groups in the [H_2(5555)-N] and [H_2(556)-N] ligand systems should render these molecules lipophilic enough for a reasonable amount of its complexes to enter the octanol phase. Using a predictive model for skin permeation rate developed by Michaels et al. [36, 37] trans-dermal flux values of 7.71×10^{-2} cm h^{-1} and 1.92×10^{-1} cm h^{-1} are determined for the Cu(II) complexes of [H_2(556)-N] and [H_2(5555)-N] respectively. These trans-dermal flux rates are encouraging enough to merit membrane crossing of complexes by passive transport.

A closer look at the structure of these ligands reveals that only the uncoordinated carbonyl oxygen can hydrogen bond to solvent molecules. However such interactions should be weak due to the low basicity of the carbonyl oxygen. Even after deprotonation of the amide groups due to metal ion complexation, the negative charge is delocalised over the amide moiety (Figure 3.25a, b and f) and the proximity of the metal ion makes hydrogen bonding with bulky water molecules insignificant.

4.2.4 Experimental

The traditional experimental method for determining partition coefficient (log $P_{oct/aq}$) is the shake-flask method, which is adapted as the standard OECD (Organisation for Economic Cooperation and Development) method [40]. It has been used to determine log $P_{oct/aq}$ values for various compounds in the range from -2.00 to 4.00. However for compounds having higher hydrophobicity, the shake-flask method cannot be used because of the formation of octanol emulsions in water.

In this study partition coefficients were measured using the shake flask method [23, 24]. 100 cm^3 of Cu(II) (0.001 mol dm^3)-L (0.003 mol dm^3) solutions were prepared. Into eighteen 20.0 cm^3 glass vials, 5.0 cm^3 portions of the metal-ligand solutions were pipetted. The first vial was left at pH 2.50 while the rest of the vials were adjusted to 0.50 pH increments apart using 0.100 mol dm^3 NaOH [23, 24]. The solutions in the vials were spiked with $^{64}CuCl_2$ solution of activity 7.5 - 9.0 mCi. To each vial containing the spiked metal-ligand solution 5.0 cm^3 portions of water saturated octan-1-ol were added. Each vial was then stoppered and shaken by hand for at least 5 minutes, swirled to collect droplets from sides of the vials and set aside to allow the two phases to separate, at a constant temperature of 25.0 ± 0.1 °C. 1 ml of each phase was pipetted into radioactive counting vials using a Gilson pipette and activity of each phase counted for 5 minutes in a Minaxi Auto gamma counter (5000 Series-Packard) using a window set at 340 - 540 keV. [41, 42, 43, 44, 45].

4.3 Superoxide dismutase (SOD) mimetic activity studies

4.3.1 Introduction

A number of Cu(II) complexes have been observed to exhibit SOD-mimic like activity and these could be viewed as alternative human therapeutics to mop up the pro-inflammatory radical, $O_2^{\cdot-}$, *in vivo*. Low molecular weight (l.mw.) Cu(II) complexes are in fact capable of catalysing the dismutation of the superoxide anion radical to molecular oxygen, water and/or hydrogen peroxide [46]. In view of such observation, Cu(II) complexes could be used as mimics of the native enzyme $Cu(II)_2Zn(II)_2SOD$. Measurement of this mimetic activity can indirectly indicate the amount of radicals generated and this can be used to predict the effect of these pharmacological agents on radical consumption, both *in vitro* and *in vivo* [47].

4.3.2 Theory

There are many ways to assay for superoxide dismutase (SOD). Each of the methods applicable has various advantages considered for SOD activity determination. The UV-Visible determination of the nitroblue tetrazolium (NBT) assay has the main advantage of sensitivity, allowing SOD activity measurement in crude homogenates of tumor tissue that generally have very low SOD activity. The use of UV-Visible is indirect, and this is based on two elements, a superoxide generator usually xanthine-xanthine oxidase system and a detector, nitroblue tetrazolium (NBT) [48]. Superoxide anion ($O_2^{\cdot-}$) acts as a one electron reducing agent to nitro-substituted aromatics such as NBT. Thus the reduction of NBT to blue diformazan is widely used as a probe of $O_2^{\cdot-}$ generation in chemical and biological systems. The reliability of this technique is based on the following assumptions;

- NBT can accept electrons from various reductants, including $O_2^{\cdot-}$.
- Superoxide dismutase (SOD), an enzyme that enhances the dismutation rate of $O_2^{\cdot-}$ inhibits the $O_2^{\cdot-}$-mediated NBT reduction by a competitive process.

In the absence of an SOD-mimetic agent (control experiment), the radicals react with the detector, while in the presence of SOD-mimetic agent (inhibition experiment), the mimetic agent competes with the detector for superoxide anion. SOD activity is then measured by the degree of inhibition of the conversion process of NBT to form diformazan using UV-Visible at 560 nm over a period of time. The absorbance versus time curves corresponding to a control and particular concentrations of an SOD mimic (Cu(II)-L complex), are generated and slopes of these curves computed. The %inhibition of the reduction of NBT to blue diformazan is then calculated using the following equation:

$$\%\text{Inhibition} = \frac{[(S_{ces} - S_{ies}) \times 100]}{S_{ces}} \qquad (4.5)$$

where S_{ces} and S_{ies} are slopes of the control and inhibition experimental solutions respectively. Plots of %inhibition against varying drug concentrations are plotted. The inhibitory concentration (IC_{50}) defined as concentration of the drug required to reduce diformazan formation by 50 % is read off from these plots.

These experiments are carried out in the presence of excess disodium salt of EDTA as compared to the other components. Such conditions simulate the competitive binding of endogenously available low molecular ligands [48, 49] and enable complexation of small amounts of metal ions such as Fe(II), that may be present in NBT and/or xanthine, which are known to catalyse the dismutation of $O_2^{\cdot-}$ [48]. It is worthy-noting that Cu(II)-EDTA complexes are inactive as SOD mimics [49].

4.3.3 Cu-L systems

Figure 4.9 and 4.10 show the percentage inhibition as a function of the concentration of the Cu(II) complexes for the ligand systems, [555-N], [H_2(5555)-N] and [H_2(556)-N]. The concentration of the drug required to reduce diformazan formation by 50 %, also known as IC_{50}, can easily be read off from these two Figures.

An IC_{50} value of 6.25 μmol dm^{-3} for MLH_{-2} species of the Cu(II)-[H_2(556)-N] system was obtained while a value of 255 μmol dm^{-3} was recorded for both ML and MLH_{-1} species of the Cu(II)-[555-N] and Cu(II)-[H_2(5555)-N] systems respectively. The MLH_{-1} species of the Cu(II)-[H(555)-N], not shown in the two Figures was observed to have an IC_{50} value of 405 μmol dm^{-3}. The IC_{50} value of the native CuZn SOD has been reported to have a value of 0.011 μmol dm^{-3} [46]. The IC_{50} values recorded in this work for the studied Cu(II) complexes are much higher than the value reported for the native CuZn SOD. This indicates that the Cu(II) complexes have low SOD activities when compared to the native enzyme.

Figure 4.9: %Inhibition as a function of the concentration of the MLH_{-2} species for the Cu(II)-[H_2(556)-N] system and MLH_{-1} species for the Cu(II)-[H_2(5555)-N] system.

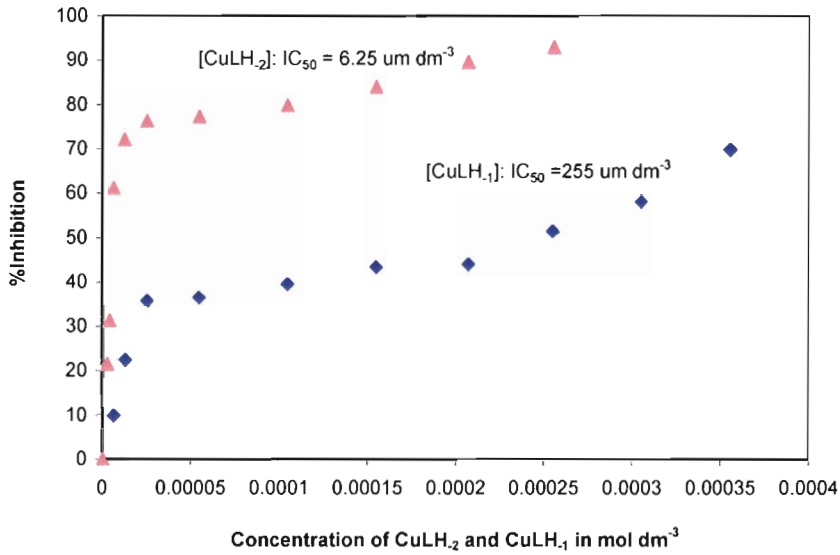

Figure 4.10: %Inhibition as a function of the concentration of ML species for the Cu(II)-[555-N] system.

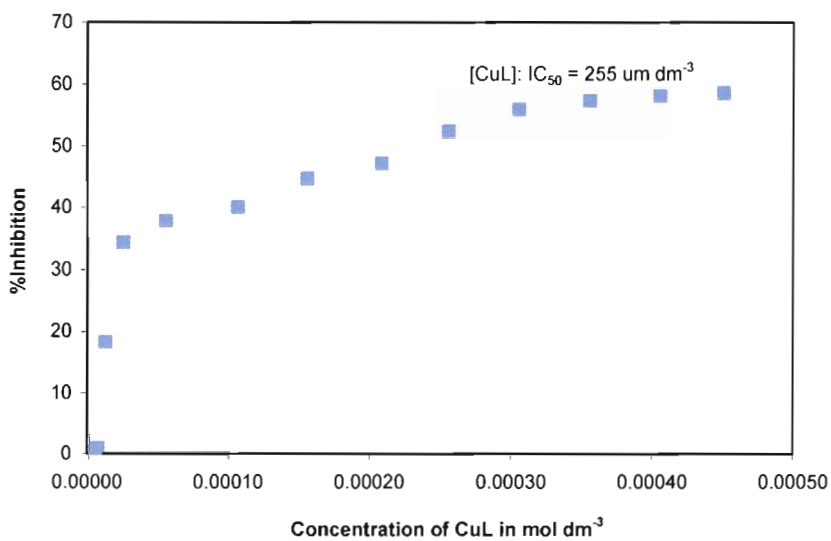

The commonly accepted mechanism [50, 51, 52] for the dismutation of $O_2^{\cdot-}$ has been proposed to occur via two steps, corresponding to the Cu(II) reduction and re-oxidation as supported by pulse radiolysis experiments [53, 54]. The reduction is suggested to occur via inner sphere electron transfer with direct $O_2^{\cdot-}$ coordination to the Cu(II) metal centre, resulting in formed Cu(I) adopting a trigonal planar coordination [55, 56, 57]. The first product is O_2 which can easily diffuse out, since it is neutral in charge, allowing for entrance of the successive substrate molecule.

The MLH_{-2} species of the Cu(II)-[H_2(556)-N] system has been observed to exhibit an IC_{50} value which is 600 times greater than that of the native enzyme, while the other three species have values that are 4 orders of magnitude greater than the native enzyme value. The rationalization of these results normally takes the approach of the non availability of binding sites on the Cu(II) complex for superoxide anion due to formation of a square planar arrangement of the ligand donor atoms around Cu(II) in these species. In view of this it is surprising to note that MLH_{-2} species of the Cu(II)-[H_2(556)-N] has the smallest IC_{50} value despite having been observed to form a typical square planar complex. This paradoxical situation can however be rationalized in terms of the dismutation mechanism. When the $O_2^{\cdot-}$ substrate radical penetrates into the active site channel and approaches the metal centre, it is protonated on its way by a proton donor. Alternatively, the MLH_{-2} of the Cu(II)-[H_2(556)-N] is capable of providing a sufficiently low local pH in the vicinity to the catalytic centre to stabilise the protonated superoxide radical due to remarkable amide bond formation ability in the ionized state at pH $\approx$ 7.00. Stability of the local pH conditions can be supported by observations on the wild-type enzyme catalytic rate, which follows a pattern of a fairly constant value within the pH range 5.00 - 8.00 [53, 58].

Overall, the dismutation of $O_2^{\cdot-}$ seems to be favoured by complexes that can provide the convenient local pH conditions that can facilitate protonation of the radical before penetrating the active site to bind to the metal centre.

4.4 Molecular Mechanics (MM)

4.4.1 Introduction

Molecular mechanics (MM) is a very popular tool for describing the structures and relative energies of many classes of molecules [59, 60, 61, 62, 63]. Advances in computing, have greatly increased the interest in computer-based molecular modelling, such that it is now used as an aid in the interpretation of experimental results and design of new materials with desirable properties. The basis of molecular modelling is that all important molecular properties; stabilities, reactivities and electronic are related to molecular structure. For a molecular modelling technique to be useful and achieve widespread application, it must readily and reliably reproduce molecular properties that closely resemble experimentally determined data. Wide use of MM is primarily due to computational simplicity and efficiency.

While quantum mechanical modelling of metal complexes with *ab-initio* or semi-empirical methods would provide better experimental evidence, this modelling method remains prohibitive because the methods used are so computationally intensive [59]. The approximations that are introduced in order to reduce central processing unit (CPU) time and allow quantum mechanical calculations to be used routinely are often severe and such calculations are then less reliable.

4.4.2 Theory

The basis of the MM method is that a good estimate of the geometry of a molecule can be obtained by taking into account all the forces between the atoms, calculated using a mechanical approach.

Molecular mechanics studies in both inorganic and organic chemistry define the strain energy $\mathbf{V}_{total}$ as arising from four principle energy terms, the general form of which is given in equation 4.6 [59].

$$V_{total} = \sum V_b + \sum V_\theta + \sum V_\varphi + \sum V_{nb} + \text{ other relevant terms} \quad (4.6)$$

where $\sum V_b$ is the total bond deformation energy, $\sum V_\theta$ is the total valence angle deformation energy, $\sum V_\varphi$ is the total torsional (dihedral) angle deformation energy and $\sum V_{nb}$ is the total non bonded (van der Waals) interaction energy.

These individual energy terms are calculated using simple functions with bonds modelled as springs obeying Hooke's law as shown below;

$$V_b = \frac{1}{2} k_b (r_{ij} - r_o)^2 \quad (4.7)$$

where k_b is the force constant or spring strength, and r_o is the ideal bond.

Valence angles are modelled in a very similar manner as above, but torsional (dihedral) angles would require a periodic function. Thus;

$$V_\theta = \frac{1}{2} k_\theta (\theta_{ijk} - \theta_o) \quad (4.8)$$

where k_θ is strength of spring holding angles at its ideal value, θ_o is the ideal angle.

$$V_\varphi = \frac{1}{2} k\varphi (1 + \cos(m(\varphi_{ijkl} + \varphi_{offset}))) \quad (4.9)$$

where k_φ is height of barrier to rotation about torsion angle φ_{ijkl}, m is the periodicity and φ_{offset} is the offset of the minimum energy from a staggered arrangement.

Non-bonded interactions are calculated using a function that includes a repulsion and attractive component as shown in equation 4.10.

$$E_{nb} = Ae^{-Bdij} - Cd_{ij}^{-6} \quad (4.10)$$

where d_{ij} is the distance between two nuclei and A, B and C are atom-based constants.

Additional components can be added to the calculation of strain energy. These include out-of-plane deformation terms, electrostatic interactions and hydrogen bonding interactions. These set of functions,

together with collection of terms that parameterize them ($\mathbf{k_b}$, $\mathbf{r_o}$, etc), is referred to as the force field. The force field therefore, represents the bond stretching ($\mathbf{V_b}$), bond angle ($\mathbf{V_\theta}$), torsion angle deformations ($\mathbf{V_\varphi}$), and non-bonded interactions ($\mathbf{V_{nb}}$) along with other relevant terms.

While force fields commonly used for description of purely organic molecules are readily available [64, 65], the choice of force field to study molecules containing a metal is not clear-cut. The extension of these force fields to inorganic chemistry is a more recent development [59, 66, 67, 68, 69]. The general lack of experimental data, especially thermodynamic, to which force field parameters can be fitted, the variability in coordination mode of the metal centre, the problem in defining reference angles around the metal centre, as well as the effect of the molecule having an overall charge, are all factors which make developing a set of transferable force field parameters more difficult for metal containing molecules than for organic molecules. Consequently, numerous molecular mechanics force fields for metal complexes have appeared in literature as research groups have parameterized their own force field for problems at hand.

A generic force field, extensible systematic force field (esff) [70] has been used to model copper complexes. The advantage of esff is its capability to model most of the elements of the periodic table. Esff employs semi-empirical rules to translate atomic-based parameters to parameters typically associated with a covalent valence force field. The atomic parameters depend not only on atom type, but also on internal type, thus resulting in a more accurate force field. The force field has been applied to molecular simulations of a wide variety of systems including nucleic acids, peptides, hydrocarbons, porphyrins, transition metal complexes, zeolites, and organometallic compounds [70] where agreement with the experimental results indicates that esff is a valuable tool in molecular simulations for understanding and predicting both crystal and gas phase molecular structures. However, esff cannot accurately represent high vibrational frequencies and conformational changes, but its hoped that in future it will provide a basis for the development

of force fields applicable to a wide variety of organic and organometallic compounds.

4.4.3 Calculations

The MM calculations were done on a SyncMaster 1100p computer using Insight II [71]. The Cu(II) complexes were constructed from fragments using the BUILDER module. The overall charge of the molecule was set equal to zero, so as to eliminate the effect of the +2 charge of the metal on the partial charges of the atoms of the organic ligand. Molecular mechanics calculations were performed using the Discover_3 program which was run as an application in the Insight II package [71]. All calculations were done in vacuum.

4.4.4 Results and discussion

4.4.4.1 Results

The energy minimized structures are given in Figures 4.11 - 4.16, while energy details of these structures are given in Table 4.2. The presented structures are compared in terms of their internal energies and not the total potential energy. This is because the total potential energy is dependent on the number of covalent bonds in the structure and also includes a contribution from the non-bonded electrostatic interactions, which is greatly influenced by the charge of the Cu(II). By virtue of the fact that these were molecular mechanics calculations the entropy associated with the chelate effect and the crystal field stabilization energy contribution to the overall stability of the complex are not included. The internal energy which was the criterion considered for stability comparison indicates the strain energy around the central metal ion.

Figure 4.11: Energy minimized Cu(II) complexes showing equatorial plane coordination by (a) three amine and a pyridyl nitrogen donor atoms, giving a 5,5,5 chelate ring sequence (28.09 kcal mol^{-1}) and (b) three amine nitrogen donor atoms giving a 5,5 chelate ring sequence (47.62 kcal mol^{-1}) for the ML species of the Cu(II)-[555-N] (L^1) system.

(a) **5,5,5** (b) **5,5**

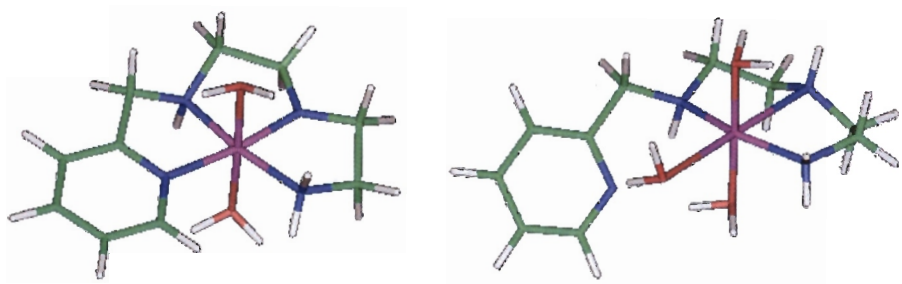

Figure 4.12: Energy minimized Cu(II) complexes showing equatorial plane coordination by (a) two amine nitrogen and one carbonyl oxygen donor atoms giving a 5,7 chelate ring sequence (35.72 kcal mol^{-1}) and (b) two amine and a pyridyl nitrogen donor atoms giving a 5,8 chelate ring sequence (48.00 kcal mol^{-1}) for the ML species of the Cu(II)-[H(555)-N] (L^2) system.

(a) **5,7** (b) **5,8**

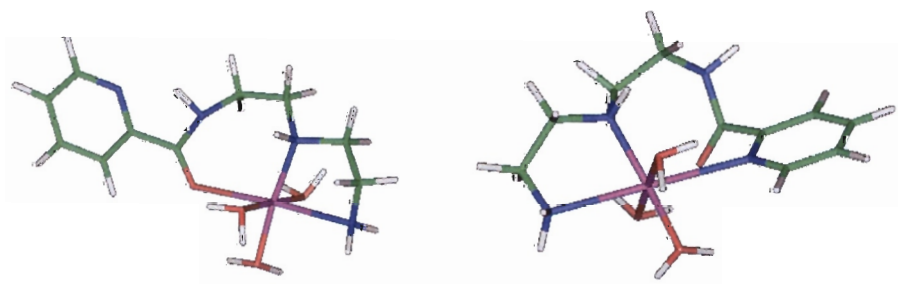

Figure 4.13: Energy minimized Cu(II) complexes showing equatorial plane coordination by (a) two amine nitrogen, one amide nitrogen and a pyridyl nitrogen donor atoms, giving a 5,5,5 chelate ring sequence (67.08 kcal mol^{-1}) and (b) two amine and an amide nitrogen donor atoms, giving a 5,5 chelate ring sequence (30.38 kcal mol^{-1}) for the MLH_{-1} species of the Cu(II)-[H(555)-N] (L^2) system.

(a) **5,5,5** (b) **5,5**

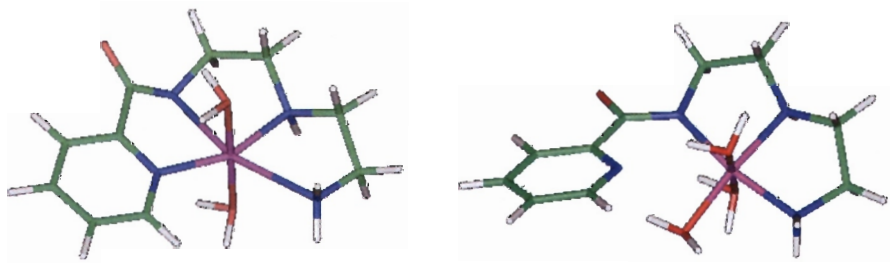

Figure 4.14: Energy minimized Cu(II) complexes showing equatorial plane coordination by (a) a central amine nitrogen, one amide nitrogen and a carbonyl oxygen donor atoms, giving a 5,7 chelate ring sequence (34.85 kcal mol^{-1}) and (b) one central amine, an amide nitrogen, a pyridyl nitrogen and a carbonyl oxygen donor atoms, giving a 5,5,7 chelate ring sequence (47.23 kcal mol^{-1}) for the MLH_{-1} species of the Cu(II)-[H_2(5555)-N] (L^3) system.

(a) **5,7** (b) **5,5,7**

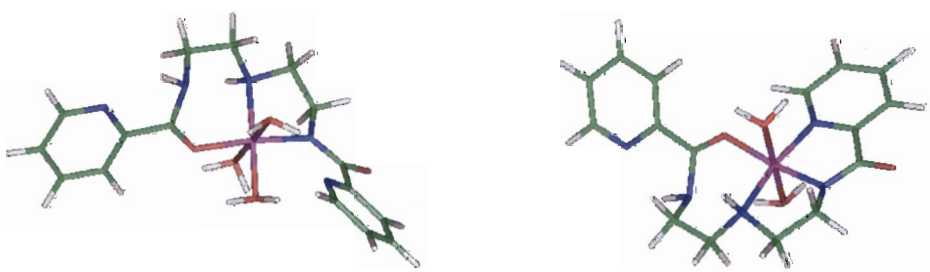

Figure 4.15: Energy minimized Cu(II) complexes showing equatorial plane coordination by (a) a central amine nitrogen and two amide nitrogen donor atoms, giving a 5,5 chelate ring sequence (60.22 kcal mol^{-1}) and (b) one central amine, two amide nitrogen and two pyridyl nitrogen donor atoms, giving a highly strained 5,5,5,5 chelate ring sequence (82.85 kcal mol^{-1}) for the MLH_{-2} species of the Cu(II)-[H_2(5555)-N] L^3) system.

(a) **5,5** (b) **5,5,5,5**

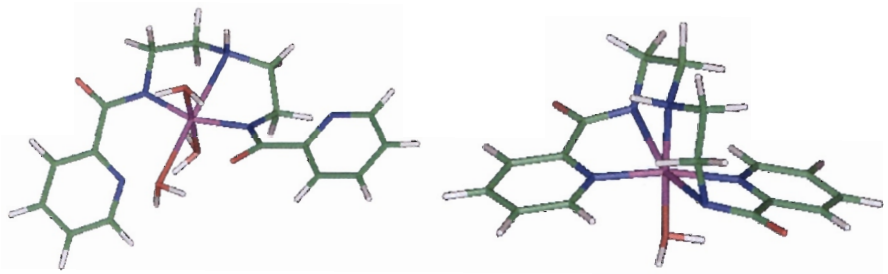

Figure 4.16: Energy minimized Cu(II) complexes showing equatorial plane coordination by (a) a terminal amine nitrogen, two amide nitrogen and a pyridyl nitrogen donor atoms, giving a 5,5,6 chelate ring sequence (21.80 kcal mol^{-1}) and (b) one terminal amine and two amide nitrogen donor atoms, giving a 5,5 chelate ring sequence (50.41 kcal mol^{-1}) for the MLH_{-2} species of the Cu(II)-[H_2(556)-N] (L^4) system.

(a) **5,5,6** (b) **5,5**

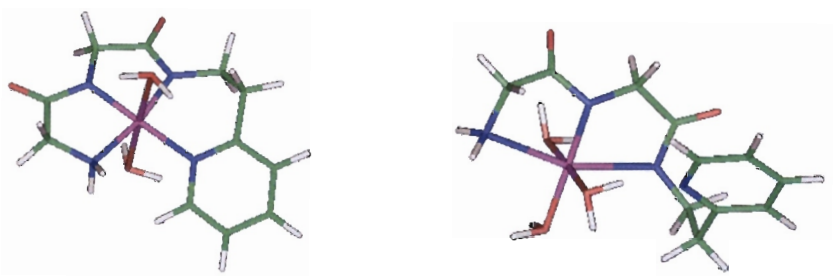

Table 4.2: Internal energy (E_{int}), bond, angle bending (Angle), bond twisting (Torsion) and out-of-plane (Oop) distortion energies (kcal mol^{-1}) for the different chelate ring size sequence associated with each structure.

	[Fig. 4.11] ML ($Cu\text{-}L^1$)		[Fig 4.12] ML (CuL^2)		[Fig 4.13] MLH_{-1} (CuL^2)		[Fig 4.14] MLH_{-1} (CuL^3)		[Fig 4.15] MLH_{-2} (CuL^3)		[Fig 4.16] MLH_{-2} CuL^4)	
	5,5,5	5,5	5,7	5,8	5,5,5	5,5	5,7	5,5,7	5,5	5,5,5,5	5,5,6	5,5
E_{int}	28.09	47.63	35.72	48.00	67.08	30.38	34.86	47.23	60.22	82.85	21.80	50.41
Bond	7.20	11.94	10.09	10.38	14.73	7.75	8.41	10.86	10.64	12.98	4.12	10.25
Angle	14.52	32.22	19.82	25.35	43.18	14.70	17.40	30.51	37.23	46.39	11.25	28.73
Torsion	6.33	3.45	5.80	11.80	8.19	7.81	8.85	5.69	12.11	20.37	6.28	10.63
Oop	0.04	0.01	0.02	0.47	0.98	0.11	0.19	0.17	0.24	3.10	0.15	0.82

4.4.4.2 Discussion

The internal energies of the energy minimized structures from Figures 4.11 - 4.16 given in Table 4.2 suggest a stability order corresponding to a chelate ring size sequence of the order 5,5,6 > 5,5,5 > 5,5 > 5,7 > 5,5,7 > 5,8 > 5,5,5,5. In coordination chemistry a 5 membered chelate is generally favoured over a 6 membered ring because the metal ion in an octahedral environment has a 90° angle between the coordination bonds. In organic chemistry where carbon is sp^3 hybridised, a six membered ring is more common.

The strain in these structures arises from both the sequence and the size of the chelate rings formed around the metal ion upon donor atom coordination. While a 5,5,5,5 chelate ring system is clearly highly strained due to its contiguous five-membered chelate rings, the 5,7 and 5,8 chelate rings tend to have unfavourably larger chelate rings. The strain of the complex in the 5,5,5,5 chelate ring system is a result of the attempt by each donor atom

to approach the metal ion at the best bonding orientation. However due to lack of ideal separation between the donor atoms in the ligand system, such ideal bonding orientation may be achieved with difficulty resulting in strain in the complex molecule. Strain energy elevates the internal energy contribution to the overall potential energy of the molecule resulting in low complex stability. The larger size (seven or more) of the chelate ring, on the other hand is an indication of the low probability of the coordination of the second donor atom that closes the ring after coordination of the first. In such a case it is possible that by the time the second donor coordinates, the first donor is about to de-coordinate. However when the coordinating atoms are separated by two or three non-coordinating atoms (to form 5- or 6-membered chelate rings), closure of the chelate ring is more probable because of the close proximity of the second coordinating atom in the coordination sphere.

The other source of strain contribution to the differences in stability is the energy associated with torsion of bonds as the different donor atoms are oriented for coordination to the metal ion. Bond stretching seems to have less significant contribution to the differences in strain energies of these structures. Most differences in internal energy contribution arises from twisting of bonds and bending of angles as coordinating atoms are accommodated around the central metal ion.

Molecular mechanics (MM) has been considered as a simple computational tool to provide more evidence in support of the solution structures postulated from potentiometric and spectroscopic data. In this regard, some structures of two reasonable sets of species postulated from both potentiometry and spectroscopy have been considered for each Cu(II)-ligand system. In all calculations no account is taken of the electronic contributions, ie Jahn-Teller distortion of Cu(II) or entropy effects, both in terms of chelate effect of the ligand and solvent.

For the two ML species for the Cu(II)-[555-N] system given in Figure 4.11, the 5,5,5 chelate structure given in (a) has lower internal energy than the 5,5 chelate structure given in (b). The high strain energy associated with

the 5,5 chelate structure is mainly due to high angle bending energy in this structure (Table 4.2). Despite a high torsion energy in the 5,5,5 chelate structure relative to the 5,5 chelate structure, formation of a 5,5,5 chelate ring is more probable because of the close proximity of the second coordinating pyridyl nitrogen donor in the coordination sphere. The 5,5,5 chelate structure supported by MM calculations has also been postulated from potentiometric data in section 3.4.5, and this therefore lends confidence to the presence of this species in solution for the Cu(II)-[555-N] system.

The two energy minimized structures given in Figure 4.12 show that a 5,7 chelate structure has slightly lower internal energy than the 5,8 chelate structure. The main contribution to the internal energy is from angle strain which is generated when forming 7 and 8 membered rings. The 5,8 structure has a high angle bending energy (25.4 kcal mol^{-1}) and torsion energy (11.8 kcal mol^{-1}). This comes about because the planarity of the amide group has been compromised. In suggesting that Figure 4.12(a) represents the structure of the ML species of [H(555)-N] the MM calculations support the structure postulated from both the potentiometric and spectroscopic data in section 3.4.5 and 4.1.3.5.

The MLH_{-1} and MLH_{-2} species for the Cu(II)-[H_2(5555)-N] system are represented by the structures given in Figures 4.14 and 4.15 respectively. In Figure 4.14, the 5,7 chelate structure has lower strain energy than the 5,5,7 chelate structure. This energy difference arises from a high angle bending energy of 30.5 kcal mol^{-1} in the 5,5,7 chelate structure as the pyridyl nitrogen donor is forced into the coordination plane of the metal. In Figure 4.15, the 5,5,5,5 chelate structure has a high strain energy of 82.85 kcal mol^{-1} compared to the 5,5 chelate structure with an internal energy of 60.22 kcal mol^{-1}. For the 5,5,5,5 structure the major contributions to the internal strain energy comes from the bend angle (43.39 kcal mol^{-1}) and torsion angle (20.37 kcal mol^{-1}) energies. In this structure both amide nitrogen donors are coordinated to the metal and are forced to adopt a more tetrahedral (sp^3) geometry rather than their preferred planar (sp^2) geometry. Here, both the

MLH_{-1} and MLH_{-2} species postulated from both potentiometric and spectroscopic data are therefore supported by MM calculations.

The two possible structures for the MLH_{-2} species of the Cu(II)-[H_2(556)-N] are given in Figure 4.16. In terms of the internal energies of the two structures, the 5,5,6 chelate structure has considerably lower strain energy (21.80 $kcalmol^{-1}$) compared to the 5,5 chelate structure (50.41 $kcalmol^{-1}$). There is twice as much angle bending energy in the 5,5 chelate structure compared to the 5,5,6 chelate structure. The coordination of the pyridyl nitrogen donor atom is likely to occur, once the amino and two amidic groups are coordinated. Moreover, the coordination of the two deprotonated amide groups ensures planarity of these groups, resulting in restriction on the chelate geometry. From the potentiometric data in section 3.4.5 we postulated a similar solution structure as predicted by these MM calculations. Moreover the spectroscopic data given in section 4.1.3.5 with a λ_{max} value of 530 nm clearly suggests a square planar geometry for the MLH_{-2} species of the Cu(II)-[H_2(556)-N] system and these MM calculations gives extra experimental evidence in support of this geometry.

The MLH_{-1} species for the Cu(II)-[H(555)-N] system was an exception in that MM calculations did not predict the structure postulated from potentiometric and spectroscopic data. In Figure 4.13, the 5,5,5 chelate structure postulated as the solution structure from potentiometry and spectroscopy, has twice as much strain energy as the 5,5 chelate structure. A closer look at the energy contributions to this total strain energy indicates that the angle bending energy in the 5,5,5 chelate structure is almost three times higher than in the 5,5 chelate structure. Such a result clearly demonstrates the limitations of MM calculations as a computational tool for Cu(II) complexes since it does not account for electronic contributions of the metal or entropy effects, both in terms of the chelate effect of the ligand and the solvent.

References

1. Atkins P.W., (1978), Physical Chemistry, Oxyford University Press. pg 583.
2. Brittain E.F.H., George W.O., Wells C.H.J., (1970), Introduction to Molecular Spectroscopy: Theory and Experiment, Academic Press, London & New York. pg 37.
3. Nicholls D., (1974), Complexes and First-Row Transition Elements. MacMillan, London.
4. Jaffĕ H.H., Orchin M., (1962), Theory & Applications of Ultraviolet Spectroscopy, John Willey & Sons, New York, London, pg 509.
5. Hartley F.R., Burgess C., and Alcock R., (1980), Solution Equilibria, pg. 33-144.
6. Lever A.B.P, (1987), Studies in Physical & Theoretical Chemistry-Inorganic Spectroscopy, 2nd Ed., 184 pg 507-544.; Hathaway B.R., In: Comprehensive Coordination Chemistry, 5 652; [Eds: SirG. Wilkins, R.D. Gillard & J.A. McCleverty, Pergamon Press.
7. Billo E.J., (1974), *Inorg. Nucl. Chem. Lett.*, **10**, 613.
8. Smith D.W., (1977), *Inorg. Chim. Acta.*, **22**, 107.
9. Hartzell C.R., Gurd F.R.N., (1969), *J. Biol. Chem.*, **244**, 147.
10. Bryce G.F., Gurd F.R.N., (1966), *J. Biol. Chem.*, **241**, 122.
11. Jackson G.E., *UV-SPEC*, *Private Communication*, University of Cape Town.
12. Voye A, (1993), *Ph.D Thesis*, University of Cape Town.
13. Drago R.S., (1965), Physical Methods in Inorganic Chemistry, New York, Reinhold Publishing Corporation, Chapman & Hall Ltd., London.
14. Prenesti E., Daniele P.G., Toso S., (2002), *Analytica Chimica Acta*, **459**, 323.
15. Jackson G.E., Nakani B.S., (1996), *J. Chem. Soc., Dalton Trans.*, 1373.
16. Nonoyama M. (1974), *Inorg. Chim. Acta.*, **10**, 59.
17. Rowland J.M., Thornton M.L., Olmstead M.M., Mascharak P.K., (2001), *Inorg. Chem.*, **40**, 1069.

18. Gizzi P., Henry B., Rubini P., Giroux S., Wenger E., (2005), *J. Inorg. Biochem.*, **99**, 1182.
19. Komorita T., Hidaka J., Shimura Y., *Bull. Chem. Soc. Japan*, (1968), **41**, 484, (1969), **42**, 168, 1782, (1971), **44**, 3353.
20. Nonoyama M., Yamasaki K., (1971), *Inorg. Chim. Acta*, **5**, 124.
21. Bojczuk M.J., Lesmak W., Schlemper W., Gatner K., Jezierski A., Smoluch M., Bal W., (2001), *J. Inorg. Biochem.*, **84**, 189.
22. Jackson G.E., May P.M., Williams D.R., (1978), *J. Inorg. Nucl. Chem.*, **40**, 1227.
23. Leo A., Hansch C., Elkins D., (1971), *Chem. Rev.*, **71**, 525.
24. Xiang T.X., Anderson B.D., (1994), *J. Membrane Biol.*, **140**, 111.
25. Briggs G.G; Bromilov, R.H.; Evans, A.A. (1982), *Pestic. Sci.*, **13**, 495
26. Veith, G.D.; Defoe, D,L.; Bergstedt B.V. (1979), *J. Fish. Res. Board Can.*, **36**, 1040.
27. Calamari, D.; Vighi, M. (1990), *Res. Environ. Toxicol.*, **4**, 1.
28. Danielson J., Ulicny J., Laaksonen A., (2001), *J. Am. Chem. Soc.*, **123**, 9817.
29. Tsang B.W., Mathias C.J., Fanwick P.E., Green M.A., (1994), *J. Med. Chem.*, **37**, 4400.
30. Tsang B.W., Mathias C.J., Green M.A., (1993), *J. Nucl. Med.*, **34**, 1127.
31. Nomkoko E.T., Graham J.E., Nakani S.B., (2004), *J. Inorg. Chem. Dalton Trans.*, 1432.
32. Nomkoko T.E., Jackson G.E., Nakani B.S., Werner Louw K.A., Zeevaart J.R., (2004), *J. Inorg. Chem. Dalton Trans.* 741.
33. Zhang Y.H., Danielson L.G., Becze Z., (1998), *Water Res.*, **32**, 2073.
34. Green M.A., (1987), *Nucl. Med. Biol.*, **14**, 59.
35. Sri-Aran M., Mathias C.J., Lim J.K., Green M.A., (1998), *Nucl. Med. Biol.*, **25**, 107.
36. Michaels A.S., Wong P.S.L., Prather R. Gale R.M., (1975), *AIChEJ.*, **21**, 1073.
37. Shaw J.E., Prevo M., Gale R., Yum Su II, (1991), in Pysiology, Biochemistry and Molecular Biology of the Skin, Oxford University Press, Oxford, 2nd edn., ch. 55, pp 1454.

38. Cassimjee R., Cassimjee F., Cassimjee A.H., Feroz Cassimjee, (1993), *S. Afr. Pat.*, ZA9204061.

39. Nomkoko E., (2002), *Ph.D Thesis*, University of Cape Town, pg 138.

40. Guidelines for Testing Chemicals, Section 1-Physical-Chemical Properties, 105 n-Octanol/Water Partition Coefficient; Organisation for Economic Cooperation and Development (OECD); Paris, 1981.

41. Ackerman L.J., West D.X., Mathias C.J., Green M.A., (1999), *Nucl. Med. Biol.*, **26**, 551.

42. Lewis J.S., Srinivasan A., Schmidt M.A., Anderson C.J., (1999), *Nucl. Med. Biol.*, **26**, 267.

43. Yu M., Qing H., Guojian H., Shu Z., You-Feng H., Kuikka T., (1998), *Nucl. Med. Biol.*, **25**, 111.

44. Jones-Wilson T.M., Motekaitis R.J., Dean-Sherry A., Martell A.E., Welch M.J., (1998), *Nucl. Med. Biol.*, **25**, 523.

45. Guerdond L.M., Ouellet R., Van Lier J.E., (1994), *Nucl. Med. Biol.* **21**, 437.

46. Roberts N.A., Robinson P.A., (1985), *Br. J. Rheumatol.*, **24**, 128.

47. Greenwald R.A., (1985), Handbook of Methods for Oxygen Radical Research, Ed., R.A. Greenwald, CRC Press.

48. Auclair C., Voisin E., (1985), In CRC Handbook of Methods for Oxygen Radical Research; Ed., R.A. Greenwald, CRC Press.

49. Frodovich I., (1985), In CRC Handbook of Methods for Oxygen Radical Research; Ed., R.A. Greenwald, CRC Press.

50. Tainer J.A., Getzoff E.D., Richardson J.S., Richardson D.C., (1983), *Nature*, **306**, 284.

51. Bordo D., Pesce A., Bolognesi M.E., S.M., Falconi M., Desideri A., (2001), In *Handbook of Metalloproteins,* Vol 2; Messerschmidt A., Huber R., Poulos T.L., Wieghardt K., Eds.; Willey & Sons: Chichester.

52. Hart P.J., Balbirnie M.M., Ogihara N.L., Nersissian A.M., Weiss M.S., Valentine J.S., Eisenberg D., (1999), *Biochemistry*, **38**, 2167.

53. Klug-Roth D., Fridovich I., Rabani J., (1973), *J. Am. Chem. Soc.*, **95**, 2786.

54. Fielden E.M., Roberts P.B., Bray R.C., Lowe D.J., Mautner G.N., Rotilio G., Calabrese L., (1974), *Biochem. J.*, **139**, 49.

55. Hough M.A., Hasnain S.S., (2003), *Structure*, **11**, 937.
56. Bailey D.B., Ellis P.D., Fee J.A., (1980), *Biochemistry*, **19**, 591.
57. Murphy L.M., Strange R.W., Hasnain S.S., (1997), *Structure*, **5**, 371.
58. Fisher C.L., Cabelli D.E., Hallewell R.A., Beroza P., Lo T.P., Getzoff E.D., Tainer J.A., (1997), *Proteins*, **29**, 103.
59. Comba P., Hambley T.W., (1995), Molecular Modeling of Inorganic Compounds, VCH, Weinheim.
60. Hay B.P., Rustad J.R., (1994), *J. Am. Chem. Soc.* **116**, 6316.
61. Cornell W.D., Cieplak P., Baylz C.I., Gould I.R., Merz K.M., Jr., Ferguson D.M., Spellmeyer D.C., Fox T., Caldwell J.W., Kollman P.A., (1995), *J. Am. Chem. Soc.* **117**, 5179.
62. Hay B.P., (1993), *Coord. Chem. Rev.* **126**, 177.
63. Comba P., (1993), *Coord. Chem. Rev.* **123**, 1
64. Burkert U., Allinger N., (1982), Molecular Mechanics; ACS Monography 177; American Chemical Society: Washington DC.
65. Schmitz L.R., Allinger N.L., (1990), *J. Am. Chem. Soc.*, **112**, 8307.
66. Rappe A., Casewit C.J., Colwell K.S., Goddard W.A., Skiff W.M., (1992), *J. Am. Chem. Soc.* **114,** 10024.
67. Kadish K.M., Smith K.M., Guillard R., (2000), (Eds.), The Porphyrin Handbook, Academic Press, San Diego, CA.
68. Root D.M., Landis C.R., Cleveland T., (1993), *J. Am. Chem. Soc.* **115,** 4201.
69. Deeth R.J., (2001), *Coord. Chem. Rev.* **212** , 11.
70. Shi S., Yan L., Yang Y., Fisher-Shaulsky J., Thacher T., (2003), *J. Comput. Chem.*, **24**, (9), 1059
71. Insight II. System Guide, July 2005.

CHAPTER FIVE

In vivo modelling and animal experiments

5.1 *In vivo* modelling

5.1.1 Introduction

The primary objective of this study was to produce a drug which is able to mobilize Cu(II) in blood plasma. Although the ligands designed in this study form more stable complexes with Cu(II) than with Zn(II) and Ca(II), this is no guarantee that the Cu(II) complex will form *in vivo* because here the Zn(II) and Ca(II) concentrations are much higher than the Cu(II) concentration and there are a myriad of other ligands which bind Cu(II). To estimate the complexing ability of these ligands *in vivo* then, their plasma mobilizing indices (p.m.i) were calculated. This calculation takes into account competition with some 10 metal ions and more than 5000 ligands present in plasma. The index is defined for Cu(II) [1, 2] as the concentration of low molecular weight (l.m.w) Cu(II) complex species in the presence of a drug divided by their concentration in the absence of the drug. Thus p.m.i defines the ability of a ligand to move Cu(II) from a protein bound form to a l.m.w form. This means that a strong specific Cu(II) chelator would have high p.m.i. values at low drug concentrations, indicating a potentially useful therapeutic agent.

5.1.2 Speciation modelling

Figure 5.1 shows the p.m.i curves for [555-N], [H(555)-N], [H_2(5555)-N] and [H_2(556)-N]. For comparison the results for glycylglycylhistamine (GGHA) are also shown. From this we see that [555-N] and [H(555)-N] are some five and two orders of magnitude better at mobilizing Cu(II) *in vivo* than GGHA. In contrast, GGHA is one and two orders of magnitude better at mobilizing Cu(II) *in vivo* than [H_2(5555)-N] and [H_2(556)-N] respectively. Figure 5.2 shows p.m.i curves for Cu(II), Ni(II), Zn(II) and Ca(II) with [555-N] and [H(555)-N] plotted against the concentration of the ligand.

Figure 5.1: Cu(II) plasma mobilizing indices for [555-N], [H(555)-N], [H_2(5555)-N], [H_2(556)-N] and glycylglycylhistamine.

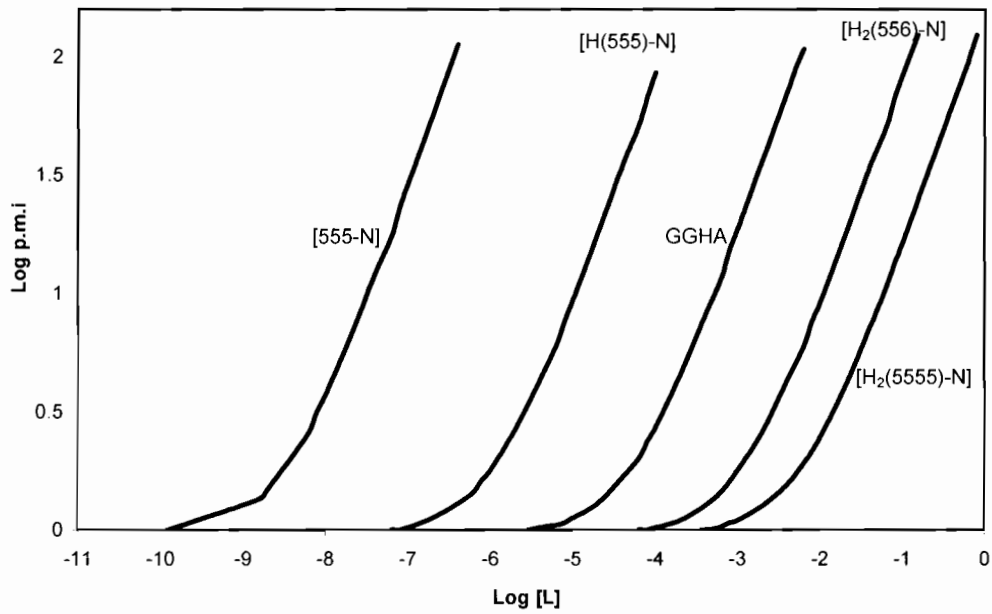

Both [555-N] and [H(555)-N] are able to cause a more than 10 fold increase in l.m.w Cu(II) concentration at a total ligand concentration of 10^{-7} and 10^{-5} mol dm^{-3} respectively. To achieve the same increase in l.m.w Cu(II) using [H_2(556)-N] or [H_2(5555)-N] a total ligand concentrations of 10^{-2} and 10^{-1} mol dm^{-3} are required respectively. The remarkably high mobilizing ability of [555-N] by a factor of three log units compared to [H(555)-N] is related to the stable three chelate rings formed with Cu(II) as well as the presence of the amide moiety in [H(555)-N]. As noted in Chapter 3, the electron withdrawing nature of such a group has been reported [3] to reduce the basicity of the donor atoms for this complex system. Reduced mobilizing ability in [H_2(556)-N] and [H_2(5555)-N] could be attributed to this same effect since these two systems contain two amidic groups. Thus the *in vivo* mobilization of Cu(II) is observed to decrease as amide groups are introduced into the ligand.

Although it has been reported that ligands containing an imidazole residue are not particularly good at mobilizing Cu(II) *in vivo* [4], it seems the better mobilization arising from GGHA as compared to [H_2(556)-N] and [H_2(5555)-N] is a result of the high basicity of the imine nitrogen of the

imidazole ring with a reported pK_a value of 6.95 [5] as compared to the very acidic pyridyl nitrogen with a $pK_a < 2.00$. Such results are not unexpected in view of the wide biological involvement of imidazole-containing ligands such as histidine as chelating agents. However better mobilization of [555-N] as compared to GGHA, could be a result of stronger coordination of the amino groups as opposed to amidic groups, which are generally hard coordinating groups, and have the effect of reducing the basicity of the ligand donor atoms.

Figure 5.2: Log p.m.i curves for (a) Cu(II), Ni(II), Zn(II) and Ca(II) with [555-N] and (b) Cu(II), Ni(II), Zn(II) and Ca(II) with [H(555)-N] plotted against log [L].

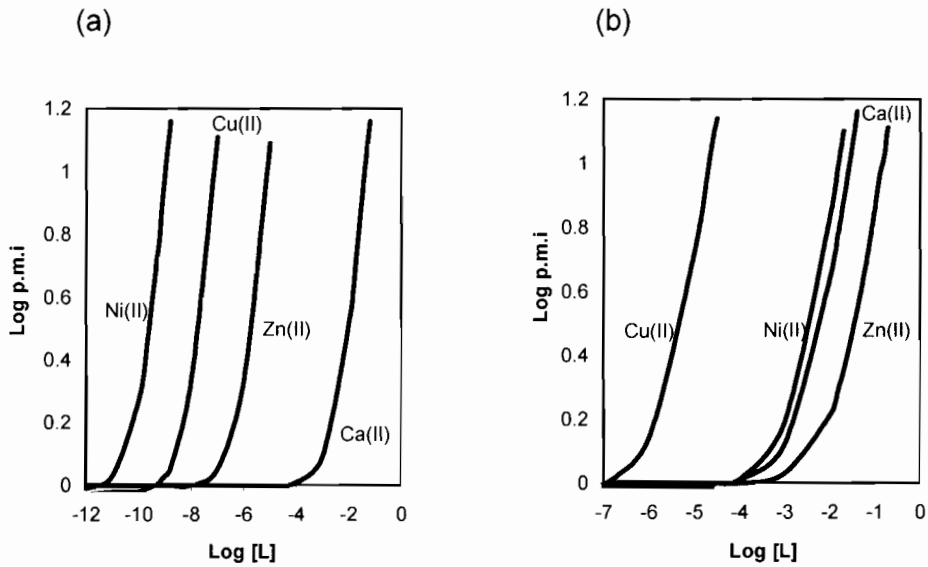

P.m.i curves for Cu(II), Ni(II), Zn(II) and Ca(II) with [555-N] and [H(555)-N] (Figure 5.2) show that the Zn(II) and Ca(II) p.m.i's are very low at ligand concentration of 10^{-7} and 10^{-5} respectively. In spite of the higher concentrations of these *in vivo* competitors and the predominance of ML and MLH_{-1} species for the two systems, the two metals generally form weak complexes with these two ligands, making them less important as competitors of Cu(II) *in vivo*.

5.2 Experimental

Computer modelling of the *in vivo* Cu(II) speciation was carried out using the program ECCLES [6]. The calculations were based on an updated model of blood plasma [7] with the relevant formation constants taken from the current potentiometric results (section 3.4.1) and references by Jackson and Kelly [8, 9]. The blood plasma model consists of data for 10 metal ions and more than 5000 ligands. The formation constants determined in this study were incorporated into the model. This enlarged database was then interrogated using the ECCLES computer program to yield the plasma mobilizing index (p.m.i) as a function of concentration. The total ligand concentration, $[L]_T$, was varied over the range 10^{-1} - 10^{-10} mol dm^{-3}. The pH was kept constant at 7.40.

5.3 Bio-distribution studies

5.3.1 Introduction

Copper is an essential trace element required by all living organisms [10, 11]. It plays a key role as an integral component of many enzymes [12, 13]. While trace amounts of copper are required for normal metabolic processes, it can be extremely toxic in excess [14]. Free copper, even in relatively low concentration, has the ability to generate free radicals through Fenton reaction and oxidize cellular components [14, 15]. This places a burden on systems that normally transport copper between organs *in vivo*.

Copper is the third most abundant transition metal element in biological systems [16], with the normal human body of an average healthy adult male (70 kg) containing 80 - 120 mg of copper as compared with 4 - 5 g of Fe and 1.4 - 2.3 g of Zn [16]. The average daily intake of copper in humans is about 1.5 - 3.0 mg per day [17]. Of the approximately 110 mg copper contained in the body, most of this is in the skeleton (46 mg), skeletal muscle (26 mg), liver (10 mg), brain (8.8 mg) and blood (6 mg) [18]. The distribution of copper in the body is such that the brain and liver have the highest tissue levels, while lesser concentrations are found in the heart, spleen, kidneys and blood. The iris and choroid of the eye also have very high copper levels [19].

Metabolic balance studies show that people with daily intakes of 2 - 5 mg of copper per day absorb 0.6 - 1.6 mg (32 %), excrete 0.5 - 1.3 mg in the bile, pass 0.1 - 0.3 mg directly into the bowel, and excrete 0.01 - 0.06 mg in the urine [20]. As these data indicate urinary excretion plays a minor role in copper clearance, and principal route of excretion is in the bile, where copper is believed to be excreted as a bile acid complex [21, 22].

In humans, copper absorption varies inversely with dietary copper intake [23]. Most copper absorption takes place from the stomach through to the small intestine [24], predominantly in the stomach and duodenum (acidic pH) of the gastrointestinal (GI) tract. Copper absorbed from the GI tract is

transported rapidly to blood serum and deposited in the liver bound metallothionen where it gets released and incorporated into ceruloplasmin (CP), a specific copper transporting protein. Maximum blood copper levels have been observed within 1 - 3 hours following oral administration, with about 50 % of ingested copper being absorbed [19]. The presence of zinc, iron, and molybdenum, decreases copper absorption, while high protein diets increase copper absorption [24, 25]. The low pH value of gastric juices also contribute to the freeing of copper bound to foodstuffs, prior to GI absorption [24]. This is important in the investigation of methods for copper administration and delivery in copper chemotherapy.

Investigation of copper bio-distribution in mice using $^{64}Cu(II)$ as a radiotracer for the copper chelating agents in this study allows determination of the improved bioavailability and efficacy of these agents in transporting Cu(II) through the body to possible sites of inflammation. Based on the high selectivity (Section 3.4.7) and encouraging mobilizing ability (Section 5.1.2) of our ligands towards Cu(II) under physiological conditions, bio-distribution studies have been carried out to verify these findings and also determine the ligands' *in vivo* stability.

5.3.2 Results and Discussion

5.3.2.1 Results

Initially, the interest was to investigate the amount of activity retained by the whole body and excreted through the urine. As a result the activity in the blood, liver, carcass and urine were investigated 1 hr post-injection. Encouraging high uptake in the carcass 1 hr post-injection, necessitated further excision of the other organs in order to investigate the localization of this activity.

The bio-distribution results are given in Tables 5.1 - 5.3. For comparison the results for $^{64}CuCl_2$, used as a control, are also included.

These readings were corrected for background noise and adjusted according to the half-life of $^{64}Cu(II)$ since the samples were counted at different times. Table 5.2 shows the degree of Cu(II) retention by the body for the various chelating agents, whereas Table 5.3 indicates into which organs $^{64}Cu(II)$ has been concentrated.

Figures 5.3 - 5.6 show the activity trend in the major organs of interest over time while the biological half life is given in Figure 5.7. Results for $^{64}CuCl_2$ (control) are also included in these Figures.

Table 5.1: Bio-distribution of $^{64}Cu(II)$ in white mice for various ligands 1 hr post-injection (% ID/organ & gram, mean ± SD, n = 3).

Organ	$^{64}Cu(II)$ complex (% ID per organ & per gram)				
	[555-N]	**[H(555)-N]**	**[H_2(5555)-N]**	**[H_2(556)-N]**	**$CuCl_2$**
Blood	0.17 ± 0.03 0.72 ± 0.06	0.32 ± 0.12 1.14 ± 0.17	0.37 ± 0.11 1.26 ± 0.09	0.43 ± 0.13 2.29 ± 0.05	0.34 ± 0.10 1.40 ± 0.44
Liver	48.63 ± 4.82 37.41 ± 2.36	61.84 ± 2.54 58.78 ± 2.89	65.09 ± 2.46 48.26 ± 2.77	68.43 ± 3.29 47.62 ± 2.62	38.45 ± 1.86 29.56 ± 4.73
Carcass	29.04 ± 3.23 1.58 ± 0.21	30.56 ± 3.19 1.81 ± 0.33	31.32 ± 2.27 1.61 ± 0.15	27.85 ± 3.06 1.97 ± 0.01	55.01 ± 1.08 3.10 ± 0.12
Urine	22.15 ± 5.56	7.28 ± 0.96	3.21 ± 0.52	3.29 ± 1.19	6.19 ± 2.16

Table 5.2: Bio-distribution of $^{64}Cu(II)$ for copper complexes (%ID / organ, mean ± SD, n = 3)

Organ	[^{64}Cu]Cu-[555-N]		[^{64}Cu]Cu-[H(555)-N]		[^{64}Cu]Cu-[H_2(5555)-N]		[^{64}Cu]Cu-[H_2(556)-N]		[^{64}Cu]$CuCl_2$	
	6 hr	24 hr	6 hr	24 hr	6 hr	24 hr	6 hr	24 hr	6 hr	24 hr
Blood	0.34 ± 0.10	0.66±0.19	0.35±0.10	0.54±0.12	0.47±0.12	0.98±0.09	0.29±0.16	1.15±0.09	0.42±0.01	0.41±0.06
Liver	52.81± 4.61	30.77±2.07	60.77±1.78	31.75±3.56	62.37±3.49	29.94±5.84	47.52±5.62	27.62±6.31	68.84±1.93	37.15±1.85
Carcass	7.97 ± 1.41	17.10±1.57	10.23±2.79	19.12±3.44	9.34±1.51	20.81±3.00	7.14±1.61	16.60±0.49	9.17±3.61	12.17±3.20
Urine	29.64 ± 2.69	32.14±5.55	10.69±2.09	30.50±2.30	8.77±1.41	27.81±3.89	30.53±6.98	32.36±11.30	4.31±0.90	33.33±4.08
Muscle	0.12 ± 0.05	0.47±0.16	0.16±0.06	0.19±0.06	0.14±0.01	0.54±0.10	0.31±0.08	0.40±0.05	0.12±0.04	0.29±0.18
Heart	0.22 ± 0.02	0.47±0.24	0.34±0.16	0.50±0.17	0.26±0.03	0.65±0.22	0.33±0.13	1.10±0.26	0.48±0.13	0.28±0.04
Lung	0.32 ± 0.04	1.29±0.60	0.49±0.22	0.99±0.22	0.48±0.05	1.18±0.29	0.41±0.04	1.36±0.37	0.53±0.10	1.28±0.11
Kidney	2.11 ± 0.48	2.60±0.31	1.07±0.04	1.90±0.10	0.91±0.02	2.36±0.10	1.48±0.80	2.67±0.17	1.18±0.14	2.61±0.41
Head	1.49 ± 0.21	3.66±0.47	1.68±0.28	3.33±0.77	1.78±0.13	4.13±0.35	1.29±0.29	3.96±1.61	2.00±0.24	4.40±0.99
Intestines	4.75 ± 0.70	10.59±1.24	13.96±1.71	11.05±2.82	14.97±3.20	11.21±1.11	10.58±2.81	11.91±2.07	12.76±3.51	22.98±1.83
Spleen	0.21 ± 0.05	0.26±0.05	0.24±0.10	0.11±0.07	0.50±0.08	0.38±0.07	0.11±0.02	0.86±0.50	0.17±0.01	0.56±0.04

Table 5.3: Bio-distribution of $^{64}Cu(II)$ for copper complexes (%ID / g, mean ± SD, n = 3)

Organ	[^{64}Cu]Cu-[555-N]		[^{64}Cu]Cu-[H(555)-N]		[^{64}Cu]Cu-[H_2(5555)-N]		[^{64}Cu]Cu-[H_2(556)-N]		[^{64}Cu]$CuCl_2$	
	6 hr	24 hr	6 hr	24 hr	6 hr	24 hr	6 hr	24 hr	6 hr	24 hr
Blood	1.41 ± 0.40	2.36 ± 0.39	0.70 ± 0.16	1.97 ± 0.27	1.84 ± 0.52	3.01 ± 0.64	0.72 ± 0.18	2.42 ± 0.52	1.01 ± 0.10	7.38 ± 0.50
Liver	41.76 ± 2.56	24.28 ± 1.93	57.85 ± 0.87	21.26 ± 3.19	53.21 ± 9.30	24.02 ± 2.57	38.51 ± 6.16	21.69 ± 5.94	52.70 ± 0.43	25.98 ± 1.32
Carcass	0.67 ± 0.04	1.45 ± 0.03	0.96 ± 0.28	1.21 ± 0.34	0.76 ± 0.17	1.50 ± 0.24	0.58 ± 0.05	1.26 ± 0.16	0.76 ± 0.25	1.78 ± 0.04
Urine	-	-	-	-	-	-	-	-	-	-
Muscle	0.32 ± 0.18	1.42 ± 0.35	0.76 ± 0.51	0.58 ± 0.17	0.78 ± 0.10	2.01 ± 0.45	1.26 ± 0.23	1.81 ± 0.07	0.50 ± 0.20	0.89 ± 0.53
Heart	2.00 ± 0.49	3.14 ± 1.46	2.85 ± 1.17	3.29 ± 1.12	2.12 ± 0.72	5.53 ± 2.57	2.39 ± 0.64	8.10 ± 2.00	2.58 ± 0.35	2.29 ± 0.48
Lung	1.48 ± 0.21	4.24 ± 1.24	2.35 ± 0.61	4.05 ± 0.93	1.61 ± 0.39	5.89 ± 1.62	2.93 ± 0.45	9.39 ± 0.91	2.11 ± 0.60	5.79 ± 0.75
Kidney	5.15 ± 0.79	6.65 ± 0.75	3.46 ± 0.14	5.45 ± 0.31	2.53 ± 0.20	7.00 ± 0.39	3.79 ± 2.22	7.64 ± 0.30	3.22 ± 0.05	7.94 ± 1.96
Head	0.53 ± 0.13	1.20 ± 0.08	0.63 ± 0.10	1.10 ± 0.08	0.61 ± 0.04	1.27 ± 0.16	0.48 ± 0.10	1.34 ± 0.43	0.65 ± 0.04	1.52 ± 0.32
Intestines	3.35 ± 0.89	4.91 ± 0.37	7.01 ± 0.06	5.13 ± 0.38	6.26 ± 1.47	6.18 ± 1.27	4.29 ± 1.29	4.73 ± 0.09	5.13 ± 0.20	11.66 ± 1.04
Spleen	2.82 ± 0.79	2.95 ± 0.23	2.80 ± 0.74	1.30 ± 0.61	4.00 ± 0.97	3.46 ± 0.44	1.88 ± 0.26	10.64 ± 1.72	1.76 ± 0.28	6.66 ± 0.81

Figure 5.3: % Injected dose per gram for Cu(II)/[555-N] [ ], Cu(II)/[H(555)-N] [ ], Cu(II)/[H_2(5555)-N] [ ], Cu(II)/[H_2(556)-N] [ ] and $CuCl_2$ [ ] in blood 1, 6 and 24 hr post-injection.

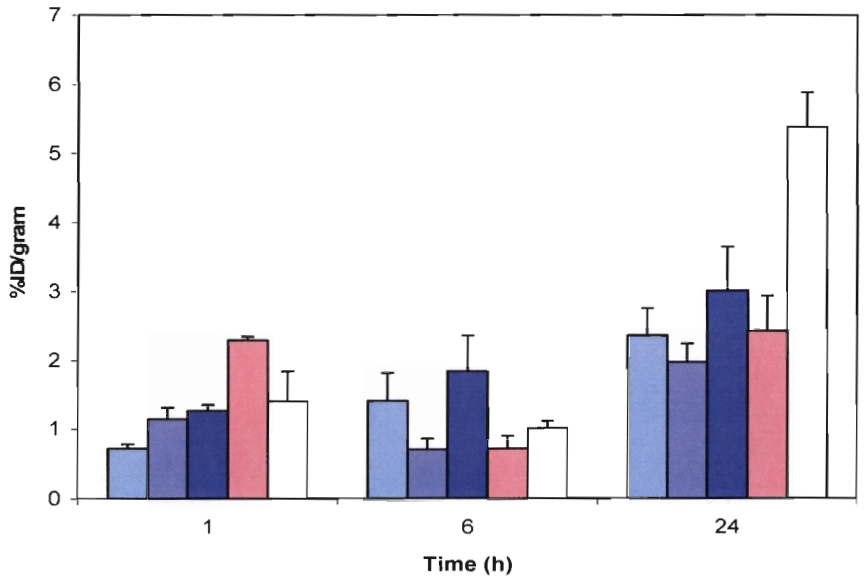

Figure 5.4: % ID per organ for Cu(II)/[555-N] [ ] Cu(II)/[H(555)-N] [ ] Cu(II)/[H_2(5555)-N] [ ] Cu(II)/[H_2(556)-N] [ ] and $CuCl_2$ [ ] in liver 1, 6 and 24 hr post-injection.

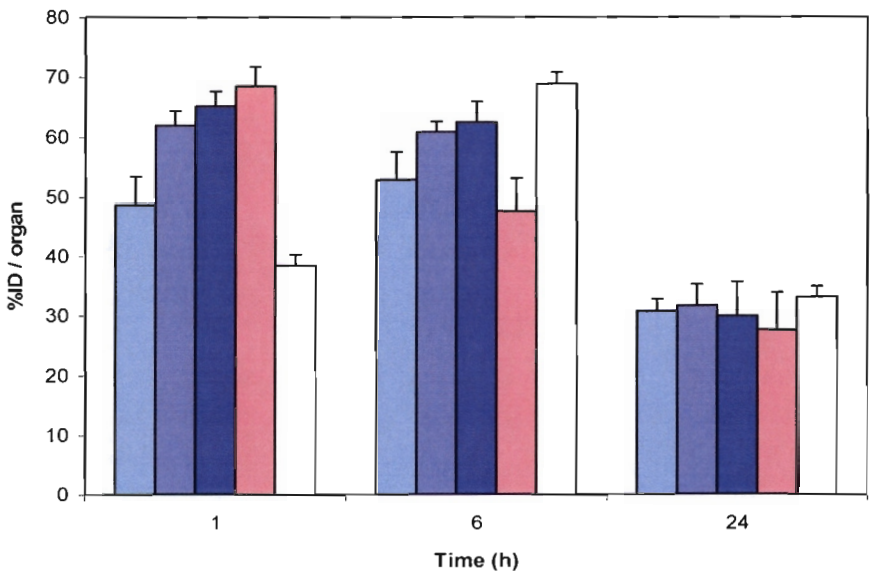

Figure 5.5: % ID per organ for Cu(II)/[555-N] [ ] Cu(II)/[H(555)-N] [ ] Cu(II)/[H_2(5555)-N] [ ] Cu(II)/[H_2(556)-N] [ ] and $CuCl_2$ [ ] in carcass 1, 6 and 24 hr post-injection.

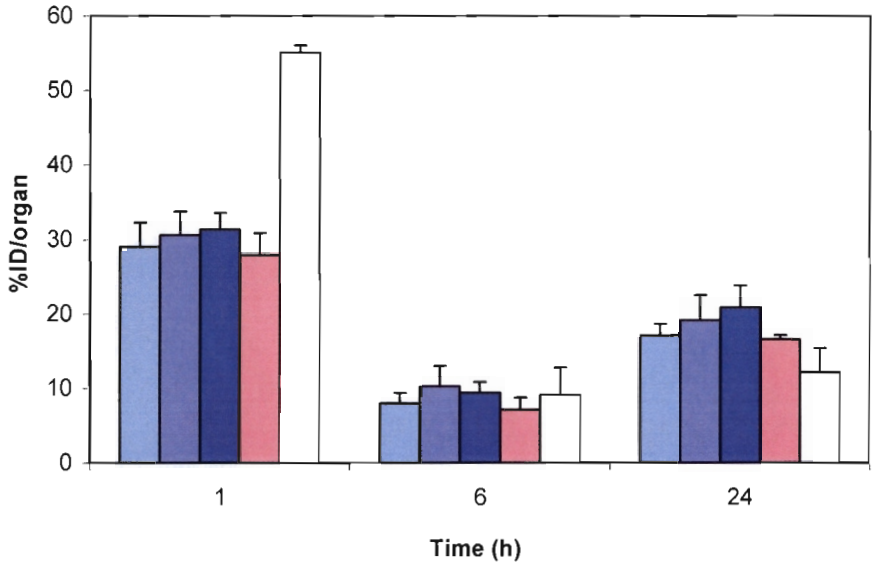

Figure 5.6: % ID per sample for Cu(II)/[555-N] [ ] Cu(II)/[H(555)-N] [ ] Cu(II)/[H_2(5555)-N] [ ] Cu(II)/[H_2(556)-N] [ ] and $CuCl_2$ [ ] in urine 1, 6 and 24 hr post-injection.

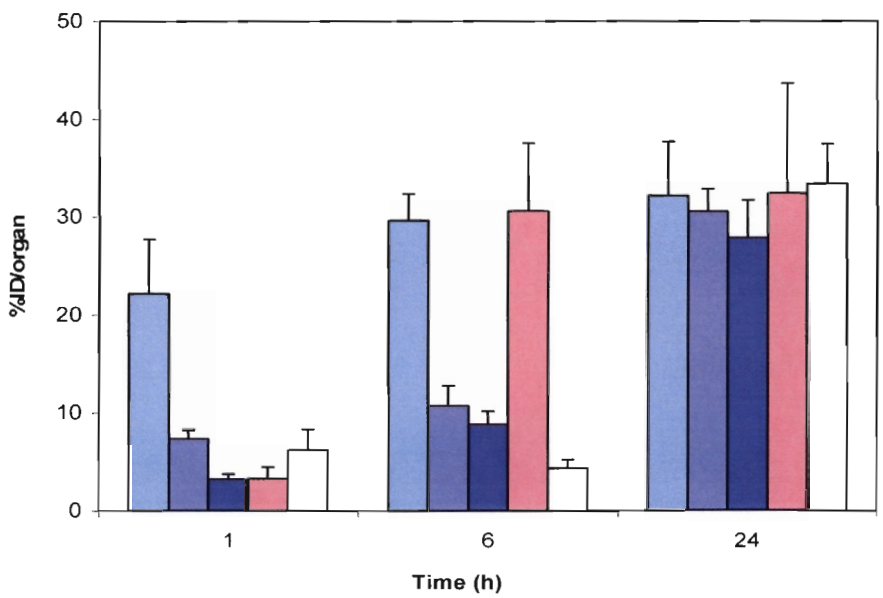

Figure 5.7: % ID remaining in the body plotted as a function of time showing the *in vivo* biological half life of copper. The dotted line denotes % ID corresponding to the half life.

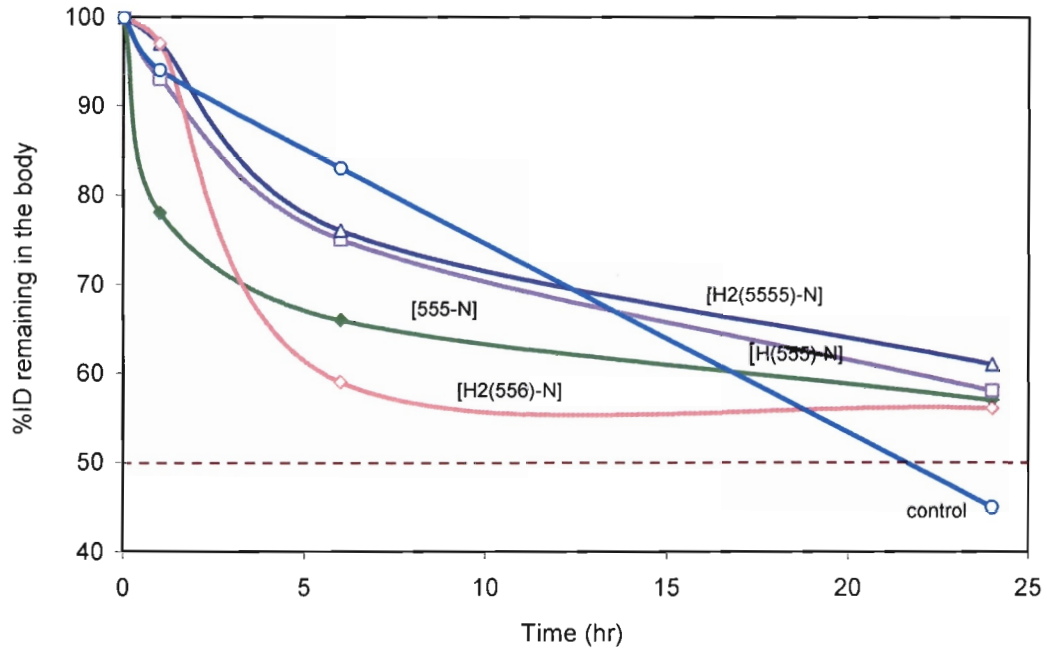

5.3.2.2 Discussion

Comparison of bio-distribution results for the $^{64}CuCl_2$ control in this study with those of the $^{67}CuCl_2$ control injected in white mice as reported by Jackson et al. [26] shows that there is no agreement between the two. The latter results show much lower uptake in the blood, liver and kidney but much higher uptake in the carcass at 24 hr. The difference between these results could be due to the injection method used in the two studies. Jackson et al. [26] used intraperitoneal injection, as opposed to intravenous injection which was used in this study. Another possible reason for the difference in the two studies is the isotopic purity of the Jackson study [26]. In their study ^{67}Cu produced as a by-product during the production of Ga from a Zn target was used. Thus it is possible that their sample of ^{67}Cu was contaminated by other long lived radio-nuclides. In our case the ^{64}Cu was produced by neutron bombardment of CuO. However, good agreement in terms of $^{64}CuCl_2$ uptake and distribution trend over time in controls of this study and controls reported

by Nomkoko et al. [27] under the same conditions is observed. This agreement lends confidence to our experimental results.

The bio-distribution results for the $^{64}CuCl_2$ control indicate that there is rapid clearance from blood upon injection with activity less than 1 % (0.34 - 0.42 % ID) remaining 1 hr post-injection. The $^{64}CuCl_2$ cleared from the blood is initially taken up by the liver which records high uptake after 1 hr (38.45 %) and 6 hr (68.84 %). The highest uptake in the liver is recorded after 6 hr and this results in some partial $^{64}Cu(II)$ excretion into the intestines where an uptake of 12.76 % is recorded. It is worthy noting that after 6 hr there is very little $^{64}Cu(II)$ activity (4.31%) in the urine. It has been shown from metabolic balance studies [20], that urinary excretion plays a minor role in copper clearance with the principal route of excretion being the intestine.

Like the liver, the carcass, recorded a high initial uptake (55.01 %) of $^{64}Cu(II)$ after 1 hr, but this drops after 6 hr (9.17 %). After 24 hr, the activity of $^{64}Cu(II)$ in the liver and carcass goes down to 37.15 % and 12.17 % respectively. This corresponds to an overall decrease in the total body load. The decrease in the total body load at the 24 hr post-injection time point suggests excretion of the $^{64}Cu(II)$ after 24 hr. High activity of $^{64}Cu(II)$ (22.98 %) recorded in the intestines at this same time indicates the principal excretion route to be hepatobiliary. An unexpected high activity of $^{64}Cu(II)$ in the urine after 24 hr (33.33 %) could be due to contamination by the stool, since this was visually present and could not be separated from the urine during extraction. Moreover low activity of $^{64}Cu(II)$ (2.61 %) in the kidneys after 24 hr suggests very little excretion via the renal route.

The bio-distribution pattern of $^{64}Cu(II)$ for the control as described above indicates a normal metabolic pathway of ionic Cu(II). This normal Cu(II) metabolic pathway consists of binding to serum albumin and rapid uptake by the liver, followed by slow release back into the blood as ceruloplasmin or excretion into the intestines as biliary copper [28].

With the exception of the [^{64}Cu]Cu(II)-[555-N] complex, the activity for the different complexes in blood are generally similar to those of the control after 1 hr (Figure 5.3). The [^{64}Cu]Cu(II)-[555-N] complex clears faster from the blood than the control with 50 % clearing after 1 hr. Bio-distribution patterns of the [^{64}Cu]Cu(II) complexes similar to the control suggest initial dissociation of the Cu(II) complexes into their components soon after injection as a result of low *in vivo* stability. This results in these [^{64}Cu]Cu(II) complexes following the ^{64}Cu(II) pathway for the control. Under such circumstances it will be expected for the [^{64}Cu]Cu(II) complexes to show elevated liver concentrations as the liberated ^{64}Cu(II) follow the normal metabolic pathway of ionic Cu(II). Indeed, significant initial uptake of all the four [^{64}Cu]Cu(II) complexes by the liver is observed after 1 hr, with more than 40 % activity absorbed compared to less than 40 % activity absorbed for the control. Thus high activity of 48.6% [^{64}Cu]Cu(II)-[555-N], 61.8% [^{64}Cu]Cu(II)-[H(555)-N], 65.1% [^{64}Cu]Cu(II)-[H_2(5555)-N] and 68.4% [^{64}Cu]Cu(II)-[H_2(556)-N] complexes are recorded in the liver 1 hr post-injection. However the liver uptake for the [^{64}Cu]Cu(II)-[555-N] complex is much lower compared to the other [^{64}Cu]Cu(II) complexes while reduced uptake of the control (< 40 %) compared to the uptake for the studied [^{64}Cu]Cu(II) complexes suggests that uptake of the [^{64}Cu]Cu(II) complexes by the liver is not solely due to these complexes following normal metabolic route only, but also a result of influence of the ligands *in vivo*. The activity for the [^{64}Cu]Cu(II)-[555-N] complex is high in the urine (22.15 %) after 1 hr while there is reduced activity in the urine for the other three [^{64}Cu]Cu(II) complexes.

The activity for all the [^{64}Cu]Cu(II) complexes in the carcass as given in Figure 5.5, indicates an initial high uptake (≈ 30 %) for all the [^{64}Cu]Cu(II) complexes after 1 hr. At this same time the activity for ^{64}Cu(II) (≈ 55 %) for the control is significantly different suggesting influence of the ligands on the [^{64}Cu]Cu(II) complexes' bio-distribution *in vivo*. There is clear correlation for the control ^{64}Cu(II) activity recorded in the carcass and liver (Figures 5.4 and 5.5) where reduced ^{64}Cu(II) activity in the liver corresponds to increased activity in the carcass 1 hr post-injection.

Generally, after 1 hr highest activity levels for the [^{64}Cu]Cu(II)-[H(555)-N], [^{64}Cu]Cu(II)-[H_2(5555)-N] and [^{64}Cu]Cu(II)-[H_2(556)-N] complexes are recorded in the liver and carcass, while relatively lower activity is recorded in blood and urine. This suggests rapid clearance from blood, minimal excretion into the urine, redistribution and accumulation into other body organs for these [^{64}Cu]Cu(II) complexes after 1 hr.

At 6 and 24 hr post-injection the [^{64}Cu]Cu(II) complexes' activity redistribution occurs resulting in activity accumulation in the major organs. Such activity accumulation in the blood suggests slow clearance of the [^{64}Cu]Cu(II) complexes from the blood stream after 24 hr. The liver retains activity of these [^{64}Cu]Cu(II) complexes up to 6 hrs before activity slowly clears by 50 % after 24 hr. Activity clearance from the liver at 24 hr would result in possible accumulation in the intestines as these [^{64}Cu]Cu(II) complexes get partially excreted into the intestines via the biliary route. Indeed, high activity of 14.0% [^{64}Cu]Cu(II)-[H(555)-N], 15.0% [^{64}Cu]Cu(II)-[H_2(5555)-N] and 10.6% [^{64}Cu]Cu(II)-[H_2(556)-N] complexes (Table 5.2) were recorded in the intestines compared to only 4.8% [^{64}Cu]Cu(II)-[555-N] complex after 6 hr. The reduced [^{64}Cu]Cu(II)-[555-N] complex activity in the intestine suggests an excretion route other than hepatobiliary. There is activity accumulation of 2.1% [^{64}Cu]Cu(II)-[555-N] complex in the kidney after 6 hr, while [^{64}Cu]Cu(II)-[H(555)-N] (1.1%), [^{64}Cu]Cu(II)-[H_2(5555)-N] (0.9%) and [^{64}Cu]Cu(II)-[H_2(556)-N] (1.4%) complexes have reduced uptake in the same organ. This then supports renal excretion for the [^{64}Cu]Cu(II)-[555-N] complex as earlier on indicated by high excretion (22.15%) of this complex after 1 hr.

Other organs were also collected to determine whether any tissue specificity existed. Concentration of the [^{64}Cu]Cu(II) complexes in the heart and lungs (Table 5.3) is observed after 6 and 24 hr. This heart and lung concentration is more significant for [^{64}Cu]Cu(II)-[H_2(5555)-N] (5.53 & 5.89 %ID/g) and [^{64}Cu]Cu(II)-[H_2(556)-N] (8.10 & 9.39 %ID/g) complexes respectively. The high uptake of these [^{64}Cu]Cu(II) complexes by the aforementioned organs could be explained in part by their high lipophilicities (log $P_{oct/aq}$ = 0.083 & -0.313) as discussed in Chapter 4. In terms of contrast

between the heart and adjacent organs, heart-to-blood ratios greater than 1.0 for the [^{64}Cu]Cu(II) complexes suggests significant uptake by the heart. However, although blood was withdrawn from the heart, this organ was not perfused so blood could be contributing to the high activity in the heart count. The concentration of the four [^{64}Cu]Cu(II) complexes in the liver at all time points ranges from 2 - 20 times the concentration in the heart. Concentrations of more than 20 times have been reported [29], suggesting that the heart count in this study could be an overestimation. No significant uptake was recorded in the head, spleen, and muscle for the [^{64}Cu]Cu(II) complexes although relatively slow accumulation was recorded in these tissues after 24 hr. On the basis of such bio-distribution patterns, none of these copper chelating agents would be expected to improve bioaccumulation of Cu(II) in the brain, despite this organ having some of the highest tissue levels of natural Cu(II) *in vivo*. This indicates the inability of these [^{64}Cu]Cu(II) complexes to cross the blood-brain barrier.

Although an estimation of the biological half life can be made from the activity remaining in the body after 24 hrs, a more accurate estimation can be obtained from an exponential decay curve (Figure 5.7) for the activity remaining *in vivo* as a function of time. The results presented (1, 6 & 24 hr post-injections) suggests that the liver readily absorbs and retains [^{64}Cu]Cu(II) complexes up to 6 hr, and thereafter releases the radionuclide for redistribution in the whole body. Activity accumulation for all the [^{64}Cu]Cu(II) complexes in the carcass after 24 hrs as shown in Figure 5.5 supports the ^{64}Cu(II) activity redistribution phenomenon, indicating reasonably encouraging biological half life of these [^{64}Cu]Cu(II) complexes *in vivo*. There is still 17.1% [^{64}Cu]Cu(II)-[555-N], 15.1% [^{64}Cu]Cu(II)-[H(555)-N], 20.8% [^{64}Cu]Cu(II)-[H_2(5555)-N] and 16.6 % [^{64}Cu]Cu(II)-[H_2(556)-N] complexes remaining in the carcass after 24 hr. At this same time only 12.17 % ^{64}Cu(II) activity for the control remains in the carcass. As is illustrated in the exponential decay curve for the activity remaining in the whole body (Figure 5.7), the *in vivo* biological half life(s) for all the [^{64}Cu]Cu(II) complexes are higher than 24 hr whereas this is much lower ($\approx$ 22 hrs) for the control. Use of ^{67}Cu(II) with a longer half life,

instead of ^{64}Cu(II) would have enabled us to count the samples for longer than 24 hr and establish the exact biological half life of each [^{64}Cu]Cu(II) complexes. However this radionuclide was not used in this study because it is difficult to produce.

The high activity in the liver is to be expected in view of the fact that the Cu(II) storing proteins and normal Cu(II) metabolism occur in this organ. The normal Cu(II) metabolic pathway consists of binding to serum albumin and rapid uptake by the liver, followed by slow release back into the blood as ceruloplasmin or excretion into the intestines as biliary copper [28]. Such high uptake of ^{64}Cu(II) labelled complexes by the liver has been reported by other workers [29, 30, 31]. It has been suggested that the high uptake of ^{64}Cu(II) labelled complexes by the liver is due to transchelation of the radioisotope by albumin and histidine. This is because these *in vivo* proteins and l.m.w ligands bind Cu(II) strongly. Since the liver is the centre of Cu(II) metabolism, the expected mode of removal of the complexes readily absorbed by the liver would be the hepatobiliary route. Reduced accumulation for the [^{64}Cu]Cu(II)-[555-N] complex in the intestines at 1 hr post-injection time point suggests removal predominantly via a route different from the hepatobiliary route.

These bio-distribution results support the *in vivo* modelling studies. [555-N] is a far stronger Cu(II) mobilizing agent than [H(555)-N], [H_2(5555)-N] and [H_2(556)-N] by several orders of magnitude, and so a bio-distribution different from $^{64}CuCl_2$ would be expected. Indeed this is seen, the [^{64}Cu]Cu(II)-[555-N] complex undergoes initial rapid renal excretion and slower liver uptake than $^{64}CuCl_2$. Such results are not unexpected for charged species [32]. Parckard and co-workers [29] have reported similar renal elimination pathways for negatively charged ^{64}Cu(II)-labelled complexes. It has been previously demonstrated that the charge of the Cu(II)-bifunctional chelator complex attached to both monoclonal antibodies and peptides had a significant effect on the clearance properties of the ^{64}Cu(II)-BFC biomolecules [33, 34]. Additionally, it has been determined that ^{64}Cu(II)-labelled macro cyclic complexes with different formal charges showed dramatically different behaviour in normal rats [32, 35]. Jones-Wilson [32] have also suggested that

many factors control the clearance of small molecules from the body, with charge on the complex playing one of the more important roles. Results reported by Rogers and co-workers [34] suggested higher uptake of some ^{64}Cu(II)-labelled macro cyclic chelates in the liver and kidneys to be due to positive charge rather than dissociation of ^{64}Cu(II) from the complex. Since the [^{64}Cu]Cu(II)-[555-N] complex is sufficiently stable within the pH range 2.00 - 10.00 as predicted by the speciation distribution results (Figure 3.7), avoidance of breakdown in the low pH environment of the stomach is possible after oral administration of this complex, but it is likely to suffer the same fate of initial rapid renal excretion after absorption.

Rapid renal loss is not a feature associated with charged complexes only, as it has been reported for uncharged polyamino [^{64}Cu]Cu(II)-DTDA and [^{64}Cu]Cu(II)-TTDA [26], which at physiological pH are presumably too hydrophilic for efficient re-absorption from the urine where they are excreted rapidly, unchanged, resulting in a poor biological half life. For the four [^{64}Cu]Cu(II) complexes investigated in this study, the bio-distribution and biological half life suggest dependence on the formal charge of the Cu(II) complexes. In particular the differences in uptake and clearance of the positively charged and neutral radiopharmaceuticals by the clearance organs were most effected, with positively charged complexes initially clearing rapidly via the renal system while neutral complexes excreted slowly via the liver. This scenario presents a challenge in terms of the nature of copper chelating agents to be developed as well as their subsequent method of administration for good biological retention and improve their bioavailability.

In conclusion, what we are attempting to design is a ligand (drug) which will improve the absorption and increase the biological half life of Cu(II) *in vivo*, so that the copper has time to exert its therapeutic potential. In this bio-distribution study we have only looked at the second stage in this process, ie biological half life. Although the [^{64}Cu]Cu(II)-[555-N] complex is initially rapidly lost via the renal route and [^{64}Cu]Cu(II)-[H(555)-N], [^{64}Cu]Cu(II)-[H_2(5555)-N] and [^{64}Cu]Cu(II)-[H_2(556)-N] complexes slowly excreted via the liver, they have encouraging biological half life(s) of greater than 24 hrs while

the biological half life for the control is less than 24 hrs. Such activity accumulation and retention in the body is encouraging and therefore merits further evaluation of these copper chelating agents for possible use as anti-inflammatory agents against inflammation associated with rheumatoid arthritis. An estimation of maximum permeation rate through human epidermis *in vitro* using a model developed by Michaels et al. [36, 37] as discussed in Chapter 4, indicated trans-dermal fluxes of 3.98×10^{-5} to 5.01×10^{-5} cm h^{-1} for these ligands. These absorption results suggest topical application at the site of inflammation to be viable for these [^{64}Cu]Cu(II) complexes. Therefore for future studies, dermal absorption measurements in mice, rather than their estimation from octanol/water partition coefficients, should be conducted to verify the amount of these [^{64}Cu]Cu(II) complexes that would actually permeate through the skin so as to establish the feasibility of percutaneous absorption as a method of drug administration.

5.4 Experimental

5.4.1 Introduction

The experimental approach adopted for animal experiments was similar to the approach of other workers in the field of nuclear medicine [32, 38, 39]. Since the ligands had been designed to be pre-organized for metal ion binding, complexation time of radio-metal labelling was expected to be reduced with the differences in stability constants not affecting the ability to label the Cu(II) complexes *in vitro*. Approval for these animal experiments was sought from the Research Animals Ethics Committee of the University of Cape Town (permission number 004/022) while authority to posses and use radioactive nuclide ^{64}Cu(II) ($t_{1/2}$ = 12.7 hrs) was requested from University of Cape Town's radiation protection and health safety committee in conjunction with the Department of Health (authority number 33/01/0327). ^{64}Cu(II) was the radioisotope of choice because of its wide application in both imaging [40, 41] and therapy [42, 43]. ^{67}Cu(II) ($t_{1/2}$ = 2.6 days) would have been a convenient choice in this study because of its longer half life, but was not considered

because it is difficult to produce. All the animal studies were performed in compliance with guidelines set by the University of Cape Town research animal ethics committee.

5.4.2 Radiation protection

Although low activity $^{64}Cu(II)$ ($t_{1/2}$ = 12.7 hr) of between 7.5 - 9.0 mCi was used during the experiment precautionary measures were taken against possible exposure to high energy radiation (β^+: 0.653 MeV, 17.4%; β^-: 0.578 MeV, 39%) from the radio active material. The most important safety aspects were to minimize exposure time and amount of activity one is exposed to during the experiments.

During the course of these experiments, safety clothing was also worn. This included disposable gowns, gloves and radiation badges. The preparation and injection of radio-labelled [^{64}Cu]Cu(II) complex solutions was performed behind a lead brick wall [44]. The aqueous solutions of the radio-labelled [^{64}Cu]Cu(II) complexes and $^{64}CuCl_2$ were kept in closed containers under refrigeration. After the experiments, all the material that included syringes, needles, disposables, the sacrificed animals and their respective excised organs were initially kept in a refrigerator for at least three weeks. This allowed the radioactivity to decay below safe levels before incineration.

5.4.3 Procedure

Approximately 1 mmol dm^{-3} solutions of the Cu(II) (0.001 mol dm^{-3})-L (0.003 mol dm^{-3}) complexes were prepared using sterile saline at pH 7.40. These prepared complex solutions (15.0 cm^3) were spiked with 7.5 - 9.0 mCi $^{64}CuCl_2$ (radiochemical purity > 98 %) to give solutions of about 12 kBq ml^{-1}.

The bio-distribution studies were carried out on a total of 45 female balb/c mice weighing between 20 - 22 g with food and water being allowed *ad libitum*. The mice were grouped in groups of three (3) per cage. These groups

of 3 mice were injected intravenously with about 5 μCi of activity via the tail vein. The injected volume did not exceed 0.2 ml giving a dose of ≈ 2.4 kBq per mouse. Another group of three mice were injected with $^{64}CuCl_2$ (aq) to serve as a control. The mice were then kept individually in polycarbonate cages, containing paper towelling for urine absorption.

At 1, 6 and 24 hr post-injection time points, groups of mice (3 at a time) were anaesthetized by carbon dioxide inhalation, aliquots of blood taken from the inferior vena cava. Various samples (liver, muscle, tail, heart, lung, kidney, intestines, spleen, head, carcass) were removed, rinsed with NaCl (0.9 %), dried and then weighed. The urine-impregnated towelling was extracted with 100 ml of 20 % v/v HCl and 10 ml used for radioactive counting.

Radioactive counting was carried out in a Minaxi Autogamma 5000 Series γ counter, using window set at 340 - 540 keV [32, 44, 45, 46, 47]. Standard samples were prepared and counted alongside with the samples. All readings were corrected for background noise by subtracting activity of an empty sample bottle as well as adjusted to activity at time zero according to the half-life of $^{64}Cu(II)$ using the exponential decay law given in equation 5.1.

$$\mathbf{N = N_o\, e^{-\lambda t}} \qquad (5.1)$$

where t is the time elapsed, λ is the decay constant, **N** is the amount of activity remaining after any time t and $\mathbf{N_o}$ is the amount of activity at time t = 0.

The percentage injected dose per organ (% ID/organ) and percent injected dose per gram (% ID/g) were calculated from the corrected activity counts.

References

1. May P.M., Williams D.R., (1977), *FEBS Lett.*, **78**, 134
2. Jackson G.E., May P.M., Williams D.R., (1978), *Inorg. Nucl. Chem.*, **40**, 1189.
3. Clark J., Perrin D.D., (1964), *Quart. Rev. Chem. Soc.*, **18**, 295.
4. Jackson G.E., Kelly M.J., (1988), *Inorg. Chim. Acta.*, **152**, 215.
5. Neckers D.C., Doyle M.P., (1977), Organic Chemistry. John Willey & Sons, New York, London, Sydney, Toronto.
6. May P.M., Linder P.W., Williams D.R., (1977), *J. Chem. Soc., Dalton Trans.*, 588.
7. Berthon G., Hacht B., Blais M., May P.M., (1986), *Inorg. Chim. Acta.*, **125**, 219.
8. Jackson G.E., Kelly M.J., (1989), *J. Chem. Soc., Dalton Trans.*, 2429.
9. Jackson G.E., Kelly M.J., (1990), *J. Chem. Soc., Dalton Trans.*, 1889.
10. DiDonato M., Sarkar B., (1997), *Biochim. Biophys. Acta.*, **1360**, 3.
11. Malmstrom B.G., Leckner J., (1998), *Curr. Opin. Chem. Biol.*, **2**, 286.
12. Bertini I., Messori L., Viezzoli M.S., in: Berthon G., (Ed), Handbook of Metal-Ligand Interactions in Biological Fluids-Bioinorganic Chemistry, Marcel Dekker, New York, 1995, p. 156.
13. Solomon E.I., Sundaram U.M., Machonkin T.E., (1996), *Chem. Rev.*, **96**, 2563.
14. Gaetke L.M., Chow C.K., (2003), *Toxicology*, **189**, 147.
15. Sandstead H.H., (1995), *Am. J. Clin. Nutr.*, **61**, 621S.
16. Hathaway B.J., (1987), Comprehensive Coordination Chemistry. The Synthesis, Reactivity, Properties & Application of coordination compounds. Vol 5, Pergamon Press, Oxford pg. 634.
17. Cox D.W., (1999), *Br. Med. Bull.*, **55**, 544.
18. Linder M.C., Hazegh-Azam M., (1996), *Am. J. Clin. Nutr.*, **63**, S 797.

19. U.S Environmental Protection Agency, (1980), Ambient Water Quality for copper. Public. No. PB81-117475. Office of Water Regulations and Standards, Criteria and Standards Deviation Washington, DC.
20. Davies G.K., Mertz W., (1987) In: Trace elements in human and animal nutrition. Vol. 1. 5th ed. W. Mertz (ed.) Academic Press, New York, NY.
21. Blower P.J., Lewis J.S., Zweit J., (1996), *Nucl. Med. Biol.*, **23**, 957.
22. Sarkar B., (2000), *J. Inorg. Biochem.*, **79**, 187.
23. Turnlund J.R., Keyes W.R., Peiffer G.L., Scott K.C., (1998), *Am. J. Clin. Nutr.*, **67**, 1219.
24. Wapnir R.A., (1998), *Am. J. Clin. Nutr.*, **67**, S 1054.
25. Lonnerdal B., (1996), *Am. J. Clin. Nutr.*, **63**, 821.
26. Jackson G.E., Mkhonta-Gama L., Voye A., Kelly M., (2000) *J. Inorg. Biochem.*, **79**, 147.
27. Nomkoko E.T., Jackson G.J., Nakani B.S., (2004), *J. Chem. Soc. Dalton Trans.*, 1432.
28. Wahner H.W., Goldstein N.P., Jenkins D., in Nuclear Medicine: Quantitative Procedures, Wahner H.W., (ed), Little, Brown & Co., Boston (1983).
29. Parckard A.B., Kronauge J.F., Day P.J., Treves S.T., (1998), *Nucl. Med. Biol.*, **25**, 531.
30. Green M.A., (1987), *Nucl. Med. Biol.*, **14**, 59.
31. Sri-Aran M., Mathias C.J., Lim J.K., Green M.A., (1998), *Nucl. d. Biol.*, **25**, 107.
32. Jones-Wilson T.M., Deal K.S., Anderson C.T., McCarthy D.W., Kovacs Z., Motekaitis D., Sherry D., Martell A.E., Welch M.J., (1998), *Nucl. Med. Biol.*, **25**, 523.
33. Anderson C.J., Pajeau T.S., Edwards W.B., Sherman E.L., Rogers B.E., Welch M.J., (1995), *J. Nucl. Med.*, **36**, 2315.
34. Rogers B.E., Anderson C.J., Connett J.M., Guo L.W., Sherman E.L.C., Zinn K.R., Welch M.J., (1996), *Bioconjug. Chem.*, **7**, 511.

35. Cutler C.S., Wuest M., Anderson C.J., Reichert D.E., Sun Y., Martell A.E., Welch M.J., (2000), *Nucl. Med. Biol.* **27**, 375.

36. Michaels A.S., Wong P.S.L., Prather R. Gale R.M., (1975), *AIChEJ.*, **21**, 1073.

37. Shaw J.E., Prevo M., Gale R., Yum Su II, (1991), in Pysiology, Biochemistry and Molecular Biology of the Skin, Oxford University Press, Oxford, 2nd edn., ch. 55, pp 1454.

38. Pastakia B., Lieberman L.M., Gatley S.J., Young D., Petering D.H., Minkel D., (1980), *J. Nucl. Med.* **21**, 67.

39. Jackson G.E., Byrne M.J., Blekkenhorst G., Hendry A.J., (1991), *Nucl. Med. Biol.* **18**, 855.

40. Dehdashti F., Anderson C.J., Trask D.D., Bass L.A., Schwarz S.W., Cutler P.D., (1997), *J. Nucl. Med.* **38**, 103P.

41. Philpott G.W., Schwarz S.W., Anderson C.J., Dehdashti F., Connett J.M., Zinn K.R., (1995), *J. Nucl. Med.* **36**, 1818.

42. Anderson C.J., Jones L.A., Bass L.A., Sherman E.L.C., McCarthy D.W., Cutler P.D., Lanahan M.V., Cristel M.E., Lewis J.S., Schwarz S.W., (1998), *J. Nucl. Med.* **39**, 1944.

43. Connett J.M., Anderson C.J., Guo L.W., Schwarz S.W., Zinn K.R., Rogers B.E., (1996), *Proc. Natl. Acad. Sci.* USA, **93**, 6814.

44. Guerdoud L.M., Ouellet R., Van Lier J.E., (1994), *Nucl. Med. Biol.* **21**, 437.

45. Ackerman L.J., West D.X., Mathias C.J., Green M.A., (1999), *Nucl. Med. Biol.*, **26,** 551.

46. Lewis J.S., Srinivasan A., Schmidt M.A., Anderson C.J., (1999), *Nucl. Med. Biol.*, **26**, 267.

47. Yu M., Qing H., Guojian H., Shu Z., You-Feng H., Kuikka T., (1998), *Nucl. Med. Biol.*, **25**, 111.

CHAPTER SIX
Concluding Remarks

It was neither the aim of this study to investigate the pathogenesis of RA nor was it to contribute to the unknown aetiological nature of the disease. The major objective has been to investigate the use of copper in chemotherapy by developing copper chelating agents that are pseudo-mimics of HSA for use in the treatment of inflammation associated with RA. Since copper has been undoubtedly shown to be involved in RA progression [1], it has been believed that control and understanding of the speciation of the metal at the site of inflammation is essential in the treatment of the disease. Thus to have a complete understanding and appreciation of the use of the copper chelating agents as anti-inflammatory agents in copper chemotherapy, an idealized approach had to be developed and followed, and this study provides a clear description of the steps that constituted the methodology followed in this investigation.

The equilibrium or formation constants determined by potentiometry with the copper chelating agents showed general formation of ML, MLH_{-1} and MLH_{-2} species with remarkable selectivity for Cu(II) over the *in vivo* competitors Ca(II) and Zn(II) (Section 3.4.7). Based on the computer modelling study of Jackson and Kelly [2], remarkable *in vivo* mobilization of Cu(II) was clearly demonstrated. With the exception of the [555-N] system, the chelation of Cu(II) by amidic nitrogen promoted a remarkable amide hydrogen ionization [3, 4] resulting in favourable speciation (MLH_{-2}) at physiological pH. The coordination of the amidic group in the complex was observed to support the reported resonance stability [5, 6] associated with this functional group as shown in Figure 6.1, with formula I as a predominant form.

Figure 6.1: Resonance structures for the amidic functional group

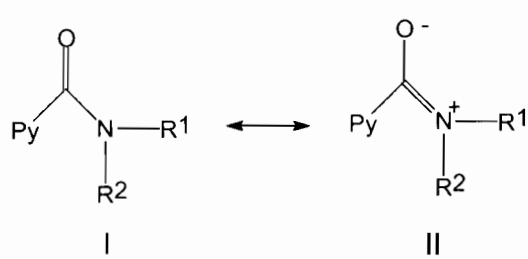

I II

Coordination through the oxygen donor was observed to increase the contribution of formula II (Figure 3.24d(ii) in section 3.4.5) at low pH. At higher pH, coordination was observed to occur through the nitrogen atom, which in order to maintain its sp^2 hybridization had to lose a proton.

However, the inclusion of amidic nitrogen groups in the copper chelating agents, though a requirement to achieve formally neutral species, was done at the expense of stability as reduced formation constants were observed for the respective species due to electronic withdrawing nature of these amidic groups. Thus further studies in future could focus on similar systems in which the effect of the amidic groups on formation constants is minimized. This can be done by incorporation of another amino group as an anchor and extending the spacer carbon chain from ethylenic to propylenic between the amidic groups in the [H_2(556)-N] system. This way the electronic withdrawing effect of the CONH groups would be distributed among more nitrogen donors (three) as opposed to only two in the current study, and the presence of five possible donor atoms would enhance some speciation variation while at the same time maintaining the desirable complex formation characteristics of these systems. Research in this direction has already been reported for the pyridylamine N_6 ligand systems analogous to [H_2(5555)-N] [7, 8] and therefore the same approach is recommended for the asymmetric system. Incorporation of a free carboxylate or an amide side chain is also desirable as this would increase the acidity of the nearby peptide, rather than forming direct coordination to the metal ion as reported for the gly-gly-his [9. 10] and gly-gly-his-N-methylamide [11], thereby further enhancing donor atom basicity in the copper chelating agents. Figure 6.2 shows the possible chelating agents of future interest. It is hoped that as in the case of pyridylamine N_6 analogues, the size of the chelate rings and steric strain, even though both factors are difficult to evaluate quantitatively, would enhance the complexation nature of the proposed copper chelating agents [12].

Figure 6.2: Proposed ligands for future studies

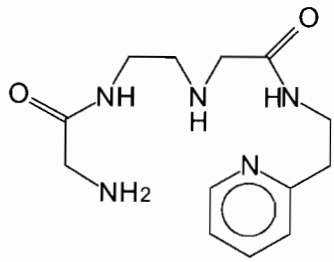

$[H_2(5556)\text{-}N]$

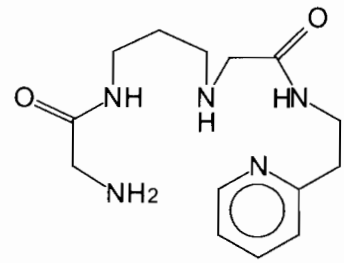

$[H_2(5656)\text{-}N]$

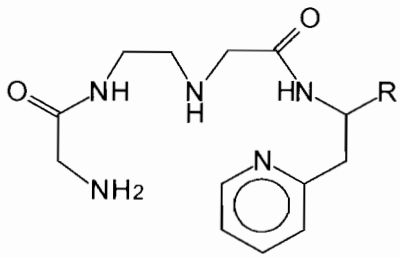

$[H_2(5556)\text{-}N]\text{-}R$

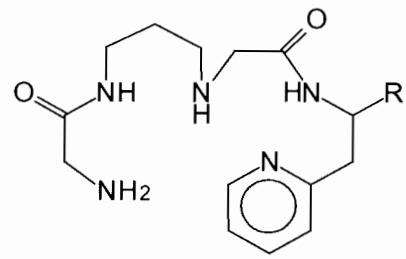

$[H_2(5656)\text{-}N]\text{-}R$

(where R = COO^-, CONHMe)

The nature of species formed with the ligands in this study depended on the nature of the metallic ion, and an attempt was made to account for the potentiometric observations by determining the actual structures of the complexes in solution by UV-Visible spectrophotometry. Since several species existed in solution, deconvolution of the spectral data as a function of pH generated extinction coefficient-based data which was used successfully to determine the actual structures of the complexes in solution. The preference of Cu(II) ion for an environment with four nitrogen donor atoms with a coordination number of four in a tetragonally distorted environment was noted. In these structures water fixation of axial positions was observed.

Having determined the actual structures of the complexes in solution using UV-Visible spectroscopy, molecular mechanics modelling was used to

calculate the strain energies (internal energy) of different possible geometries By consideration of the differences in strain energy on complexation in various species, the stability of the postulated solution complexes were successfully explained. Thus it was shown that molecular mechanics calculations, though not a comprehensive tool, can still be used to rationalize the stability of related complex species in solution.

Speciation modelling of blood plasma was useful in showing *in vivo* selectivity for Cu(II) of the individual ligands, and these computer simulations could be used to predict the *in vivo* tissue distribution results obtained for the Cu(II)-[555-N] complex system in the animal experiments (see section 5.3). Such observations were however unexpected since these simulations do not take into account factors such as hydrophilicity of the complexes. These simulations have failed to predict rapid urinary excretion of stable and formally uncharged Cu(II)-TTDA and DTDA complexes [2] before. Although the Cu(II)-[555-N] complex would be initially excreted rapidly in urine, it is retained *in vivo* in contrast to the Cu(II)-TTDA and DTDA complexes. Thus, the long biological half life of greater than 24 hr for all the Cu(II) complexes in this study is encouraging enough to merit further evaluation of these chelating agents for use in copper chemotherapy.

The use of percutaneous application of the Cu(II) complexes is favourable as demonstrated by encouraging absorption estimates from octanol/water partition coefficients. It has been demonstrated that incorporation of bulky groups on the ligand is essential because they enhance and improve their dermal absorption, and for the first time to our knowledge besides results reported by Green and co-workers [13, 14] positive octanol/water partition coefficients are reported. With the use of permeation enhancers topically-applied anti-arthritic agents could be developed and considering the difficulties associated with intravenous injection of these agents, further studies should be directed along these lines. As a result, this form of drug administration would require the development of appropriate vehicles to enhance percutaneous absorption. A water/dimethyl sulfoxide mixture as an initial vehicle model will be worth trying while encapsulation of

the species in liposomes might offer some advantages over the two phase water/DMSO mixture. Moreover, in future, instead of estimating the dermal absorption using a two phase bio-phase system, the actual dermal absorption measurements should be carried out in mice.

Overall, although this study has not led to the development of new anti-arthritic agents for use in the treatment of R.A, the knowledge gained from such a study provides further advances in our understanding of the role of these copper chelating agents in normal physiology and in their application as therapeutic agents in diseases. It is therefore hoped that this study has contributed to the understanding of a number of some aspects and problems involved in the development of copper-chelating agents for alleviation of inflammation associated with RA. Furthermore, besides introducing new ideas that can be successfully applied in solution chemistry, the study has clearly outlined the approach that could be followed in future studies in the development of new metal ion based drugs.

References

1. Bonta I.L., Parnham M.J., Vincent J.E., Bragt P.C., (1980), In: G.P. Ellis, G.P. West (Eds.) Progress in Medicinal Chemistry, North Holland Biomedical Press, North Holland, pg. 185.
2. Jackson G.E., Kelly M., (1988), *Inorg. Chim. Acta.*, **152**, 215.
3. Conley H.L., Martin R.B., (1965), *J. Phys. Chem.* **69**, 2914.
4. Nawata Y., Iwasaki H., Saito Y., (1967), *Bull. Chem. Soc. Jpn.*, **40**, 515.
5. Sigel H., Martin R.B., (1982), *Chem Rev.* **82**, 385.
6. Robin M.B., Bovey F.A., Basch H., (1970), in Basic Principles of Amides, ed. J. Zabicky, Interscience, London, pg. 1.
7. Jubert C., Mahamadou A., Gerard C., Brandes S., Tobard A., Bardier J.P., (2002), *J. Chem. Soc., Dalton Trans.*, 2660.
8. Jubert C., Mohamadou A., Gerard C., Brandes S., Tobard A., Bardier J.P., (2003) *Inorg. Chem. Commun.*, **6**, 900.
9. Kruck T.P.A., Sarkar B., (1975), *Inorg. Chem.*, **14**, 10, 2383.
10. Lau S., Sarkar B., (1981), J. Chem. Soc., Dalton Trans. 491.
11. Kruck T.P.A., Lau S., Sarkar B., (1976), *Can. J. Chem.*, **54**, 1300.
12. Kim S.D., Kim J.K., Jung W.S., (1988), *Polyhedron* **17**, 1223.
13. Green M.A., (1987), *Nucl. Med. Biol.*, **14**, 59.
14. Sri-Aran M., Mathias C.J., Lim J.K., Green M.A., (1998), *Nucl. Med. Biol.*, **25**, 107.